



# The Interstellar Probe (ISP): Pre-Perihelion Trajectories and Application of Holography

*G.L. Matloff*  
*Pace University, New York, New York*

*G. Vulpetti*  
*Telespazio Company, Rome, Italy*

*C. Bangs*  
*Art Resource Transfer, Inc., New York, New York*

*R. Haggerty*  
*Pace University, New York, New York*

Prepared for Marshall Space Flight Center  
Under Contract H-29712D



# The Interstellar Probe (ISP): Pre-Perihelion Trajectories and Application of Holography

*G.L. Matloff*

*Pace University, New York, New York*

*G. Vulpetti*

*Telespazio Company, Rome, Italy*

*C. Bangs*

*Art Resource Transfer, Inc., New York, New York*

*R. Haggerty*

*Pace University, New York, New York*

Prepared for Marshall Space Flight Center  
Under Contract H-29712D



# The Interstellar Probe (ISP): Pre-Perihelion Trajectories and Application of Holography

*G.L. Matloff*

*Pace University, New York, New York*

*G. Vulpetti*

*Telespazio Company, Rome, Italy*

*C. Bangs*

*Art Resource Transfer, Inc., New York, New York*

*R. Haggerty*

*Pace University, New York, New York*

Prepared for Marshall Space Flight Center  
Under Contract H-29712D

National Aeronautics and  
Space Administration

## Acknowledgments

The contribution of many people to this research is discussed throughout the text. We would like to thank R. Baggett, M. Herrmann, J. Hood, and Les Johnson, NASA Marshall Space Flight Center (MSFC), for their assistance and hospitality. During our stay in Huntsville, many people affiliated with The University of Alabama in Huntsville, especially Jeanelle Hodge, Gerald Karr, and Chuck Karr, were most generous and effective in expediting the Summer Faculty Program.

Robert Foward of Tethers Unlimited supplied invaluable information about the effectiveness of white-light holography as an information storage medium. We appreciate additional discussions of holograms with Nikolai Kukhtarev of Alabama A & M University and David Maker of Teledyne Brown.

The research supported by NASA Contract H-29712D was expedited by a number of people. They include Contracting Officer Ronald Smith, NASA MSFC, and Pace University grant office personnel Lindsley Homrighausen and Len Williams.

Available from:

NASA Center for AeroSpace Information  
7121 Standard Drive  
Hanover, MD 21076-1320  
(301) 621-0390

National Technical Information Service  
5285 Port Royal Road  
Springfield, VA 22161  
(703) 487-4650

**The Interstellar Probe (ISP) :**  
**Pre-Perihelion Trajectories and Application of Holography**

Dr. Gregory L. Matloff, NASA Contract H-29712D (continuation)

**TABLE OF CONTENTS**

Chapter I : Abstract (Executive Summary)	Page I-1
Chapter II : Introduction : ISP goals and Parameters	Page II-1
Chapter III : Advantages of Retaining the Sail to the Heliopause	Page III-1
Chapter IV : Sailcraft Trajectory Options for ISP : Math, Theory, and Results	Page IV-1
Chapter V : A Prototype Holographic Message Plaque for ISP	Page V-1
Chapter VI : Simuated Space Environmental Effects on Holograms	Page VI-1
Chapter VII : Conclusions	Page VII-1
Bibliography	Page B-1
Appendix : A Near-Earth Application for Holographic Solar Sails	Page AP-1
Acknowledgements	Page AC-1



## CHAPTER 1. ABSTRACT (EXECUTIVE SUMMARY)

Between February and September 2001, a number of aspects of the solar-sail launched Interstellar probe (ISP), which is under consideration by NASA for launch in the 2010-2015 time frame, were researched. The effort was conducted in New York City during February-May, at MSFC in May-July (when the PI served as a NASA Summer 2001 Faculty Fellow) and in New York City during August and September. as well as the people listed on the title sheet, many people in NYC and at MSFC participated in this research.

The goals of the planned ISP mission are to launch a solar sail on a trajectory with a close perihelion pass (about 0.2 -0.25 AU) so that the scientific payload could reach the heliopause (at about 200 AU) from the Sun after a flight of about 20 years duration. The scientific payload is less than 30 kg and the mission is devoted to the study of particles and fields.

Current JPL planning disposes of the sail at 5 AU from the Sun on the outbound trajectory leg. we show that it may be advisable to retain the sail during the interstellar mission for two reasons. First, analysis indicates that sail can still increase terminal velocity by a few percent in the outer solar system. second, an electrically conducting sail or sail segment could function as magnetometer and consequently reduce payload mass.

Using a computer code developed by consultant Giovanni Vulpetti , we considered many aspects of preperihelion sail trajectory. These computer runs indicate that there are two launch windows every year to project the spacecraft towards the same portion of the heliopause. Both require an initial trajectory directed outward from the Sun, and then a dip in towards perihelio. As well as the posigrade trajectory considered in NASA / JPL planning for the proposed mission, Vulpetti's code considers an angular-momentum-reversal option.

An advantage of Vulpetti's code over many other models is its realistic parameterization of sail reflectance. The latest MSFC Space Environment Group determination of sail optical degradation by the solar wind were used as inputs for Vulpetti's code.

Many optimized configurations are capable of performing the ISP mission. Most intriguing are a series of trajectories in which a higher Earth-escape velocity results in less technologically-demanding ISP mission configurations.

Artist C Bangs supervised creation of a prototype white-light (rainbow) holographic message plaque for the ISP, following a suggestion by Dr. Robert Forward. After mounting and framing, the completed art piece was delivered to the MSFC Transportation Directorate. Under proper illumination, 5 of the 6 multiplexed holographic images on the photographic plate can be readily viewed.

Les Johnson of MSFC Space Transportation concluded that holography might have propulsive space applications as well as artistic ones. Ryan Haggerty and c bangs assisted the MSFC Space Environments group in determining the resistance of commercial holograms to simulated solar-wind radiation.

The PI suggested a new method of analyzing radiation resistance of holograms. After exposure to simulated solar wind, the hologram was scanned into a computer

and compared to non-irradiated control hologram using the color-histogram option of the Adobe Photoshop™ computer package. Red, green, and blue image quality was evaluated. As indicated by previous studies in the literature and confirmed by photographic comparisons of the subject samples, holograms are very resistant to space radiation.

The PI was asked to present an application of holography to solar-sail propulsion. As indicated by this presentation (which is included as the Appendix to this report), holographic sail elements may enable the technology of solar-photon thrusting (SPT) , which allows some control of the radiation-pressure vector's direction. multi-sail SPTs may allow sail operations closer to low-Earth orbit (LEO) than possible with other sail configurations.

## CHAPTER II : INTRODUCTION: ISP GOALS AND PARAMETERS

NASA's ambitious Interstellar Probe (ISP) Mission is the outgrowth of decades of research in travel beyond the solar system, summarized by Mallove and Matloff (1989). Initial interstellar-travel concepts utilized nuclear propulsion schemes, such as the American Orion (Dyson, 1968) and British Daedalus (Martin, 1978) concepts. These thermonuclear-pulse proposals would be capable of propelling large payloads to velocities in excess of  $0.1c$  (where  $c = 3 \times 10^8$  m/sec, the speed of light).

As an alternative to thermonuclear pulse, Matloff and Mallove (1981 and 1983) considered the interstellar capability of hyperthin solar sails unfurled at distances of 0.01-0.03 AU from the Sun's center. These craft could conceivably achieve solar-system escape velocities in excess of 0.005c. In landmark papers, Martin (1984) and Bond and Martin (1984) concluded that of all peopled interstellar-travel proposals, only the "1000-year ark" or "worldship" is possible and the only ultimately feasible propulsion systems for these craft are the thermonuclear-pulse, or solar-sailing option. In a more near-term but much less challenging proposal, NASA/JPL considered the Thousand Astronomical unit (TAU) probe in a studied authored by Jaffe et al (1980). Instead of targeting one of the nearer stars, TAU would explore near-interstellar space out to about 100 AU. Exiting the solar system at about 100 km/sec, TAU would reach 1000 AU from the Sun within a human lifetime. The TAU propulsion system would be nuclear electric, which is feasible for such interstellar-precursor missions but may never be capable of true interstellar travel.

Development and construction of a large nuclear spacecraft such as TAU presents many political, sociological, and environmental problems. So in the early 1990's, researchers in Europe and the US turned their attention to sail-launched missions to the Sun's gravity focus at 550 AU from the Sun (Heidmann and Maccone, 1994). As pointed out by Vulpetti (1996) in his "Aurora" proposal, a less-demanding "technology demonstrator" for a gravity-focus or TAU mission would be a probe to the heliopause, the boundary between the sun's influence and interstellar space. The heliopause is estimated to be about 200 AU from the Sun.

Starting in the mid-1990's, NASA / MSFC and JPL have studied sails that could be launched in the 2010-2015 time frame and would require about 15 years to reach the heliopause (Johnson and Leifer, 2000, Liewer et al, 2000 and Mewaldt and Liewer, 2000). Such near-term ISP configurations would carry a scientific payload of about 30 kg, have a total spacecraft mass of a few hundred kilograms and be launched to earth-escape by a Delta-class booster. To achieve a sufficiently high interstellar cruise velocity, the sailcraft would first use the sail after Earth-escape to spiral out to about the orbit of Mars (1.5 AU) and then dip in towards a perihelion of about 0.25 AU. Sail-aspect angle would be varied appropriately during the pre-perihelion pass and would be near-normal to the Sun at and after perihelion. The ISP sail radius would be a few hundred meters. Sail areal thickness or mass loading would be about 1 gram/meter<sup>2</sup> and total spacecraft areal mass loading would be about 2 gm/m<sup>2</sup>. Currently, NASA plans to drop the sail from the payload section at about 5 AU from the Sun. the next chapter of this report considers advantages of

retaining the sail beyond this solar distance.

As well as being a technology demonstrator for a propulsion system which could be developed to true interstellar capability, ISP has a number of scientific goals. These include the *in situ* study of the interaction between the solar wind and the interstellar medium, the nature and composition of the interstellar medium and the interstellar magnetic field. Stated objectives for the mission are to explore the interstellar medium and its implications for evolution of the galaxy and universe; to explore the influence of the interstellar medium in the solar system and the impact of the solar system on the interstellar medium; and to explore the outer solar system for clues to the origin of planetary systems.

A wide variety of scientific instruments are under consideration for the (approximately) 30 kg science payload. These include neutral and charged-particle instruments, spectrometers to determine isotopic composition of the local interstellar medium, and detector for suprathermal ions and electrons, cosmic-ray detectors, a magnetometer and a plasma/radio-wave detector to monitor fluctuations in the electric and magnetic fields at and beyond the heliopause, an energetic neutral-atom imager, ultraviolet and infrared photometers and a small telescope to survey Kuiper belt objects near the spacecraft's trajectory.

Although designed for a 15-year flight to the heliopause, ISP may well survive for 30 years or more, as has been the case for the first interstellar probes Pioneer 10/11 and Voyager 1/2. It is not impossible that ISP could survive to return data from 400 AU or even the Sun's gravitational focus at 550 AU.

## Chapter 2 References

- A. Bond and A. R. Martin, "World Ships -- An Assessment of the Engineering Feasibility," *JBIS*, **37**, 254-266 (1984).
- F. Dyson, "Interstellar Transport," *Physics Today*, **21**, No. 10, 41-45 (October, 1968).
- J. Heidmann and C. Maccone, "ASTROSail and SETIsail : Two Extrasolar System Missions to the Sun's Gravitational Focus," *Acta Astronautica*, **37**, 409-410 (1994).
- L. D. Jaffe, C. Ivie, J. C. Lewis, R. Lipes, H. N. Norton, J. W. Sterns, L. D. Stimpson, and P. Weissman, "An interstellar Precursor Mission," *JBIS*, **33**, 3-26 (1980).
- L. Johnson and S. Leifer, "Propulsion Options for Interstellar Exploration," AIAA-2000-3334.
- P. C. Liewer, R. A. Mewaldt, J. A. Ayon, C. Garner, S. Gavitt, and R. A. Wallace, "Interstellar Probe using a Solar Sail : Conceptual Design and Technological Challenges," presented at COSPAR Colloquium, *The Outer Heliosphere : The Next Frontier*, Potsdam, Germany, July 24-28, 2000.

E. Mallove and G. L. Matloff, *The Starflight Handbook*, Wiley, NY (1989).

A. R. Martin, ed., "Project Daedalus : The Final Report on the BIS Starship Study," supplement to *JBIS* (1978).

A. R. Martin, "World Ships -- Concept, Cause, Cost, construction, and Colonization," *JBIS*, 37, 243-253 (1984).

G. L. Matloff and E. Mallove, "Solar Sail Starships : the Clipper Ships of the Galaxy," *JBIS*, 34, 371-380 (1981).

G. L. Matloff and E. Mallove, "The Interstellar Solar Sail : Optimization and Further Analysis," *JBIS*, 36, 201-209 (1983).

R. A. Mewaldt and P. C. Liewer, "An Interstellar Probe Mission to the Boundaries of the Heliosphere and Nearby Interstellar Space, presented at Space 2000, Sept. 19-21, 2000, Long Beach, CA.

G. Vulpetti, "The Aurora Project : Flight Design of a Technology Demonstration Mission," in *Missions to the Outer Solar System and Beyond*, 1st IAA Symposium on Realistic, Near-Term Scientific Space Missions, ed. G. Genta, Levrotto & Bella, Turin, Italy (1996), pp 1-16.



### CHAPTER 3. ADVANTAGES OF RETAINING THE SAIL TO THE HELIOPAUSE

Current planning for the NASA Interstellar Probe (ISP) mission assumes that the spacecraft will be accelerated by solar-sail from starting from a perihelion as close as 0.2 AU from the Sun and will detach from the solar sail at or near the orbit of jupiter (5.2 AU from the Sun). This report chapter considers the kinematical advantages of not dropping the sail.

We start this analysis with Eq. (4.26) of Matloff, *Deep-Space Probes* (Matloff, 2000) :

$$V_{fin} = \left[ V_{init}^2 + (\eta_{sail} - 1)V_{para, init}^2 - V_{para, fin}^2 \right]^{1/2} \quad (3-1)$$

where  $V_{fin}$  = final spacecraft velocity relative to the Sun,

$V_{init}$  = initial spacecraft velocity relative to the Sun,

$V_{para, init}$  = solar parabolic (escape) velocity at perihelion

$V_{para, fin}$  = solar parabolic velocity at end of sail acceleration

$\eta_{sail}$  = sailcraft lightness factor (the ratio of solar radiation pressure force to solar gravitational force on the sailcraft).

It is assumed in the derivation of Eq. (3-1) that the sail is fully opaque, is fully unfurled at perihelion and is always oriented normal to the Sun.

We next simplify Eq. (3-1) by assuming that the pre-perihelion trajectory is parabolic. Therefore,  $V_{init} = V_{para, init} = V_{para-peri}$ , where  $V_{para-peri}$  is the solar parabolic velocity at perihelion. Substituting in Eq. (3-1) and manipulating,

$$V_{fin} = V_{para-peri} \eta_{sail}^{1/2} \left[ 1 - \frac{(\eta_{sail} - 1)V_{para, fin}^2}{V_{para-peri}^2 \eta_{sail}} \right]^{1/2} \quad (3-2)$$

In any interstellar solar sail expedition, the solar parabolic velocity at the end of solar-sail acceleration will be small compared with the perihelion velocity. Therefore,

$$V_{fin} \approx V_{para-peri} \eta_{sail}^{1/2} \left[ 1 - \frac{(\eta_{sail} - 1)V_{para- fin}^2}{2V_{para- peri}^2 \eta_{sail}} \right] \quad (3-3)$$

Equation (4-27) of Matloff (2000) is an approximate expression for the

calculation of spacecraft final velocity if the sail is dropped an infinite distance from the Sun. For such a situation,

$$V_{fin,\infty} \approx V_{para-peri} \eta_{sail}^{1/2} \quad (3-4)$$

We next define the parameter K, where K is the fractional loss in final interstellar cruise velocity if the sail is dropped at 5.2 AU from the Sun instead of an infinite distance from the Sun:

$$K = \frac{V_{fin,\infty} - V_{fin,5.2au}}{V_{fin,\infty}} = \left( \frac{\eta_{sail} - 1}{\eta_{sail}} \right) \frac{V_{para, fin=5.2au}^2}{2V_{para-peri}^2} \quad (3-5)$$

From the definition of solar parabolic or escape velocity,

$$K = \left( \frac{\eta_{sail} - 1}{\eta_{sail}} \right) \left( \frac{R_{peri,au}}{10.4} \right) \quad (3-6)$$

Applying Equation (4.19) of Matloff (2000), we can approximate sail lightness factor :

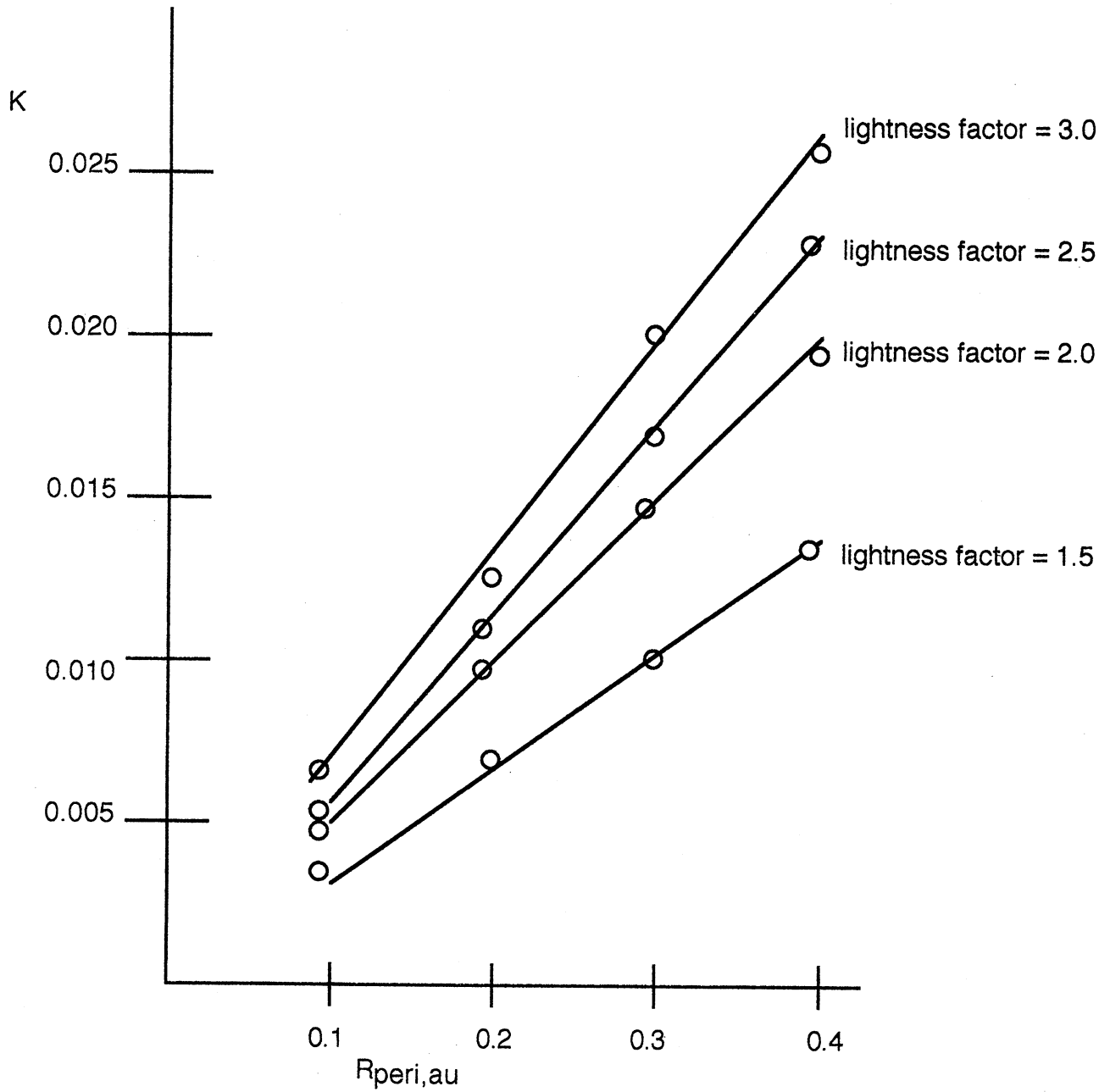
$$\eta_{sail} \cong \frac{0.000787(1 + REF_{sail})}{\sigma_{s/c}} \quad (3-7)$$

where  $REF_{sail}$  = (fully opaque) sail fractional reflectivity and  $\sigma_{s/c}$  is the sailcraft areal mass thickness in MKS units.

Figure 3-1 shows parametric solutions of velocity loss factor K as a function of sailcraft lightness factor and perihelion distance. Note that retaining the sail beyond Jupiter can increase terminal interstellar cruise velocity by a few percent. Velocity loss factor K increases for low-mass missions and high perihelion velocities. Using the software described in the next chapter, Giovanni Vulpetti has also found a kinematical advantage to retaining the sail throughout the ISP mission.

There are potential non-propulsive applications for a retained ISP sail. a properly shaped sail could function as a communications antenna. also, if circuitry is emplaced around the outer edge of a disc-shaped ISP sail, the sail could function as a magnetometer during interstellar cruise without a substantial payload mass penalty.

Fig. 3-1 Terminal Velocity Fractional Loss factor K as a Function of Sailcraft Lightness Factor and Perihelion Distance.



### Chapter 3 References

G. L. Matloff, *Deep-Space Probes*, Springer-Praxis, Chichester, UK (2000).

# CHAPTER IV

## SAILCRAFT TRAJECTORY OPTIONS FOR THE INTERSTELLAR PROBE: MATHEMATICAL THEORY AND NUMERICAL RESULTS

*Giovanni Vulpetti<sup>1</sup>, Telespazio SpA, Via Tiburtina 965, 00156 Rome, ITALY*

### IV.1 Introduction

Gregory Matloff dealt with the purposes of NASA Interstellar Probe (ISP) in the previous chapters of this report to NASA George C. Marshall Space Flight Center. Les Johnson provided report authors with basic input (Johnson, 2001). Preliminary design of ISP baseline mission and sailcraft systems can be found in (Mewaldt *et al.*, 2000) and (Liewer *et al.*, 2000). This chapter aims at identifying other options for the ISP mission based on solar-sail propulsion. Unavoidably, mission strategies and results are interrelated to the sailcraft technology, in general, and the sail system, in particular. Although literature on solar sailing has been enriching since the Eighties, perhaps the general reader is not full aware of all aspects on advanced space sailing. Thus, we arranged this chapter as follows: §IV.2 and §IV.3 present a background on fast solar sailing and considerations about modeling the translational motion of a sail in space. §IV.4 focuses on the important topic of optical sail degradation, whereas §IV.5 shortly describes the computer code we have employed to get the numerical results presented in §IV.6 and §IV.7. Considerations on the ISP feasibility and suggestions about some items of next ISP research & design are given in §IV.8 and §IV.9.

### IV.2 Background on Fast 3D Trajectories by Solar Sailing

In this section, we summarize the basics of *fast* heliocentric sailcraft trajectories by using a formalism developed in the last decade of the 20<sup>th</sup> century. Details can be found in Vulpetti (1996, 1999a, 1999b) and the references inside. With regard to nomenclature, symbols will be explained on the way; normally, bold letters refers to as three-dimensional *column* vectors whereas capital Greek letters denotes matrices, unless otherwise specified. Although the used formalism is coordinate-free, however, we shall use coordinates, implicitly or explicitly, that are defaulted to the Cartesian ones.

#### 2.1 Frames of Reference and Units

In the present theory and related numerical code, we use two heliocentric reference frames and one sailcraft-centred frame. The first frame, hereby called the Heliocentric Inertial Frame (HIF), has been built starting from the realization, named the *International Celestial Reference Frame* (ICRF), of the International Celestial Reference System (ICRS) that is provided by the International Earth Rotation Service (IERS). The strict definition of ICRF and its related documentation can be found at <http://www.iers.org>. Here, we very briefly report that the origin of the ICRF is the barycenter of the Solar System and its orientation is close to dynamical equinox and mean equator at J2000. HIF has been obtained by rotating the YZ-plane of ICRF counterclockwise about its X-axis by the value of Earth obliquity ( $23^{\circ} 26' 21.16''$ ) at J2000. HIF is centred on the Sun barycenter and it is oriented close to the dynamical equinox and mean ecliptic at J2000. That is particularly useful when planetary perturbations are included, via standard ephemerides, in the sailcraft motion (as a matter of fact, *a-priori* one does not know whether the sailcraft will be flying-by some planet).

The second frame, hereby named the Extended Heliocentric Orbital Frame (EHOF), is defined as follows:

**2D motion in HIF** with trajectory curvature supposed not to diverge at any time

1. If motion is direct or counterclockwise (in HIF), then the reference direction & orientation are those ones of the sailcraft position vector  $\mathbf{R}$ ; the reference plane is given by  $(\mathbf{R}, \mathbf{V})$ ,  $\mathbf{V}$  denoting the sailcraft

---

<sup>IV-1</sup> Chief Scientist, Full Member of the International Academy of Astronautics

velocity vector, and the Z-axis coincides with the direction & orientation of the orbital angular momentum per unit mass  $\mathbf{H}=\mathbf{R}\times\mathbf{V}$

2. If motion is retrograde or clockwise (in HIF), then the X-axis is the same as in (1), but the Z-axis is oriented opposite to  $\mathbf{H}$  and, consequently, the Y-axis is in the semi-plane  $(\mathbf{R}, -\mathbf{V})$ .
3. At some time, say,  $t^*$  where  $\mathbf{H}=\mathbf{0}$  (if any), the Z-axis is the limit of the Z-direction of either (1) or (2) when  $t$  approaches  $t^*$ . It is easy to show by considerations of geometry and vector analysis that such a direction, here denoted by  $\mathbf{h}^*$ , exists and is unique.

**3D motion in HIF** with trajectory torsion assumed to be limited at any time

a. If flight *begins* with a direct motion (in HIF), then EHOV axes are defined the same way in 2D-1

b. If flight *begins* with a retrograde motion (in HIF), then EHOV axes are defined the same way in 2D-2.

The direction of the Z-axis is denoted by  $\mathbf{h}$ , whereas  $\mathbf{r}$  is the direction of  $\mathbf{R}$ . At any time  $t$ , there is a well-posed triad  $(\mathbf{r}, \mathbf{h} \times \mathbf{r}, \mathbf{h})$ , which defines the extended orbital heliocentric frame. The attribute *extended* refers to the fact that a general sailcraft trajectory may be composed of pieces separated by at least one point where the orbital angular momentum vanishes. General discussion on the EHOV can be found in (Vulpetti, 1999a). The case characterized by  $\mathbf{H}=\mathbf{0}$  for a finite interval of time can be also dealt with appropriately, but is beyond the scope of this report and the realistic options related to the Interstellar Probe.

The third frame, named the Sailcraft Orbital Frame (SOF), has its origin on the vehicle's barycenter and it is instantaneously at rest, according to Special Relativity (SR). In general, its orientation differs from that of EHOV by an amount due to the aberration of light, which is a first-order effect in speed. For ISP, the orientations of EHOV and SOF are very close to one another.

The computer code described in §IV.5 is fully based on SR. However, we shall use the classical approximation for ISP, here, to simplify presentation of solar sailing theory and discussion/comparison of the results. Evenly, HIF/EHOV-related time and SOF proper time scales can be considered equal to each other. Julian Date (JD) has been used for astronomical events and coordinates such as position and velocity of planets in HIF at different times, whereas sailcraft thrusting and/or coasting time intervals could be specified in either SI seconds or days (1 day = 86400 SI seconds) or standard years (1 standard year = 365.25 days).

## 2.2 The Lightness Vector Formalism

Let us consider the vector solar-pressure acceleration that acts on the sailcraft center of mass. Think about this vector (1) *resolved* in EHOV, (2) normalized to the *local* solar gravitational acceleration. Let us denote it by  $\mathbf{L}$  and name it the *lightness vector*. We call its components the *radial*, *transversal* and *normal numbers* as follows:

$$\mathbf{L} = [\lambda_r \quad \lambda_t \quad \lambda_n]^T \quad \lambda \equiv |\mathbf{L}| \quad (\text{IV-1})$$

$\mathbf{L}$  is a function of time. Its magnitude is called the *lightness number* here; it should not be confused with the same-name parameter defined in (Wright, 1993); that one is a particular case of the current  $\lambda(t)$  function. The motion of the sailcraft barycenter in HIF can be described by the following system of ordinary differential equations (ODE)

$$\begin{aligned} \frac{d}{dt}\mathbf{R} &= \mathbf{V} \\ \frac{d}{dt}\mathbf{V} &= -\frac{\mu}{R^2} + \frac{\mu}{R^2}\Phi\mathbf{L} + \left(\sum_{j=1}^{N_p}\mathbf{P}_j\right)P = \\ &\quad \frac{\mu}{R^2}\left[-(1-\lambda_r)\mathbf{r} + \lambda_t\mathbf{h}\times\mathbf{r} + \lambda_n\mathbf{h}\right] + \left(\sum_{j=1}^{N_p}\mathbf{P}_j\right)P \\ \frac{d}{dt}m &= -\dot{m}_{\text{sail ACS}} \end{aligned} \quad (\text{IV-2})$$

where  $m$  is the sailcraft mass,  $\mathbf{V}$  its velocity,  $R=|\mathbf{R}|$  is the Sun-sailcraft distance;  $\mu$  denotes the solar gravitational constant, whereas  $\mathbf{P}_j$  represents the gravitational perturbation of the  $j$ -th of  $N_p$  planets on the spacecraft,

according to Celestial Mechanics. The symbol  $p$  denotes a switch, either 1 or 0, for including planetary perturbation(s) or not, respectively.  $\Phi$  denotes the matrix of rotation from EHO to HIF; it is equal to  $(\mathbf{r} \times \mathbf{h} \times \mathbf{r})_{HIF}$ , according to what defined in sect. IV-2.1. The scalar differential equation in IV-2 accounts for any mass consumption, for instance due to some small-rocket control of the sail orientation; one supposes that mass is exhausted at zero total momentum in SOF, namely, no residual force acts on the vehicle barycenter.

Some remarks are in order: *first*, although in principle equation IV-2b may be valid also for an (ideally) rocket-controlled spacecraft, in practice, however, only a sailcraft is characterized by the fields appearing in the acceleration equation, namely, two conservative fields and one non-conservative (aside from planetary perturbations). *Second*, if  $\lambda$  is sufficiently high, the features of the heliocentric spacecraft trajectory are determined mainly by solar gravity and solar pressure (even though some close planetary fly-by may affect low-speed trajectory arcs). *Third*, as such, equations IV-2 do not contain any reference to sailcraft technology; in other words, all sailcraft trajectory classes can be studied by reasoning only in terms of  $\mathbf{L}$ 's magnitude and components. Subsequently, a real mission shall be analyzed by connecting dynamics and vehicle technology (§IV.3). Such observation is particularly important since it allows the analyst to be aware of strong non-linear behaviors that a conventional spacecraft does not have.

From the above observations, it is convenient to focus our attention on the solar fields here for illustrating and discussing solar sailing behaviors. Thus, unless otherwise specified, we refer to the following simplified equations

$$\begin{aligned} \frac{d}{dt} \mathbf{R} &= \mathbf{V} \\ \frac{d}{dt} \mathbf{V} &= \frac{\mu}{R^2} [-(1-\lambda_r) \mathbf{r} + \lambda_t \mathbf{h} \times \mathbf{r} + \lambda_n \mathbf{h}] \end{aligned} \quad (\text{IV-2A})$$

It is a simple matter to show how sailcraft energy and (orbital) angular momentum evolve under equations IV-2A. By introducing the quantity

$$H = \mathbf{H} \cdot \mathbf{h} \quad \Leftrightarrow \quad \mathbf{H} = H \mathbf{h} \quad H = \pm \|\mathbf{H}\| \quad (\text{IV-3})$$

which is an invariant, named the  $H$ -function, one gets the following equations for energy

$$\begin{aligned} E &= \frac{1}{2} V^2 - (1-\lambda_r) \frac{\mu}{R} \\ \frac{d}{dt} E &= \frac{H}{R^2} \frac{d}{dt} H \end{aligned} \quad (\text{IV-4})$$

and the following equations for angular momentum and invariant:

$$\begin{aligned} \mathbf{H} \times \frac{d}{dt} \mathbf{H} &= H \lambda_n \frac{\mu}{R} \mathbf{r} \\ \frac{d}{dt} \mathbf{H} &= \frac{\mu}{R} (\lambda_t \mathbf{h} - \lambda_n \mathbf{h} \times \mathbf{r}) \\ \frac{d}{dt} H &= \lambda_t \frac{\mu}{R} \quad \Rightarrow \quad \frac{d}{dt} E = \lambda_t \frac{H \mu}{R^3} \end{aligned} \quad (\text{IV-5})$$

In words, sailcraft energy depends of the radial number; energy rate does on the transversal number (through equation IV-5c), whereas the normal number drives the angular momentum bending. The evolution of  $\mathbf{H}$  does not depend explicitly on the radial number. Equation IV-5c is a basic equation for controlling sailcraft trajectory; trajectory classes depend on the initial *invariant* value and how it evolves (Vulpetti, 1996, 1997, 1999a). One should note that, unless the analyst knows the vector functions  $\mathbf{L}(t)$  and  $\mathbf{h}(t)$  in advance, equations IV-2 and IV-5c have to be integrated *simultaneously* to propagate a sailcraft trajectory. As a point of fact, in general, one does not know whether/when sailcraft may reverse its motion or not.

If vector  $\mathbf{L}$  were aligned with the radial direction  $\mathbf{r}$ , for instance after the sail deployment at some suitable perihelion  $R_p$  from the Sun, the sailcraft energy change would amount to  $\lambda_r \mu / R_p$ ; as a result, the hyperbolic excess would be  $V_\infty = \sqrt{V_p^2 - 2(1 - \lambda_r) \mu / R_p}$ . A very good way to get a high cruise speed would be to make a sailcraft with high lightness number and launch it on either parabolic or quasi-parabolic orbit down to  $R_p$ . This results in the following speed

$$V_\infty = \sqrt{[(1+e)\mu/\ell]^2 - 2(1-\lambda_r)\mu/R_p} \quad (\text{IV-6})$$

In equation IV-6,  $(e, \ell)$  denote the eccentricity and the magnitude of angular momentum, respectively, of the pre-perihelion orbit. Options for pre-perihelion acceleration have been investigated extensively (Matloff and Mallove, 1983) and summarized critically (Matloff, 2000). One should realize that the value, say,  $V_\infty^p$  obtained from equation IV-6 (or an equivalent one) by parabolic pre-perihelion mode could be taken as a useful reference with which *actual* fast trajectories may be compared. As a point of fact, one knows that a mission obeying equation IV-6 is somewhat hard to implement, in practice. In addition, one should note that  $V_\infty^p$  represents an upper limit only for supercritical sailcraft (§IV.6).

When perturbations are added to the sailcraft motion, equations IV-4 and IV-5 are to be modified. For instance, the invariant's evolution equation changes to:

$$\frac{d}{dt}H = \lambda_t \frac{\mu}{R} + R \mathbf{h} \times \mathbf{r} \cdot \mathbf{P} \quad (\text{IV-7})$$

In equation IV-7,  $\mathbf{P}$  denotes the sum of sailcraft accelerations other than solar gravity and photon-sail interaction. However, a good quasi-optimal profile of a 3D trajectory could be carried out by using the simpler form again, especially around the perihelion.

### 2.3 The Motion Reversal Mode

A sailcraft with  $\lambda = \lambda_r$  moves on a "generalized" keplerian orbit inasmuch as it senses the Sun with an effective mass equal to  $(1 - \lambda_r)\mu$ . However, there is no way to change energy, according to the last equation in IV-5, since any transversal components of the lightness vector vanishes. Thus, if one wants to increase sailcraft speed, some non-radial control has to be applied. The problem is not simple even because, if any non-radial component of the lightness vector is different from zero, the sailcraft equations of motion admit no Lagrangian. It is possible to show strictly by the theory of Lie Groups that no analytical solution to IV-2A exists (Vulpetti, 2001). However, many important properties and features of solar sailing trajectories can be drawn by analyzing equations IV-2A through IV-5 appropriately.

Let us consider the evolution equation of the invariant. It is easy to recognize that, if the transversal number is negative (and not too low) and the trajectory arc time is sufficiently long, some point can be reached where either  $H$  vanishes or achieves a local low minimum (or a local high maximum, if the initial motion is retrograde). It can be proved that the first possibility can arise in 2D motion (Vulpetti, 1997), whereas the second one pertains to either mixed 2D/3D-trajectory arcs or full 3D-trajectory arcs (Vulpetti, 1996, 1999a). Only for special cases, conditions can cast them in simple form such as

$$\begin{cases} \frac{1}{2} \leq \lambda_r < 1 \\ -1 < \lambda_t \frac{(t_p - t^*)\mu}{R_p V_p R^*} < -\frac{R_p}{R^*} \end{cases} \quad \text{2D trajectories, } \mathbf{L} = \text{constant} \quad (\text{IV-8})$$

Here, the lightness vector is assumed constant throughout the flight. The subscript p denotes quantities evaluated at the perihelion, whereas starred quantities refer to the  $H=0$  event. Another special case is the mixed 2D/3D trajectory in which one has a piecewise-constant lightness vector. In this case, one gets

$$t \in [t_0, t_A] \quad t_A > t^* \quad \begin{bmatrix} \lambda_r \\ \lambda_t \\ 0 \end{bmatrix} = \mathbf{L}_A \quad (\text{with constraints IV-8}) \quad (\text{IV-9})$$

$$t \in (t_A, t_f] \quad \begin{cases} \frac{1}{2} < |\mathbf{L}_B| < 1 \\ \lambda_t < 0 \\ \lambda_n \neq 0 \end{cases} \quad \begin{bmatrix} \lambda_r \\ \lambda_t \\ \lambda_n \end{bmatrix} = \mathbf{L}_B = \text{const.} \neq \mathbf{L}_A$$

A realistic 3D trajectory class shall be dealt with extensively in §IV.3.

*Why an analysis on sailcraft mission should consider the option in which the orbital angular momentum of the vehicle may reverse somewhere?*

The strict mathematical treatment of the motion-reversal sailing mode is beyond the scopes of this report. Here, we limit ourselves to show what happens semi-quantitatively. Let us begin by calculating the along-track component of the total acceleration, namely, the time derivative of the sailcraft speed

$$\frac{d}{dt}V = \mathbf{V} \cdot \dot{\mathbf{V}} / V = [-(1-\lambda_r)\cos\varphi + \lambda_t \sin\varphi] \mu / R^2 + \mathbf{v} \cdot \mathbf{P} \quad (\text{IV-10})$$

In IV-10, the quantity  $\varphi: \varphi \in [0, 2\pi)$ ,  $RV \sin\varphi = H$  denotes the generalized angle between sailcraft's position and velocity vectors.  $\mathbf{v}$  stands for the direction of  $\mathbf{V}$ . Note that the *normal* number does not appear in equation IV-10. If one ignores small perturbations, this along-track quantity vanishes when

$$\cot\varphi = \lambda_t / (1-\lambda_r) \quad (\text{IV-11})$$

For simplifying discussion, let us assume both radial and transversal numbers constant throughout the flight; this means that there are two values of the  $\varphi$  angle satisfying equation IV-11 as follows

$$\begin{cases} 0 < \varphi_s < \pi/2 & \lambda_t > 0 & \lambda_r < 1 \\ \pi/2 < \varphi_s < \pi & \lambda_t < 0 & \text{"} \\ \varphi_e = \varphi_s + \pi & & & \end{cases} \quad (\text{IV-12})$$

$$\begin{cases} \pi < \varphi_e < \frac{3}{2}\pi & \lambda_t > 0 & \text{"} \\ \frac{3}{2}\pi < \varphi_e < 2\pi & \lambda_t < 0 & \text{"} \end{cases}$$

It is possible to show that the angle labeled by  $S$  refers to local maximum or minimum of sailcraft speed, occurring at time  $t_S$ , if  $\lambda_t$  is positive or negative, respectively. Typically, if sailcraft starts from a near circular orbit such as the Earth-Moon barycenter orbit (plus an hyperbolic excess) with a sufficiently *positive* transversal number, say,  $\lambda_t \approx \lambda/3$ , it accelerates while increasing its distance from the Sun. Rapidly, it achieves the maximum of speed, then decelerates though it can escape the solar system radially (if the lightness number is high enough). There is no local minimum of speed, since  $dV/dt$  is always negative past the maximum. As a point of fact, the invariant  $H$  is positive and increases monotonically; consequently, the angle between position and velocity can pass through neither zero nor 180 degrees. In such a trajectory class,  $\varphi_e$  does not represent a physical solution. Even more, this happens for slow spiraling-out trajectories (for which  $\lambda$  is low), whereupon sailcraft speed changes through local maxima and minima characterized by  $\varphi = \varphi_s$ .

A quite asymmetrical situation arises from a sufficiently *negative* transversal number. Since  $H$  may vanish, the  $\varphi = \varphi_e$  solution can physically exist at some time  $t_e$ . Consequently, one may integrate (the main terms of) equation IV-10 from time  $t_S$  to time  $t_e$

$$(V_{max} - V_{min})/\mu = - (1 - \lambda_r) \int_{t_s}^{t_e} \frac{\cos \varphi}{R^2} dt + \lambda_t \int_{t_s}^{t_e} \frac{\sin \varphi}{R^2} dt \quad (IV-13)$$

(The fact we are dealing with the simplified problem of  $L=\text{constant}$  (throughout the flight of interest) has been highlighted). If  $\lambda_r < 1$ , the first term gives its highest positive contribution when  $\varphi \cong \pi$ , namely, around a point where the angular momentum is zero or close to zero, whereas the second term is strongly positive when  $\varphi \cong 3\pi/2$ , that is around the perihelion of the *reverse* motion arc. Around the perihelion, the first integral gives a total vanishing contribution, while the far dominant term is that one related to the transversal number. In addition, perihelion is not the point of maximum speed; in fact, maximum speed is achieved past the perihelion because of  $\varphi_e > 3\pi/2$ . Thus, sailcraft goes on accelerating for a long (asymmetric) arc of solar fly-by performed by reversing its initial motion. The sailcraft speed amplification may be high indeed, depending on the perihelion and lightness vector. It is an easy matter to show that the escape point ( $E=0$ ) is achieved *before* the perihelion. Many other properties of sailcraft trajectories can be inferred by studying trajectory curvature and torsion (Vulpetti, 1996, 1997). Among them, the pseudo-cruise branch is of concern here. It has the following properties: (a) it begins at few AU from the Sun, (b) it passes through the solar system with a small speed decrease, (c) although it is generally lower than  $V_{max}$ , however  $V_{cruise}$  can be significantly higher than  $V_0$ , the sailcraft injection speed (close to the mean Earth Orbital Speed, or EOS, that equals  $2\pi$  AU/yr). These considerations apply to 2D trajectories for which the normal lightness number is zero. This is an ideal case useful for reference mission:  $\varphi_e - \varphi_s = \pi$ . It is possible to prove (Vulpetti, 1999a) that a real 3D reversal trajectory must have both non-radial numbers *variable* at least in a time interval around the reversal time. Such variability is essential to guarantee the orbital frame to be *smooth* and to cause motion reversal. Here,  $H$  does vanish, but its magnitude exhibits a local minimum. In such trajectory class,  $\varphi(t)$  approaches  $\pi$  closely, then it reverses back to values less than  $\pi/2$ . One gets  $\varphi_e + \varphi_s = \pi$ ; when perturbations are active, such relationship is well approximated.

Equation IV-13 admits non-reverse motion solutions, plainly. As a simple good example, one could think of performing an attitude maneuver at some time (to be determined) in the  $[t_s, t^*]$  interval such that  $\lambda_t \rightarrow -\lambda_t$ , (the transversal number being high enough as above). Since  $H$  remains positive this case, the angle between position and velocity never achieves 180 degrees; thus, the second term in equation IV-13 is dominant and positive again for a long trajectory arc about the Sun. At, say, 1-2 AU another attitude maneuver adjusts the sail orientation in either the inertial or the orbital frame. The cruise speed for this class of direct motion and that related to the motion reversal may be quite comparable in realistic cases; they also depend on the departure planet position and velocity at the sailcraft injection time or epoch.

Both the direct and the reverse motion strategies share a basic rule: *if a sufficiently light sailcraft is planned to exit from the solar system with high speed, it has to lose most of its initial heliocentric energy (passing through a minimum) before accelerating fully.*

It is not difficult to show that the  $H$ -reversal class for sailcraft trajectories exhibits large launch windows, from several days to a few weeks, depending on the distant target coordinates. For targets well beyond Pluto, e.g. the heliopause or the solar gravitational lens, wide favorable injection into the solar field repeats on annual basis.

Thus, the motion reversal represents a full mission opportunity, which has the following additional features: confirming/extending the feasibility of a mission from a dynamical viewpoint, examining the critical role of the (external) optical degradation on unconventional sailcraft trajectories. Both points are among the main aims of this report.

### IV.3 Specifying Sailcraft Barycenter Motion: the Connection Equations

As emphasized above, each component of the lightness vector may act as a dynamical control variable. However, any real  $L$  stems from the actual physical interaction between the solar photons and the sail material and configuration. Such interaction generates a thrust in the sailcraft frame of reference. Thus, there is a link between the *direct* control variables/parameters of the sailcraft and  $L$ 's components. We call them *the connection equations*. Moreover, such equations contain geometrical/physical features of the source(s) of light

and environment-related effects. Here, we shall, very briefly, report sailcraft-related phenomena and source-related perturbations. Very extensive explanations of photon-metal interactions, both from physical and mathematical viewpoints, can be found in many excellent classical textbooks on optics. A sailing-oriented description of the solar radiation pressure can be read in (McInnes, 1999, chapter 2). Intrinsic and environment-induced changes of the ideal sail behavior will be mentioned in §IV.4.

In terms of radiant flux, 99 percent of the solar spectrum ranges from 1000 Å to 40,000 Å in wavelength that can affect space sailing. The light a sail receives can be specularly reflected, diffusely reflected, absorbed, transmitted. A good solar sail should exhibit vanishing transmittance<sup>2</sup>, low absorptance ( $a$ ), low diffuse reflectance ( $d$ ) and high specular reflectance ( $r$ ). Therefore,  $r + d + a = 1$ , a condition well achieved even by very thin Aluminium-Chromium films. For the moment, we only mention that such optical quantities are somehow averaged over the essential solar spectrum. We shall return on that below. In general, the local solar radiant flux impinges onto the sail surface at an angle  $\theta$  of incidence, as seen from the sailcraft. (If  $\alpha_n$  and  $\delta_n$  denote the azimuth and elevation in EHO, respectively, of the sail axis  $\mathbf{n}$ , oriented *backward* with respect to the reflective sail side, then one has  $\cos\theta = \cos\alpha_n \cos\delta_n$  strictly only if the vehicle speed is zero). Specularly reflected light generates (main) momentum along  $\mathbf{n}$ , while absorption causes a momentum along the incident radiation direction. The process of light diffusion by the sail's front side induces two additional momenta on the sail: the first one acts along the incident direction, the second one is along  $\mathbf{n}$  and is proportional to the surface coefficient, say,  $\chi_f$  (for an ideal Lambertian surface  $\chi = 2/3$ ) and the  $d$ -value (which, in turn, depends on the sail roughness). The energy absorbed by the sail materials is re-emitted from front-side and backside according to their respective emissivities,  $\epsilon_f$  and  $\epsilon_b$ . We suppose that each sail side behaves as a uniformly diffuse gray surface. Emissivity is only function of the sail temperature: the sail thickness is so small that one can use the same temperature  $T_S$  across the sail film. This value follows from the equality between absorbed power and emitted power in vacuum at any distance  $R$  from the Sun. By neglecting the cosmic background radiation temperature, the absorption-induced thermal effect consists of a net momentum along the normal-to-sail direction proportional to the following factor

$$\kappa = \frac{\chi_f \epsilon_f(T_S) - \chi_b \epsilon_b(T_S)}{\epsilon_f(T_S) + \epsilon_b(T_S)} \quad (\text{IV-14})$$

(In equation IV-14, we have highlighted the dependence on sail temperature). The sail of a fast sailcraft should be composed of a high-reflective layer and a high-emissivity coating. As a result, the function  $\kappa$  is negative for Aluminum-Chromium sails; in other words, there is a thrust acceleration, along  $-\mathbf{n}$ , stronger as absorptance and temperature increase. Even this component of the total thrust is not negligible, especially around the perihelion and for a degraded sail.

The above picture of sail-photon interaction is rather simplified. In addition to detailed aspects of this interaction, a more general treatment should include other meaningful items. These ones are photon aberration, features of the light source, curved sail, and optical degradation, in the order, according to the progressive removal of some underlying assumptions such as:

- A1. direction of incident light along to the X-axis of the sailcraft frame
- A2. point-like Sun
- A3. flat sail
- A4. ideal optics.

We have mentioned that physics in the spacecraft orbital frame does not coincide with that of the heliocentric orbital frame. By neglecting 2<sup>nd</sup>-order and higher terms in the vehicle speed, it is possible to carry out the following connection equations

---

<sup>IV-2</sup> We use optical terms ending in 'ance' since they apply to real specimens regardless of their geometric thickness and physical surface state. Terms ending in 'ivity' are normally used to highlight optically smooth specimens.

$$\mathbf{L} = \lambda_0 n_x \left\{ \left[ (2r n_x + \chi_f d + \kappa a)(1 - 2\beta_x) - 2r n_y \beta_y \right] \mathbf{n} + (a + d) \begin{bmatrix} 1 - 2\beta_x \\ -\beta_y \\ 0 \end{bmatrix} \right\} \quad (\text{IV-15})$$

In equation IV-15, we have set

$$\boldsymbol{\beta} \equiv \frac{V}{C} \begin{bmatrix} \cos \varphi \\ \sin \varphi \\ 0 \end{bmatrix} \equiv \begin{bmatrix} \beta_x \\ \beta_y \\ 0 \end{bmatrix}, \quad \varphi \equiv \text{angle}(\mathbf{R}, \mathbf{V}), \quad V \equiv |\mathbf{V}|, \quad \lambda_0 \equiv \frac{\sigma_c}{\sigma}, \quad \sigma \equiv \frac{m}{S}$$

$$\sigma_c \equiv 2 \frac{W_{1AU}}{g_{1AU} C} = 0.001538 \text{ kg } m^{-2}, \quad W_{1AU} = 1367 \text{ W } m^{-2}, \quad g_{1AU} = 0.00593 \text{ m } s^{-2} \quad (\text{IV-16})$$

$$\text{with the sail direction in EHOFF given by } \mathbf{n} = \begin{bmatrix} \cos \alpha_n \cos \delta_n \\ \sin \alpha_n \cos \delta_n \\ \sin \delta_n \end{bmatrix} \equiv \begin{bmatrix} n_x \\ n_y \\ n_z \end{bmatrix}$$

where  $m$  is the (instantaneous) sailcraft mass,  $S$  denotes the sail area,  $C$  is the speed of light.  $\sigma$  is the total vehicle mass divided by the sail area and is usually named *the sailcraft sail loading*. The quantity denoted by  $\sigma_c$  is the so-called critical density. Vector  $\boldsymbol{\beta}$  accounts for photon aberration, which is linear in the sailcraft speed. The  $\kappa$  factor is given by equation IV-14. An important thing to be noted about vector equation IV-15 is that the various optical sail parameters are *weighted* by quantities of significantly different physical nature. Each optical parameter appears in two independent terms.

Ideally, by a perfectly reflecting planar sail at rest in HIF and orthogonal to the vector position, one would get  $\mathbf{L}_{ideal} = [1 \ 0 \ 0]^T \sigma_c / \sigma$  with the maximum allowed thrust, or equivalently, with a thrust efficiency equal to 1. Thus, in general, sailcraft thrust efficiency can be defined as the actual-on-ideal thrust ratio at any time. It is related to the sailcraft sail loading by the following relationship:

$$\tau = \lambda \sigma / \sigma_c \quad (\text{IV-17})$$

When the sailcraft sail loading equals the critical density,  $\lambda < 1$  since thrust efficiency is less than unity in any real case.

We have removed assumption A1 in carrying out equations IV-15, which hold for a point-like Sun. If sailcraft comes sufficiently close to the Sun, say, at  $R \approx 15 R_\odot$  ( $1 \text{ AU} \approx 214.94 R_\odot$ ), then it begins by sensing the finite size *and* the limb darkening of the photosphere. They ultimately cause a reduction of the thrust on sail; the nearer the spacecraft is the weaker the thrust is (standing the same sail orientation, distance and speed) with respect to the point-like Sun thrust. Thus, by removing assumption A2 and using the standard gray-atmosphere model, it is possible to carry out exact formulas for an *arbitrarily* oriented sail (and in relativistic motion too). A modern symbolic-math system on computer is appropriate for achieving this goal. Closed-form solutions are very long. However, we like to report simple classical-dynamics formulas without any terms in vehicle velocity for isolating the mentioned effects on the sail. This results in the following modified connection equations:

$$\mathbf{L} = \lambda_0 \left( \left[ 2r u_1 + (\chi_f d + \kappa a) u_2 \right] \mathbf{n} + (a + d) \mathbf{w} \right) \quad (\text{IV-18})$$

In equations IV-18, we employed the following definitions:

$$\xi \equiv R/R_\odot \quad u_2 \equiv n_x \mathbf{w}^T \equiv -\frac{1}{192 \xi} (2 n_x k \quad n_y q \quad n_z q)$$

$$u_1 \equiv \left[ \begin{aligned} & 2(59 - 9n_x^2)\xi^2 - 64\xi\sqrt{\xi^2 - 1} + 2(3n_x^2 - 1)(9 + 16\sqrt{1 - 1/\xi^2}) + \\ & + 9[(n_x^2 - 3)\xi^3 + 2(n_x^2 + 1)\xi + (1 - 3n_x^2)/\xi] \ln \frac{\xi + 1}{\xi - 1} \end{aligned} \right] / 192$$

$$k \equiv 9(\xi^2 - 1)^2 \ln \frac{\xi + 1}{\xi - 1} + 32(\xi^2 - 1)^{3/2} - 2(25\xi^2 + 9)\xi$$

$$q \equiv 9(3\xi^4 - 2\xi^2 - 1) \ln \frac{\xi + 1}{\xi - 1} + 32(2\xi^2 + 1)\sqrt{\xi^2 - 1} - 2(59\xi^2 - 9)\xi$$

Obviously, even though sunlight distribution has a cylindrical symmetry in this model, a non-radially oriented sail destroys this symmetry in generating thrust. If the sailcraft moves at a distance  $\xi \gg 1$ , the actual-Sun lightness vector approaches that one from the point-like Sun, as described by equation IV-15 with zero speed. (The general formulas are coincident in the limit of  $\xi \rightarrow \infty$  for any sail orientation and velocity, of course). We close this topic here with mentioning a few values for the pure radial case: at  $\xi = 4$  (that is at 3 solar radii from photosphere), a correction factor equal to 0.9858 should be applied to the point-like model, whereas at  $\xi = 21.49$  (0.1 AU), the correction factor would amount to 0.99951. Finally, at 0.2 AU, deviation would result in -0.00012, namely, about  $1/4$  of the photon aberration for a sailcraft traveling at such distance with 15 AU/yr.

Now, let us remove the assumption A3 to have a flat sail. Currently envisaged sails may be grouped into two large classes: (I) plastic substrate sails, (II) all metal sails. A representative of class-I is a three-layer sail consisting of a plastic layer of a few microns thick on which thin reflective and emissive films may be deposited (one film per side, typically). Such a sail may be suitable for (many) interplanetary transfers. Class-II regards bilayer sail configuration consisting of reflective and emissive films alone. Since sailcraft of class-II has a sail loading considerably lower than class-I, it would be appropriate for high-speed missions. Photon pressure on a large surface induces a large-scale curvature that, in turn, causes pressure redistribution and thrust decrease. In class-I, curvature increases when sail temperature increases. Depending on the supporting structure, large-stress values can result in small-scale folds in the sail materials known as the wrinkles. One deems that wrinkles may interact with large-scale curvature by producing hot spots. During the AURORA Collaboration (January 1994 – December 2000), a few promising experiments (Scaglione, 1999) were performed for getting a light sail for the AURORA concepts of mission to either the heliopause or the solar gravitational lens. The sail would be manufactured in the following multi-layer mode: Aluminum-Chromium-buffer-UVTplastic, where the buffer layer consists of diamond-like carbon (DLC)<sup>3</sup>. UVTplastic stands for plastic substrate transparent to the solar UV photons. Once deployed in a high orbit about Earth, solar UV light reaches the DLC buffer and weakens its chemical bonds at the interfaces such that it and the plastic film soon detach from the Al-Cr layers. Closely related to techniques for achieving metallic sails without infrastructures in orbit, are the deployment and the sail-keeping methods. The AURORA collaboration studied a circular Al-Cr sail to be deployed in orbit by a small sail-rim-located torus. This is a hydrostatic beam-based deployment system with load-supporting web (Genta *et al.*, 1999); deployment is effected by inserting gas into this peripheral ring. The sail shall take a pillow-like shape, symmetric with respect to the sail axis, with a maximum axial shift depending on the Sun-sailcraft distance (and sail orientation). For instance, a circular sail of 300-m radius exhibits maximum slope of 4.4 degrees at a perihelion as low as 0.15 AU (or, equivalently, a sunward shift of 14 m). Large-scale curvature radius takes on 3.3 km, by entailing a thrust reduction factor of about 0.998 (with respect to the ideal case of flat sail). These figures would hold only around such perihelion distance. Although some differential equations used for this sail deformation analysis are simplified, nevertheless there is a strong indication that the whole flight of smaller-sail AURORA-type spacecraft, designed for higher perihelion ( $R_p \geq 0.2 AU$ ), is compliant with the assumption of a large-scale flat sail. This statement is of great concern with regard to ISP, here.

Finally, we shall remove the assumption A4 regarding *ideal* optics for a sail. Since this is a special topic with strong consequences on dynamics, we shall devote next section to it. However, before proceeding, we have to be

<sup>IV-3</sup> DLC is a metastable disordered solid that shows a mix of diamond and graphite structures.

more precise about the meaning of the optical parameters entering the connection equations. The set  $\{r, d, a\}$  represents the fractions of the incident photons that are specularly reflected, diffusely reflected and absorbed, respectively. Although they are not defined as one usually does in Optics, nevertheless they can be related to the strict optical quantities known as the bi-directional spectral reflectance  $\rho_{spec}(\mathcal{L}, \theta, \{p\})$ , the directional hemispherical spectral reflectance  $\rho_{diff}(\mathcal{L}, \theta, \{p\})$  and the directional spectral absorptance  $\alpha(\mathcal{L}, \theta)$ . (The reader may consult some standard handbook such as the *Handbook of Optics* by Optical Society of America, 2001, <http://www.osa.org>). Here,  $\mathcal{L}$  denotes the wavelength of the incident light, whereas  $\{p\}$  emphasizes parameters characteristic of the reflective sail layer. The above reflectance terms are averaged over all possible orientations of the incident electric field. Note that easy measurable quantities are the total spectral reflected light, giving  $\rho(\mathcal{L}, \theta, \{p\})$ , and the scattered light (via laser, for example). It is possible to show (Vulpetti, 1999b) that the parameters entering the sailcraft motion equations (through the connection equations) have the following meaning

$$\begin{aligned}
\mathcal{J} &\equiv \int_{\mathcal{L}_{min}}^{\mathcal{L}_{max}} \mathcal{U}(\mathcal{L}) d\mathcal{L} \\
r &= \rho_{spec}(\theta, \{p\}) = \frac{1}{\mathcal{J}} \int_{\mathcal{L}_{min}}^{\mathcal{L}_{max}} \rho_{spec}(\mathcal{L}, \theta, \{p\}) \mathcal{U}(\mathcal{L}) d\mathcal{L} \\
d &= \rho_{diff}(\theta, \{p\}) = \frac{1}{\mathcal{J}} \int_{\mathcal{L}_{min}}^{\mathcal{L}_{max}} \rho(\mathcal{L}, \theta, \{p\}) \mathcal{U}(\mathcal{L}) d\mathcal{L} - r \\
a &= 1 - (r + d)
\end{aligned} \tag{IV-19}$$

In the above equations,  $\mathcal{U}(\mathcal{L})$  denotes the spectral radiant exitance of the Sun, which may be assumed as blackbody source with 5777 K, (corresponding to the solar constant value of  $1367 \text{ W/m}^2$ , §IV.5.4). Wavelength could range from  $1,000 \text{ \AA}$  to  $40,000 \text{ \AA}$  for a number of physical reasons. For a given sail material and film deposition method, entries in the thrust parameter set  $\{r, d, a\}$  depend only on the photon incidence angle, though, in some case, some parameter may exhibit a quasi-independence on this angle. Anyway, they are assumed to *not* change with time. That is what we mean by *ideal optics* here. Actually, any  $d > 0$  entails a sort of *intrinsic* degradation in terms of thrust because of the different coefficients that the specular and diffuse terms have in the connection equations. One needs a device separating these contributions to the total reflectance. Particularly appropriate to the solar sailing thrust modeling is the Scalar Scattering Theory (SST), where the main parameter is the root mean square roughness of the reflective layer, hereafter denoted by  $\delta$ . It is closely related to the sail making process that causes irregularities in the deposited Aluminum film, for instance. The underlying assumptions of SST are discussed in (Vulpetti, 1999b) relatively to space sailing. Here, we limit to report the simple equation between total and diffuse reflectance:

$$\rho_{diff}(\mathcal{L}, \theta, \delta) = \rho(\mathcal{L}, \theta) \left[ 1 - e^{-\left(4\pi \frac{\cos \theta \delta}{\mathcal{L}}\right)^2} \right] \tag{IV-20}$$

Total spectral reflectance does not depend on  $\delta$ ; however, light scattering causes specular and diffuse components to be distributed differently. Equation IV-20 shows that diffuse reflectance augments non-linearly with roughness. Strange enough at first glance,  $\rho_{diff}$  achieves its maximum value at normal incidence  $\theta = 0$ . Depending on the actual sail, consequences to sailcraft dynamics could be significant, through equation IV-15.

#### IV.4 External Optical Degradation

Space is known to be a very complex environment that behaves very differently, even as seen from different artifacts and with respect their goals. In addition to classical design items (spacecraft thermal control, spacecraft system & sub-system protection, payload degradation and so forth), modern objectives regard tests on inflatable structures too (Stuckey *et al.*, 2000). These systems can include different structural elements that have to be capable of tolerating space environment for the time necessary to allow the payload mission. From this point of view, any sail system is a special deployable system. Apart from some simple Russian tests in orbit, a full

preliminary experimental mission sailcraft has yet to be flown (August 2001). There are only very scarce experimental data specifically oriented to solar sailing hitherto. We shall use part of them for exploring consequences on fast sailcraft trajectory such as the ISP's. To this aim, we have to build some model that accounts for the environment a deep-space sailcraft sail is able to sense. Since our interest is in all-metal sails, as explained above, we may focus on two major causes that could induce a decrease of the sail performance, that is a modification of the ideal-optics conditions as stated in §IV.3. These causes are the solar ultraviolet photons and the solar wind particles that will continuously impinge on a space sail. In this current investigation for NASA, it has been agreed that, considering the very limited amount of experimental data, only effects stemming from solar wind should be considered. Nevertheless, we present calculations that should hold even in a next research phase about the influence of the solar UV flux on the mission design of a *fast* sailcraft, namely a sailcraft flying-by the Sun at low perihelion. By using the concepts of exitance, radiance and irradiance from classical optics, it is a simple matter to carry out the integrated flux of UV photons onto a sail of a sailcraft in the time interval  $[t_0, t]$ . One gets the energy *fluence*

$$\Psi_{UV} = f_{UV} W_{1AU} \int_{t_0}^t a(\theta) \frac{\cos(\theta)}{R^2} dt \quad (\text{IV-21})$$

Equation IV-21 holds for a sail having absorptance  $a$  and distance  $R$  from a point-like Sun. UV beam impinges on sail with an incidence angle  $\theta$  from the sail normal  $\mathbf{n}$ . (The relativistic energy shift, sensed in the sailcraft frame, has been neglected). Symbol  $f_{UV}$  represents the ultraviolet fraction of the solar constant; it may be easily estimated by the blackbody distribution at 5777 K. For instance,  $f_{UV} = 0.122$  over the 1,000-4,000 Å range, namely, 167 W/m<sup>2</sup> of UV flux at 1AU. An important thing to be noted in equation IV-21 is that the absorptance function is not exhaustively given by equations IV-19 as they hold for (time-independent) ideal optics. We shall return on this topic in § IV.4.1 since it regards the lightness vector computation.

As far as the energy deposited by the solar-wind particles on a moving sail, we make ~~some~~ simplifying assumptions here. They are: (i) solar wind flows radially from the Sun with a speed constant from  $\approx 20R_{\odot}$  to the termination shock, (ii) solar-wind number density scales as  $1/R^2$  everywhere in this range of distance, (iii) interplanetary magnetic field does not interact with sail. A few remarks about these points. Solar wind is an expanding momentum-dominated high-conductivity super-alfvénic (pseudo) supersonic collisionless plasma for which a continuum description applies. Very schematically, it may be viewed at large as composed of *quiet* background plasma of low speed, on which non-radial *fast streams* of essentially electrons and protons overlap almost periodically. Solar-wind speed changes with the helio-magnetic latitude and reaches a minimum close the interplanetary current sheet. Our assumption (i) is somewhat elementary, but it has the great advantage to make calculations affordable in the context of this report. In contrast, assumptions (ii) and (iii) appear rather realistic also on considering that here one is interested in fast sailcraft receding from the Sun. Thus, in the sailcraft frame of reference, the (differential) flux of proton energy arriving at the sail during the time  $dt$  is given by

$$\frac{d}{dt} \Psi_{SW} = \frac{v_{1AU} m_p (W^2 - 2WV \cos \varphi + V^2)}{2R^2} \left( \begin{bmatrix} W - V \cos \varphi \\ -V \sin \varphi \\ 0 \end{bmatrix} \cdot \mathbf{n} \right) \quad (\text{IV-22})$$

In equation IV-22,  $W$  is the solar-wind speed in heliocentric frame,  $m_p$  denotes the proton mass and  $v_{1AU}$  represents the (mean) proton number density at 1 AU. The energy per unit area absorbed by the sail in the time interval  $[t_0, t]$  can then be written down as

$$\Psi_{SW}(t) = \int_{t_0}^t (1 - y_p \epsilon_p) \left( \frac{d\Psi_{SW}}{dt} \right) dt \quad (\text{IV-23})$$

In IV-23,  $y_p$  and  $\epsilon_p$  denote the proton backscattering yield and the proton backscattering energy fraction, respectively. Actually, computation of IV-23 is a long iterative process, which may be simplified by estimating the proton backscattering properties in the energy range related to the sail and sailcraft under consideration. By using a sophisticated Monte Carlo code, such as SRIM 2000 (Ziegler, 2001), it is possible to study the

interaction of protons and Aluminum. We have focused attention on a number of fast sails and missions; for instance, *fast-stream* proton energy, as sensed by the sailcraft, ranges from 1.8 to 3.4 keV. A radial-in-EHOF 200-nm sail, moving at 15 AU/yr, is characterized by a backscattering yield equal to 0.039 and a backscattering energy fraction of 0.205; therefore, 99.2 percent of the solar-wind proton energy flux is deposited on the sail (in a max depth equal to 110 nm). On the other side, a 130-nm 22-AU/yr sail at perihelion absorbs 97.8 percent of the proton energy flux (in 115 nm). Along a trajectory, sailcraft experiences differential proton energy flux, which changes as sail orientation and sailcraft position & velocity evolve.

Energy from UV photons and solar-wind protons, absorbed by the reflective sail material through a very short thickness, alters reflectance and absorptance *permanently*. Mathematically, the independent variable is the energy fluence, of which equations IV-21 and IV-23 represent our present evaluation. Here, we adopt the following model of optical-parameters change

$$\begin{aligned} \delta a &\equiv a_{actual} - a_{ideal} = A(\Psi) \\ (r_{ideal} + d_{ideal})(1 - \zeta) + a_{ideal} + \delta a &= 1 \\ \Rightarrow \\ r_{actual} &= (1 - \zeta) r_{ideal} , \quad d_{actual} = (1 - \zeta) d_{ideal} \end{aligned} \tag{IV-24}$$

This model entails that we should have some experimental data about absorptance change, namely, the function  $A$  of fluence at time  $t$ , from which we could calculate the alteration in reflectance (since we know how to calculate the ideal or reference optics discussed in §IV.3). The second equation in IV-24 assumes that the relative changes of both specular and diffuse reflectance are equal to one another. Thus, immediately we get

$$\zeta = A(\Psi) / (r_{ideal} + d_{ideal}) \tag{IV-25}$$

Equations IV-24 have been written to having changes as positive quantities. Finally, though sail material emissivity does not change as a temperature function, however its actual range is shifted according to the absorptance change. Thus, all thermo-optical sail parameters entering the sailcraft motion equations are modified by the UV field and solar plasma that the sail gradually experiences.

On a conceptual basis, one can note that when surface roughness (an internal degradation) is introduced, part of the specular reflectance turns into diffuse reflectance. In contrast, when external degradation is considered, part of the total reflectance turns into absorptance.

#### 4.1 Integro-Differential Equations of Sailcraft Motion

Despite the simplicity of the above particular model, the mathematical problem that stems from any optical degradation model consists of parameters depending on some quantity that is, at any time  $t > 0$ , function of the *previous* history of the sailcraft trajectory. The optical parameters, modified through the energy fluence that depends on the sailcraft state evolution in  $[t_0, t]$ , determine the *actual* lightness vector at time  $t$  that affects the sailcraft motion during the interval  $(t, t + dt]$ . Equations IV-2, IV-15 (or IV-18), IV-24 and IV-25 are coupled. As soon as the last three equations are substituted into IV-2, equations of sailcraft motion appear as a system of integro-differential equations (IDE). In other words, whereas the ideal optics for sail entails a system of ODE, the introduction of optical degradation requires the numerical integration of a system of IDE for computing the sailcraft motion.

In the computer code shortly described in §IV.5, we had to modify some of the routines of the numerical integrators used for ODE in order to deal with the problem of optical degradation (even though model IV-24 is formally simple). In §IV.6, we shall show that some sailcraft trajectories are significantly affected by a progressive change of the thermo-optical sail parameters.

## 4.2 Experimental Data Fitting

What remains to do here is to discuss the determination of the function  $A(\Psi)$ . We began with the experimental data reported in (Wertz *et al.*, 2000), but we proceeded with using a different fitting procedure in order to be compliant with our present optical model. As of September 2001, the paper by Wertz was the only one, on this matter, supplied by NASA/MSFC to the author of this chapter. In addition, some of the public space literature on the UV-photon-induced degradation either regards organic materials or has contradictory results about thin metal films. In such literature, topics are not oriented specifically to solar sailing materials. Thus, in using data from Wertz paper, we had to assume that electron-dose damage may be similar to solar-wind proton's. No reliable data about UV-induced damage of Al-Cr films have been found by the author at the writing time. Nevertheless, the theoretical model described in this section and some consequences reported in §IV.6 may be of considerable importance for solar sailing in general, even though we deal with only one of the pieces to the actual change of the thermo-optical sail parameters. With this in mind, we proceeded to the computation of the  $A$ -function into two steps. *First*, we fitted the experimental data of absorptance as function of the (electron) dose by considering that (1) if dose is very low, then the actual absorptance practically coincides with the ideal one, (2) if dose is very high, then the material is completely degraded, in practice  $a_{actual} \rightarrow 1$ . This has carried out the following fit

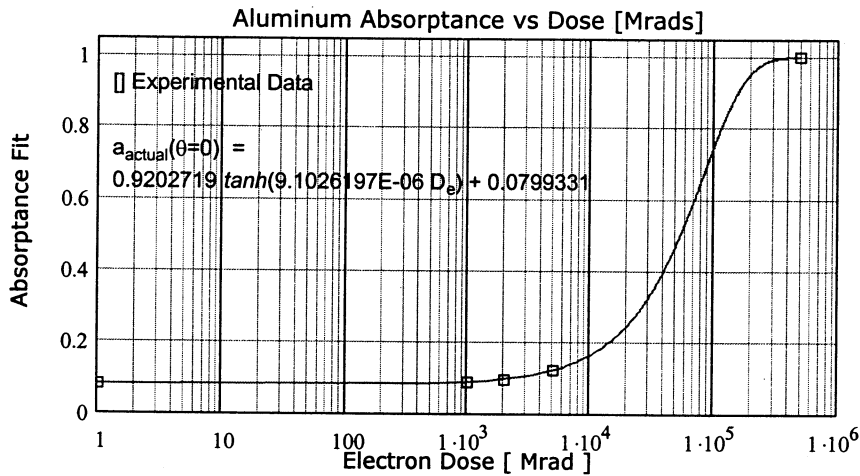


Figure IV.4-1

In the above plot,  $D_e$  denotes the electron dose expressed in Mrads (1 Mrad =  $10^4$  Gy). Experimental data regarded beams incident orthogonally to the specimen surface. This fit produces absorptance residuals of zero mean ( $<1E-14$ ) and standard deviation equal to 0.00085.

The *second* step consisted of transforming dose into energy fluence by utilizing the specimen materials, their geometrical configuration (Wertz, 2000) and noting that  $a_{ideal}(\theta=0) = 0.0720$  (independently of roughness) for Aluminum. That has resulted into the following absorptance change law

$$A(\Psi) = 0.92027 \tanh(0.25215 \Psi_{sw}) + 0.00793 \quad (IV-26)$$

In IV-26, the energy fluence is expressed in  $\text{MJ/m}^2$ . The last term in equation (IV-26) represents the difference between the experiment control value, taken at (small) non-zero fluence, and the ideal absorptance value given above. It has been retained as a small conservative bias; for a real mission, some bias will probably happen due to the non-negligible time between sail making (on ground) and sail deployment (in space).

## IV.5 A Computer Code

The numerical cases of trajectory optimization presented extensively in §IV.6 have been computed by using a computer code named Starship/Spaceship Mission Analysis Code (SMAC). The author has implemented SMAC on PC in the 1986-2001 timeframe.

### 5.1 General Description

SMAC has been designed and is maintained for computing spacecraft trajectories related to propulsion modes such as nuclear/solar electric propulsion, antimatter propulsion, space ramjet, laser/microwave sailing, solar sailing, plasma-driven sailing and any physically-admissible combination two-three modes. Obviously, some combinations of modes are hard to be realized in practice; they are useful for evaluation analysis and/or performance limit. User can perform trajectory computation in either classical or (full) relativistic dynamics. (SMAC was used by the author in his research on interstellar flight in the 1988-90 timeframe and during the AURORA Collaboration mentioned in §IV.3). SMAC is now in full Fortran-90/95 and currently runs under MS-Windows 98-SE. User graphic interface (GUI) has been designed in MS-Visual Basic 5. SMAC includes a 3D graphic module for quick output visualization.

Current SMAC version (A.45.93a) consists of about 24,600 lines. Employed compiler is a commercial highly optimized compiler for Pentium-III.

Solar-sail mode is one of the most detailed propulsion modes in SMAC. The whole of the solar sailing theory described in the previous sections comes from as special case of a more general solar-sailing model embedded in a set of Fortran modules and procedures; these ones are designed to grow with the user needs.

With regard to the Interstellar Probe mission concept, Normalized Solar Units (NSU) have been used by setting  $GM_{SUN} = 1$  and Astronomical Unit (AU) = 1. Internal computations have been performed in full double precision according to IEEE 754.

### 5.2 Integrators

SMAC user can select different numerical integrators for different trajectory arcs, according to the propulsion types, star and planetary fields. The available methods for integrating ODE are:

- Adams-Bashforth-Moulton (variable stepsize, variable order)

- Bulirsch-Stoer (variable stepsize)

- Runge-Kutta-Shank (modified)

  - Fixed step

  - Automatic variable stepsize

  - User-defined variable stepsize

The above three methods are known to be based on quite different principles. They are useful also to compare high-precision integration of *difficult* mission profiles. Each integrator consists of Fortran procedures arranged into three nested levels: the *driver* routine, the *stepper* routine and the *algorithm* routine. The above integrators were originally implemented only for ODE in SMAC. Subsequently we have modified the drivers for also dealing with the integro-differential equations system stemming from the optical degradation problem.

### 5.3 Optimizers

The user can use SMAC in either propagation-mode or optimization-mode. Trajectories can be optimized in the Non-Linear Programming (NLP) sense; the analyst can minimize one objective function chosen out of five criteria. Optimization may be constrained on either control or state, or both. Additional linear/non-linear constraints, relevant to special propulsion modes (e.g. the solar sailing) are dealt with. Very shortly, a trajectory can be segmented into a number of arcs each of which is characterized by its own propulsion mode (one or more depending on the research purposes), star field, planetary perturbation(s), attitude control parameters, state/control constraints and so on. Through the GUI, the analyst can choose which controls are to be optimized arc-by-arc, including launch date and/or part of the initial spacecraft state relatively to either the departure star or the departure planet. Similarly, the final spacecraft state (at target) can be partially left open.

SMAC knows two *robust* optimization algorithms: the Marquardt method revised by Levenberg-Marquardt-Morrison (or the LMM algorithm), the Levenberg-Marquardt method improved by Moré (Argonne Lab., 1980)

or the LME algorithm. The original implementation of LME was in FORTRAN-IV; it was ported to Fortran-90 by Vulpetti in the Nineties. Its current version in SMAC is either standard or interactive. Due to the different minimum-search policies of the two methods, the analyst may utilize both algorithms for solving problems exhibiting many local minima that differ slightly in value or by small amounts of the (optimized) control parameters, or both.

#### 5.4 Constants and Standard Files

In addition to what explained in § IV.2.1, the following constants have been used in the present investigation by this computer code:

Solar Gravitational Constant	1.327124400180E+20 m <sup>3</sup> /s <sup>2</sup>
Astronomical Unit	1.495978706910E+11 m
Unit Mass	the spacecraft initial mass [kg]
Solar Constant	1367 W/m <sup>2</sup>
1 AU/standard year	4.740470 km/s
Solar radius	6.961E+05 km

Basic physical constants have been taken from Particle Data Group (2000) available from CERN, LBNL and at <http://pdg.lbl.gov>. File DE403/LE403 from Jet Propulsion Laboratory (JPL) has been used for planetary ephemerides. With regard to the assumed value for the solar constant, it is an excess-rounded (by about 0.7 W/m<sup>2</sup>) average of the daily-means of the total solar irradiance (that is time-variable) measured by satellite throughout the year 2000. For details, visit the site <http://obsun.pmodwrc.ch>. We have considered such value in this mission analysis of the Interstellar Probe, for a presumable launch in 2010/2011, namely, about one solar cycle from now. Some care about it should be used, in general. Sometimes, one might adopt a round value (1.4 kW/m<sup>2</sup>) in rapid computation of solar sail trajectories. This entails higher lightness numbers that, in turn, could induce some non-negligible shift of some key quantity (e.g. the perihelion distance). The result may be a non-linear (generally optimistic) change of the trajectory performance index.

### IV.6 The Case for Interstellar Probe

We shall study ISP mission opportunities involving sailcraft motion reversal. They might be added to the mission profiles already analyzed by JPL (Mewaldt *et al.*, 2000). We deal with trajectories from sailcraft injection into the solar gravitational field to the target distance of 200 AU in the heliopause nose direction.

#### 6.1 Investigation Line and Problem Statement

In its most general form, the lightness vector depends on variables and parameters of different physical origin that one may group as follows: (a) source-of-light parameters, (b) physical/geometrical sail parameters, (c) sailcraft state variables (mass, position, velocity), (d) environmental parameters, and the time elapsed since deployment. In particular,  $L$  is proportional to  $\sigma_c/\sigma$ ;  $\sigma$  is a (technological) control parameter. We shall analyze aspects of the ISP mission concept through different values of the sailcraft sail loading that, in turn, is strongly related to the whole sailcraft technology, including the scientific payload. For each value of  $\sigma$ , typically we first discuss one (optimized) trajectory opportunity with ideal sail optics and, then, the *corresponding* opportunity with optical sail degradation. For the case  $\sigma = 2 \text{ g/m}^2$ , more than one ideal-optics profiles will be presented. The meaning of the term “corresponding” used above is the following: once the ideal-optics trajectory has been optimized (in the sense described below), one switches from ODE to IDE by considering optical sail degradation; then, optimization is performed by inserting the ideal-optics optimal controls as the guessed or starting control set. In the next sub-sections, we will discuss six profiles by  $\sigma$  ranging from 2.2 to 1 g/m<sup>2</sup>.

We computed admissible ranges of geocentric vector position and velocity (or the hyperbolic state) of a sailcraft in the fuzzy boundaries of the Earth-Moon-Sun system. We considered some of the current launchers capable to deliver a spacecraft of (at least) 200-350 kg with hyperbolic excess up to 1 km/s. Significantly higher values of the hyperbolic excess are excluded here, simply because both direct and reverse motion modes have to obey the

basic rule stated in §IV.2.3. (Obviously, launcher is a primary constraint; however, indicating any specific launcher is not a item of this report). The hyperbolic sailcraft state is added to the Earth state at the injection time, or the mission epoch, of the sailcraft into the solar field. We assume that, at such JD value, sail deployment & attitude acquisition and any other preliminary operations have been completed. The whole sailcraft trajectory is here segmented in five parts: four sailing thrusting arcs (or T-arc) plus one coasting arc (or C-arc) from sail jettisoning to target. The first three T-arcs entail a three-axis stabilized attitude control, whereas sailcraft is spun in the fourth one. (Why sail is not jettisoned at few AU past the perihelion has been explained in Chapter-III of this report). In order to simplify the ISP  $H$ -maneuver, we have considered the following trajectory control parameters:

- (1) Epoch ( $t_0$ )
- (2) Direction of the geocentric hyperbolic position (resolved in HIF) at  $t_0$
- (3) Geocentric hyperbolic excess
- (4) 1<sup>st</sup> T-arc duration and sail direction *constant* in EHO $\Phi$  (IV-27)
- (5) 2<sup>nd</sup> T-arc duration and sail direction *constant* in HIF
- (6) 3<sup>rd</sup> T-arc duration and sail direction *constant* in EHO $\Phi$
- (7) 4<sup>th</sup> T-arc duration and sail direction *constant* in HIF
- (8) 1<sup>st</sup> C-arc duration

Control sets 4-5-6 represent a simple realization of the 3D  $H$ -reversal motion detailed in (Vulpetti, 1999a). In addition, we have set the following constraints:

$$\begin{aligned}
 \min(H) &> 0 \\
 \min(R) &\geq 0.2 \text{ AU} \\
 \max(T_s) &< 600 \text{ K} \\
 t_f - t_0 &\leq 18 \text{ yr}
 \end{aligned}
 \tag{IV-28}$$

The following endpoint conditions have been applied

$$\begin{aligned}
 |\mathbf{R}(t_0) - \mathbf{R}_{Earth}(t_0)| &= 0.01776 \text{ AU} \\
 R(t_f) &= 200 \text{ AU} \\
 \Lambda(t_f) &= 254.5^\circ \quad \Theta(t_f) = 7.5^\circ
 \end{aligned}
 \tag{IV-29}$$

We chose the flight time upper limit in IV-28 such that, combined with the optimized coasting speed, the whole ISP mission, with a *potential* prolongation from 200 AU to 400 AU (Liewer *et al.*, 2000), may last less than a typical human job time (HJT) or 35 yr. However, the sailcraft distance baseline was fixed at 200 AU. The third row of IV-29 represents the ecliptic longitude-latitude coordinates of the sailcraft target position. The other endpoint values have been left free and optimized according to NLP. The index of performance, here, is the sailcraft speed at 200 AU. Thus, the current problem of astrodynamics can then be stated as follows:

*Given either the previous ODE or IDE system, describing the motion of a sailcraft in the solar system, with vector state  $\mathbf{S} \equiv [m \quad \mathbf{R} \quad \mathbf{V}]^T$  driven from  $\mathbf{S}_0$  to  $\mathbf{S}_f$  (partially-fixed states) by the control  $\{U\}$  (defined in IV-27), find the special set  $\{U^{opt}\}$  that maximizes the sailcraft speed at  $t_f$  while satisfying the linear and non-linear constraints IV-28.* IV-30

As far as the planetary perturbations are concerned, we considered both inner and outer planets; eventual planetary swing(s)-by of the sailcraft is(are) computed during the trajectory optimization process. When in the solar field, gravitational perturbation from the Earth-Moon system to the sailcraft is modeled as stemming from their barycenter.

## 6.2 Arrangement of the Results

In the following subsections, we discuss the numerical results of the problem stated in §IV.6.1. For each case and for each optimization, we have arranged the main results in six-Figure tables (on a one-per-page basis), which are grouped sequentially in §IV.6.11. Each table contains an header reporting the values of the quantities by which we made mission profiles distinct. They are: sailcraft sail loading (input), root mean square roughness (input), optical sail degradation switch (input), actual sailcraft perihelion (output). Each Figure in a set is labeled by both paragraph (of discussion) and progressive number. Figures 1-2 regard the projection of the sailcraft trajectory onto the ecliptic, or the XY plane, and the YZ plane. The orbits of the first four planets are also shown in the two plot windows. Figure 3 shows the evolution of the  $H$ -invariant. On the left side of the  $H$  minimum, the sailcraft motion is direct, whereas on the right side it is reversed. The ensuing sailcraft cruise phase “saturates” the invariant. This behavior, which looks like a sort of “square root”, is quite general for the 3D  $H$ -reversal mode aimed at getting away from the solar system. Time at which the vector  $\mathbf{H}$  crosses the ecliptic plane is shown by a vertical segment in Fig.-3. Reversal time decreases with the sailcraft sail loading. Figure 4 is the plot of the time-history of the lightness vector components (in EHO). Motion reversal line is shown again. Controlling the first three T-arcs entails  $L(t)$  continuous, whereas the optimal spin-stabilized T-arc requires an attitude maneuver. After such a maneuver, *supercritical* sailcraft results in a quasi-radial lightness vector. In contrast, *sub-critical* sailcraft shows high non-radial numbers: the transversal number increases energy while the normal number steers to the target direction. During the spin phase, the radial number is close to unity or higher, so counterbalancing or overcoming the solar gravitational acceleration. Sailcraft speed and orbital energy are graphed in Figure 5. There, the perihelion time (vertical) line is added to show that maxima of speed and energy take place past the perihelion, with the following distinction: *supercritical* sailcraft exhibits a local maximum of speed and an asymptotic maximum of energy, whereas *sub-critical* sailcraft evidences asymptotic maxima of both. With regard to Figure 6, we plotted the history of sail temperature for the ideal sail optics (i.e. switching degradation to off); when degradation=ON, we reported temperature, fluence and change of optical sail parameters altogether.

All Figures focus on suitable time windows that highlight the behaviour of functions. In discussing results, we limit ourselves to some points, whereas other considerations, which can be read out easily from Figures, are left to the reader.

Table IV.7-1 summarizes the main input and output values. We shall refer also to this table in discussing results.

Unless otherwise specified, the root mean square roughness has been fixed to 20 nm. This means that a roughness uncertainty from 3 standard deviations or 60 nm is reasonably compliant with the construction of a large surface with Aluminum-Chromium film nominally 200 nm thick.

Sailcraft sail loading will be given with two decimal digits. Units are grams per square meter. This means that, *in the range considered in the present analysis*, two mission profiles differing by less than  $0.01 \text{ g/m}^2$  in this technological quantity can be considered identical, in practice.

## 6.3 The $2.20 \text{ g/m}^2$ case

This case has been considered to show the difficulty of a sailcraft of  $2.2 \text{ g/m}^2$  to move as fast as the ISP mission concept would require.

Figures IV.6.3-[1-6] show the optimized profile for ideal optics. Radial, transversal and normal lightness numbers are such that motion reversal can take place. Orbital angular momentum decreases in magnitude and bends progressively until it lies on the ecliptic plane, 1.492 years after injection. At such a time, the transversal number vanishes and the normal number achieves its local positive maximum, according to the theory. Since this instant on, the transversal component of the lightness vector becomes positive whereas angular momentum bending continues as the normal number is still positive. As a result, sailcraft motion reverses while energy increases. Sailcraft moves toward the Sun with increasing speed not only because potential energy decreases but also since total energy augments significantly. It achieves the escape point ( $E=0$ ) and rapidly rises before the perihelion. Acceleration keeps on after the perihelion, but now the normal number goes to zero from the right side, while the sailcraft distance from the Sun rapidly increases because of the very high speed. All this means that angular momentum stops bending and the  $H$ -function evolves asymptotically. The subsequent attitude

maneuver for getting a spinning sailcraft completes both speed keeping and steering of sailcraft toward the target direction.

In the current framework, the above description applies qualitatively to any  $H$ -reversal evolution. However, as we decrease the sailcraft sail loading, we will find a corresponding progressive *shifting of values* (not of behavior) that is important in the ISP context.

In the present case, the direct motion arc – always characterized by the  $H$ -invariant decrease – is slow because the transversal number, responsible for the energy change, is not negative enough. Even the radial number is not sufficiently greater than  $1/2$  for allowing a high perihelion. Consequently, if one wants a cruise speed satisfying the mission flight-time constraint, then perihelion has to be low. Getting a cruise speed more than 14 AU/yr entails a non-negligible perihelion violation, namely,  $R_p=0.175$  AU here. Such a low perihelion may not be a problem, in general, for an advanced sailcraft. The true problem arises in the presence of optical degradation.

To figure out better, a sailcraft trajectory - satisfying active constraints - may be generally regarded as a sort of delicate compromise between conflicting key quantities such as hyperbolic state (with respect to the departure planet), time interval to perihelion, perihelion distance, sail temperature effects, range of lightness numbers, and so on. They “interact” to each other, of course. As pointed out, in the current case the lightness numbers are not so high to decelerate sailcraft fast enough. Thus, solar-wind energy fluence increases and induces a strong absorptance change. This one, in turn, increases sail temperature significantly. On the other side, if one decreased the hyperbolic excess at epoch, then a time-to-perihelion reduction could take place; nevertheless, since the *radial* lightness number does not depend on hyperbolic excess, one would have a further lowering of perihelion and an additional increase of the fluence on the sail. Thus, in getting a trajectory satisfying perihelion and temperature constraints, both baseline and extended-mission flight times exceed their limits, as reported in Table IV.7-1, as cruise speed falls down to 11 AU/yr. The present value of  $\sigma$  may be considered in a transition zone (relatively to the ISP mission concept) where *some* constraint, unavoidably, cannot be satisfied.

#### 6.4 The 2.10 g/m<sup>2</sup> case

As pointed out above,  $L$  depends on  $\sigma$  non-linearly. With respect to the previous case, a decrease of 4.5 percent in  $\sigma$  induces a change of 9.6 percent in the range of the optimal *transversal* lightness number of the direct-motion arc (ideal optics, Figures IV.6.4-[1-6]). This quantity is the major responsible for the change of key values with respect to those ones related to 2.20-g/m<sup>2</sup>. As a point of fact, even though the radial number varies by about 1 percent,  $H$ -reversal time and perihelion time are back shifted by 15.7 and 13.1 percent, respectively. Every constraint is satisfied; in particular, perihelion takes place at 0.204 AU. Note that the duration of the 2<sup>nd</sup> T-arc decreases from about 60 to 33.5 days. In this arc, the angular momentum bends and reverses by passing through a minimum in magnitude. The interval of such a T-arc is a non-linear function of the sailcraft sail loading. Its allocation after the 1<sup>st</sup> T-arc, where the sailcraft’s deceleration occurs, is a key factor for achieving the condition of motion reversal.

Optical degradation brings on perihelion rising of 0.044 AU with a delay of 84 days (or about 14.9 percent) with respect to the just-mentioned ideal-optics case. However, relatively to the 2.20 g/m<sup>2</sup> case, the “gain” in terms of mean distance and time in the pre-perihelion motion is such that fluence at perihelion decreases down to 0.57 MJ/m<sup>2</sup> or –3.4 percent. This is enough to not violate the temperature limit and get a good margin. Fluence saturation is achieved two years after injection, namely, one year (or 30 percent) in advance with respect to the 2.20-case. Trajectory profiles are shown in Figures IV.6.4-[7-12]. One has only a slight violation (0.1 yr) of the baseline flight time. Cruise speed amounts to 12.23 AU/yr.

In the current framework, the 2.10 g/m<sup>2</sup> case could be considered the lower bound of the above-mentioned transition from mission infeasibility to mission feasibility.

#### 6.5 The 2.00 g/m<sup>2</sup> case

The present  $\sigma$  value is very close to that considered for ISP in (Mewaldt and Liewer, 2000) and (Liewer *et al.*, 2000). We first present a number of trajectory profiles with different values of the root mean square roughness. Key values are collected in background-colored rows of Table IV.7-1.

In principle, the best case one may envisage is a sail with neither roughness nor degradation. Plots related to this special case of optimized trajectory are shown in Figures IV.6.5-[1-6]. Pre-perihelion trajectory is almost tangential to the Mars orbit. Motion reversal begins after 321 days (since injection) with  $H_{\min}=0.0226 \text{ AU}^2/\text{yr}$ . The sailcraft proceeds to perihelion, in about 76 days, with a speed of 16.78 AU/yr; maximum speed is as high as 17.79 AU/yr. However, since the max value (0.736) of the lightness number is less than unity even in this ideal case, speed has to decrease while sailcraft recedes from the Sun. Nevertheless, a cruise speed of 15.22 AU/yr is achievable by satisfying constraints widely. This results in baseline flight time of about 14.2 yr with additional 13 yr to accomplish the prolonged mission. In one HJT, sailcraft could reach 516 AU.

Figures IV.6.5-[7-12] show that this performance is decreased only slightly if the sail were made with a root mean square roughness equal to 10 nm. This is a direct consequence of the diffuse-reflectance law given by equation IV-20. The most visible differences are: earlier launch date (on October 7) by almost three days, the increase of the hyperbolic excess from 10 m/s to 70 m/s. Both compensate for the (low) reduction of transversal lightness number; thus, without remarkable changes in the other decision parameters, perihelion remains unchanged and cruise speed can be kept over 15 AU/yr. In one HJT, sailcraft could reach 509 AU.

There is still a good margin in accepting a sail made with higher roughness  $\delta$  and, at the same time, finding a perihelion very close to the value given in (Liewer *et al*, 2000). The set of plots for  $\delta=20 \text{ nm}$  and *ideal* optics are displayed in Figures IV.6.5-[13-18]. The pre-perihelion arc elongates beyond the Mars orbit,  $H$ -reversal delays by 61 days ( $H_{\min}=0.0115 \text{ AU}^2/\text{yr}$ ) and perihelion occurs at 0.24 AU. As a result, cruise speed decreases to 13.17 AU/yr. However, both baseline and extended mission flight times satisfy the related constraints (even though the extended mission lasts four years more). In one HJT, sailcraft could reach 443 AU.

This  $\delta=20$  ideal-optics solution is important since it is changed exiguously, injection date included, by the optical degradation (Figures IV.6.5-[19-24]). As a point of fact, the lightness numbers are still sufficiently high to ultimately keep fluence below  $0.55 \text{ MJ/m}^2$  around the perihelion. Thus, temperature constraint is not violated ( $T_{\max}=587 \text{ K}$ ). Fluence achieves saturation ( $0.7 \text{ MJ/m}^2$ ) in 1.7 yr. From Table IV.7-1, one can see that both time to and speed at 200 AU are such that 441 AU could be achieved in one HJT. In addition, the current cruise speed of 13.13 AU/yr compares well to  $V_{\infty}^p$  or 14.41 AU/yr, given by equation IV-6 (which does not include any degradation).

From what so far described, one should note that decreasing the sailcraft sail loading from 2.2 to 2.0  $\text{g/m}^2$  means moving from risk to feasibility, at least from the *nominal*-mission viewpoint.

## 6.6 The 1.80 $\text{g/m}^2$ case

In full degradation conditions, the value of 2.00  $\text{g/m}^2$  would cause a temperature violation if one attempted to use a perihelion even reduced by 0.011 AU. For instance, some sail control errors may force to flyby the Sun at a lower distance during the real flight. On the other hand, some meaningful perihelion decrease is necessary to increase the cruise speed. That may be accomplished by further reducing the sailcraft sail loading. In the ideal-optics mode, 1.80  $\text{g/m}^2$  would allow the sailcraft to flyby the Sun at  $R_p=0.20 \text{ AU}$  and to complete the extended mission in 26.2 years. One would get 538 AU in 1 JHT.

However, in the optical-degradation mode, perihelion cannot be lower than 0.22 AU. At this value, fluence takes on  $0.5 \text{ MJ/m}^2$  that induces 597 K of max sail temperature. Fluence saturates at  $0.64 \text{ MJ/m}^2$ , practically achieved in 1.1 yr. With this perihelion, cruise speed comes to 14.8 AU/yr; whence, baseline flight time amounts to about 14.4 yr and the extended mission lasts 27.9 yr. After a time equal to 1 HJT, sailcraft would achieve 505 AU. Plots of the current case are displayed in Figures IV.6.6-[1-12].

The main advantage stemming from making the ISP sailcraft with 1.8  $\text{g/m}^2$  instead of 2.0  $\text{g/m}^2$  would consist of flight error counterbalance through a set of admissible backup trajectories with respect to a nominal trajectory having  $0.22 \text{ AU} < R_p < 0.25 \text{ AU}$ , especially if the actual energy fluence were to result meaningfully different from the predicted one.

## 6.7 The Critical Case

As we know, the attribute *critical* refers normally to the equality between the sailcraft sail loading and that ideal value, which would allow a sailcraft to balance the solar gravity exactly. We mentioned in §IV.3 that such value pertains to a perfectly reflecting sail (at-rest in HIF) oriented radially and receiving light from the point-like Sun. However, any real sailcraft at criticality, i.e. with  $\sigma = \sigma_c$ , would exhibit a maximum value of the lightness number lower than unity at any time, as its thrust efficiency is certainly less than unity throughout the flight. Besides, the max value of this efficiency in this case is close to 0.87. Consequently, such a sailcraft would not be *dynamically* critical, inasmuch as the lightness number would be meaningfully lower than one throughout the flight. We shall go forward to analyzing some sub-critical cases.

## 6.8 The 1.28 g/m<sup>2</sup> case

In terms of  $\sigma$ , this sub-critical 1.28 is as distant from  $\sigma_c$  as 1.80 is. For an ideal-optics sail, the pre-perihelion arc is characterized by a mean value of the transversal number equal to  $-0.375$ . This is sufficient negative to lower aphelion, increase energy loss and achieve perihelion (0.20 AU) in 212 days. After the attitude maneuver at the beginning of the fourth T-arc (at 0.27 AU), the post-perihelion trajectory arc exhibits comparable values of all components of the lightness vector. This allows both energy and speed to evolve with profiles practically flat throughout the fourth T-arc (that ends at 120 AU). Strictly speaking, the local maximum of sailcraft speed still exists, but it is so broad, on the right, that it is rendered indistinct from the cruise level or 20.8 AU/yr. Baseline mission could be accomplished in 10.2 yr. Sailcraft could reach 716 AU in 1 HJT.

When optical sail degradation is considered, the pre-perihelion arc is still so fast that, very close to the perihelion, solar-wind energy fluence is as low as 0.37 MJ/m<sup>2</sup> at which sail temperature rises to 578 K, its max value. Sail achieves fluence saturation (0.48 MJ/m<sup>2</sup>) in 0.7 yr since injection. The optimal profiles for optical-degradation are very similar to those ones without it. One value for all, ISP would reach a distance, again, equal to 716 AU in 1 HJT.

This case is shown in Figures IV.6.8-[1-12].

## 6.9 The 1.00 g/m<sup>2</sup> case

In contrast to the above cases, some lightness number can now be greater than unity in some T-arcs; in particular, one gets  $\lambda \cong 1.24$ ,  $\lambda_r \cong 1.17$ ,  $\lambda_t \cong 0.34$  (ideal optics) in the spinning-sail T-arc. The main result consists of obtaining the sailcraft speed increasing as sailcraft moves far away from the Sun. As a point of fact, once the sailcraft overcomes the perihelion, some maneuver can be accomplished in order to reorient the sail with a radial number constantly greater than unity. Thus, the local speed maximum of the previous cases has “evolved” into an asymptotic *absolute* maximum. The *H*-reversal arc duration is still quite manageable (2 days). The optimal profiles are shown in Figures IV.6.9-[1-6].

By including optical degradation, the above set of lightness values changes into  $\lambda \cong 1.14$ ,  $\lambda_r \cong 1.08$ ,  $\lambda_t \cong 0.29$ , which allows sailcraft to accelerate again asymptotically. The related profiles are shown in Figures IV.6.9-[7-12]. Sail temperature takes on a max value of 547 K at fluence equal to 0.31 MJ/m<sup>2</sup>. The dynamical output one gets at 200 AU consists of sailcraft speed equal to 23.5 AU/yr. Baseline mission lasts 9.03 years, whereas the extended mission to 400 AU may be accomplished in less than 18 years. 809 AU could be reached in one HJT.

From Table IV.7-1, one can note that the current max value of sail temperature is the lowest one out of all cases hitherto analyzed. (The temperature margin may be used to design a new profile with perihelion less than 0.2 AU, but still keeping fluence sufficiently low not to violate 600 K. Such an analysis may be among the topics of a future study on faster ISP). Finally, one should note that, in this case of sub-critical sailcraft sail loading,  $V_\infty^p$  amounts to 21.34 AU/yr, namely, *lower* than the current cruise speed. It is to be ascribed mainly to the large transversal lightness number that can change energy (equation IV-5c) to overcome the pure-radial solution significantly.

## 6.10 Further Remarks

1. Keeping the sail attitude constant, or so, in the sailcraft orbital frame entails that the sail axis has to be rotated sufficiently fast in the inertial frame, especially when sailcraft moves around the perihelion. For instance, the attitude control system has to output about 9.7 deg/day and 15.1 deg/day for the 2 g/m<sup>2</sup> and 1 g/m<sup>2</sup> case, respectively. In the present model of sailcraft, although detailed system description and modeling is beyond the scope of this report, we assumed a small-rocket attitude control; each pair of micro-engines (endowed with small solar panel) is placed on the sail rim. In the fastest trajectories here analyzed, maximum fuel consumption is less than 1 percent of the initial sailcraft mass. In general, a “mixed” attitude control system may be considered: non-rocket devices (Wright, 1993) and micro-thrusters, depending on the distance from the Sun and the trajectory control requirements.
2. The optimal trajectory profiles presented in this report are characterized, among many things, by a double-crossing of the ecliptic plane, with the perihelion between the two. Perihelion latitude ranges from -14.8° to -47.8°. Therefore, there is no geometric problem in the sailcraft-Earth communication around the perihelion. What shall be analyzed in detail is the location of the onboard antenna with respect to the sail.
3. In addition to the mission unfeasibility-feasibility transition, there exist another special value of the sailcraft sail loading. For the ISP-mission Al-Cr sail spacecraft with *H*-reversal motion, this value is very close to 1.3 g/m<sup>2</sup>. Below it, the pre-perihelion trajectory arc can be so fast that (despite the angle between sailcraft position and velocity is significantly greater than 90° for over 50 percent of time), the optimal performance indexes of the ideal-optics and the optical-degradation flights can be considered equal to one another (< 1 percent). Above this limit, the influence of the energy fluence on mission feasibility cannot be neglected. Reasonably, such a feature should hold even for a direct-motion fly-by of the Sun. At the time of this writing, though, it is not known.
4. A sailcraft with 1.2 g/m<sup>2</sup>, or less, would be able to fast explore the solar gravitational lens in deeper focal zones. For instance, if sailcraft were able to fly-by the Sun at perihelion equal to 0.15 AU (Vulpetti, 2000), it could navigate the interval from 763 AU to 821 AU in 2.3 yr and reach 821 AU after 32.2 yr since injection. That would be appropriate for observing distant photon sources in the range from 160.4 GHz to 122.3 GHz (Maccone, 2000). At 122.3 GHz, the photon path bending due to the solar gravity is counterbalanced by the contrary deflection caused by the solar corona plasma. Photon frequencies different from such *no-lensing* value behave differently in total deflection. In the context of a generalized ISP mission concept, such a potential flight may be revisited by adding optical degradation, telecommunication system and launcher constraint.

## 6.11 Figures

Case id:  $\sigma=2.20 \text{ g/m}^2$ , r.m.s.  $\delta=20 \text{ nm}$ , Degradation=off, perihelion=0.175 AU

Figure IV.6.3-1

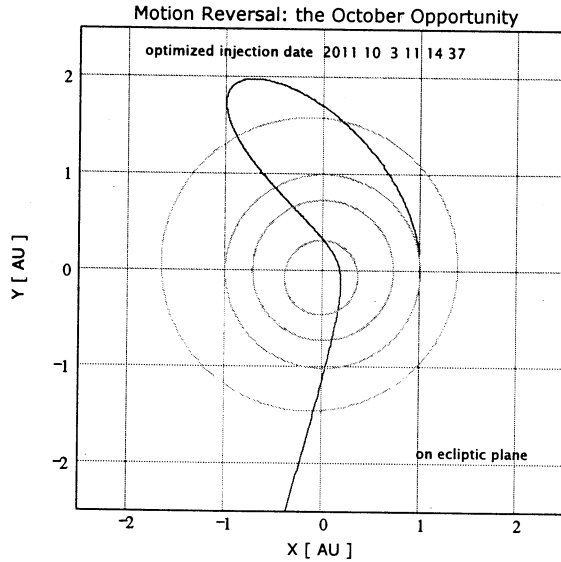


Figure IV.6.3-3

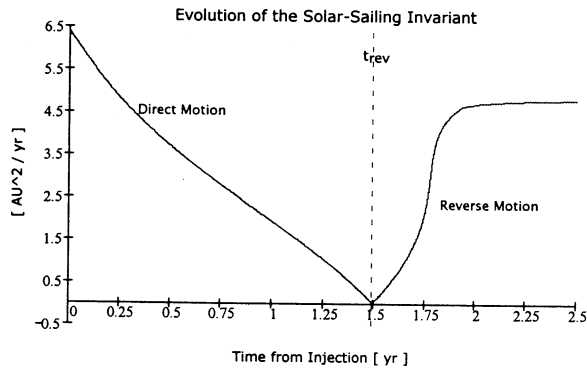


Figure IV.6.3-5

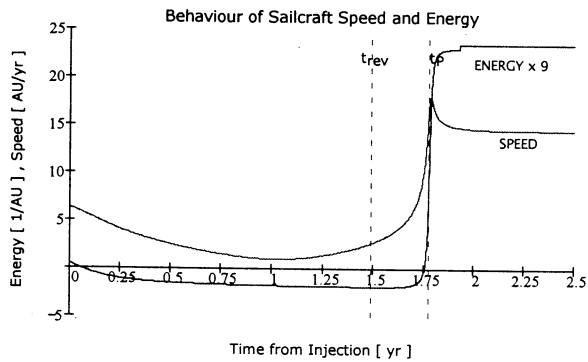


Figure IV.6.3-2

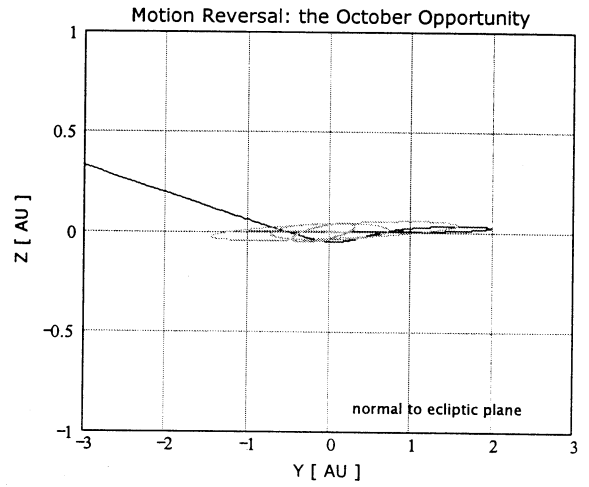


Figure IV.6.3-4

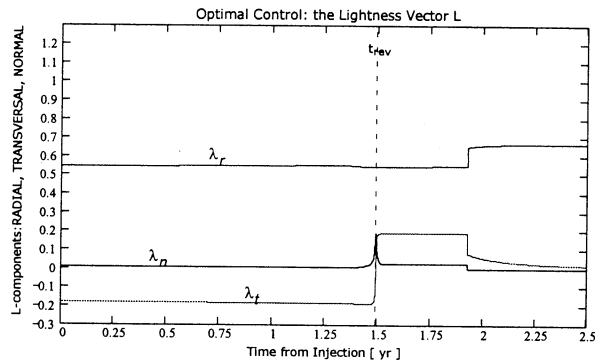
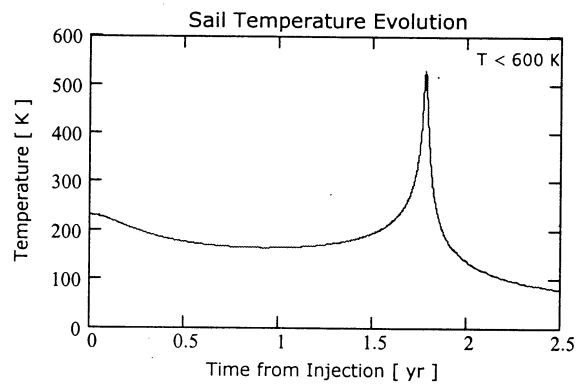


Figure IV.6.3-6



Case id:  $\sigma=2.20 \text{ g/m}^2$ , r.m.s.  $\delta=20 \text{ nm}$ , Degradation=ON, perihelion=0.261 AU

Figure IV.6.3-7

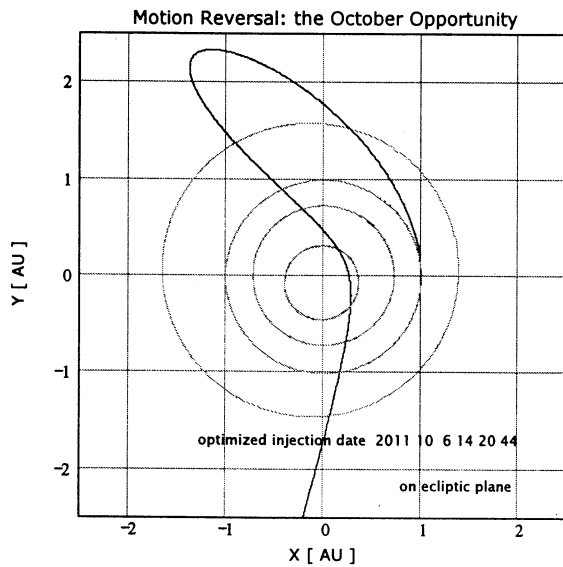


Figure IV.6.3-8

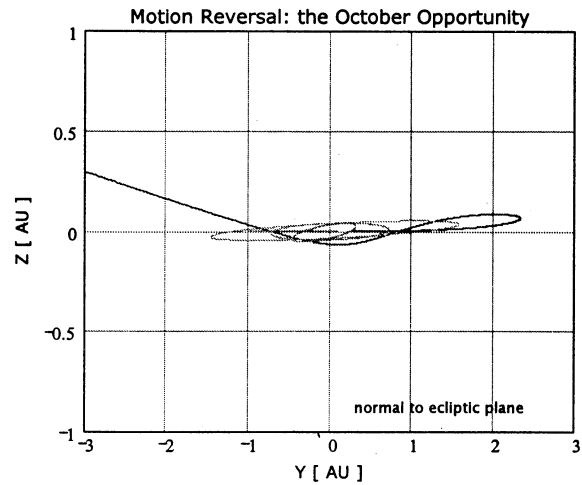


Figure IV.6.3-9

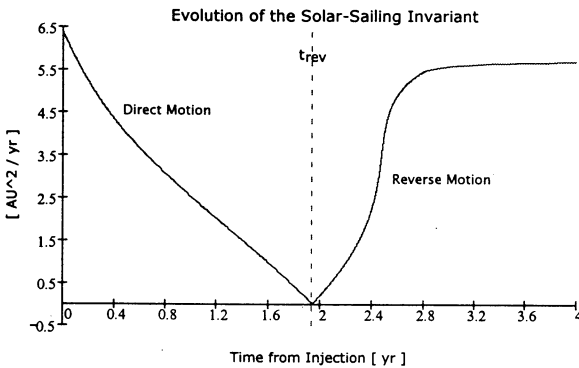


Figure IV.6.3-10

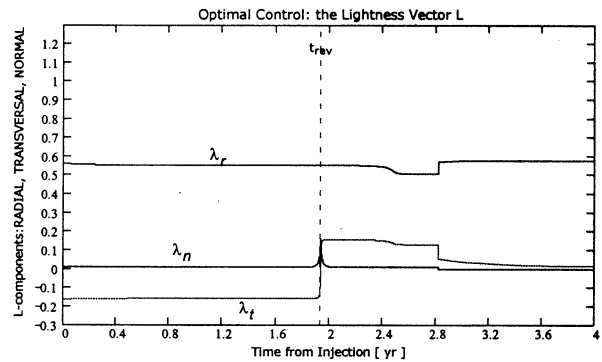


Figure IV.6.3-11

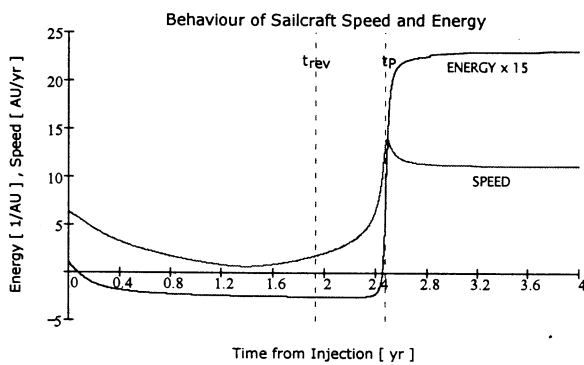
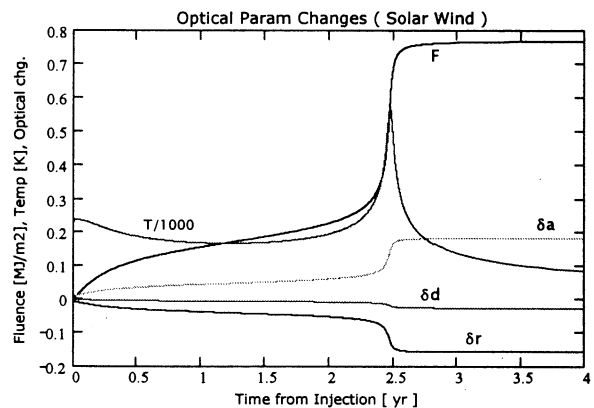


Figure IV.6.3-12



Case id:  $\sigma=2.10 \text{ g/m}^2$ , r.m.s.  $\delta=20 \text{ nm}$ , Degradation=off, perihelion=0.204 AU

Figure IV.6.4-1

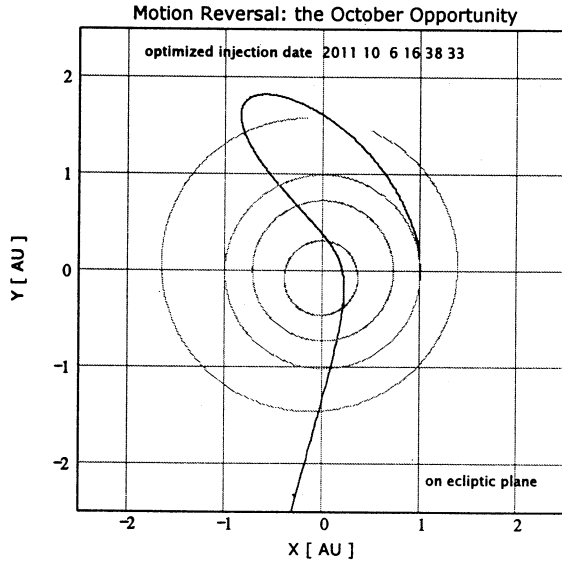


Figure IV.6.4-2

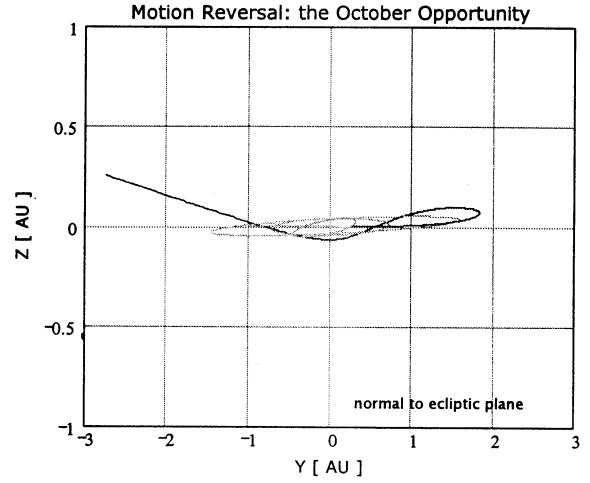


Figure IV.6.4-3

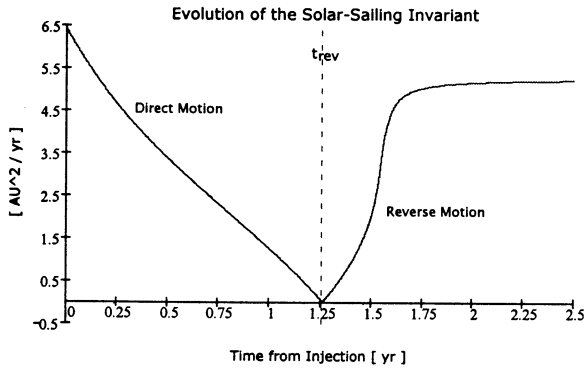


Figure IV.6.4-4

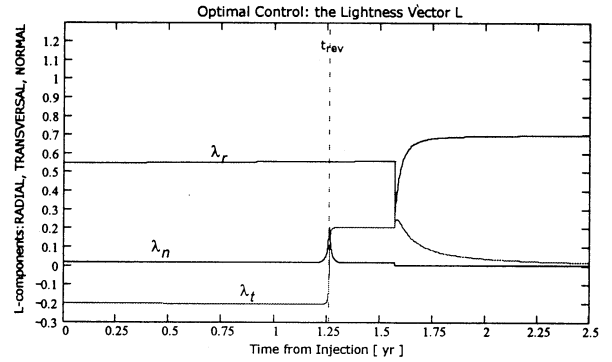


Figure IV.6.4-5

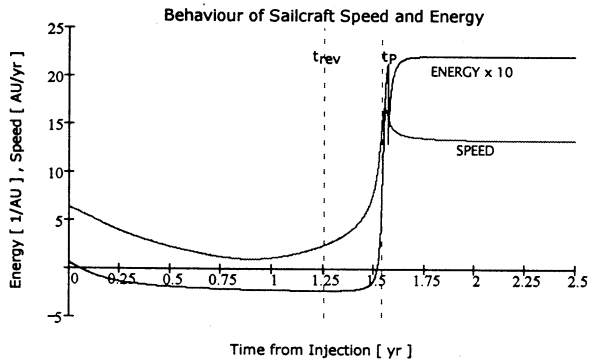
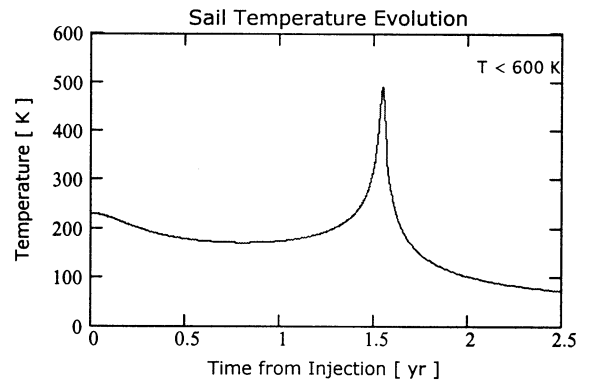


Figure IV.6.4-6



Case id:  $\sigma=2.10 \text{ g/m}^2$ , r.m.s.  $\delta=20 \text{ nm}$ , Degradation=ON, perihelion=0.248 AU

Figure IV.6.4-7

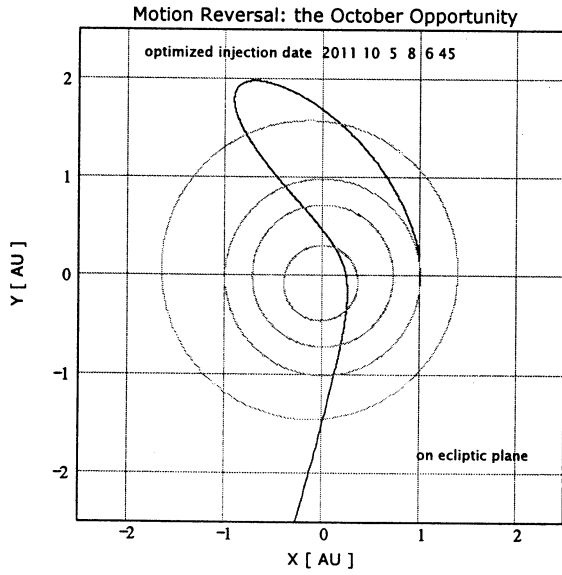


Figure IV.6.4-8

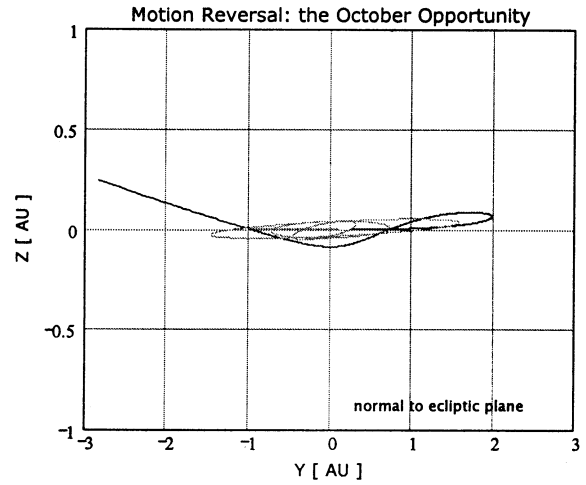


Figure IV.6.4-9

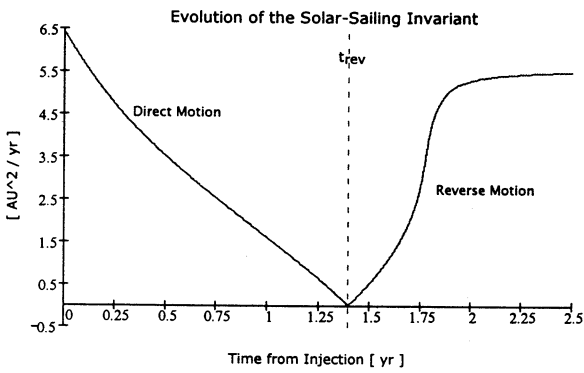


Figure IV.6.4-10

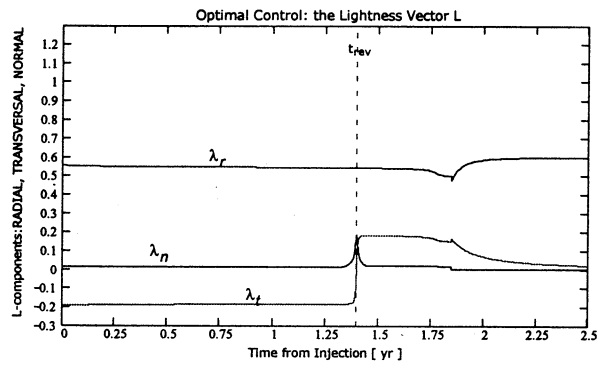


Figure IV.6.4-11

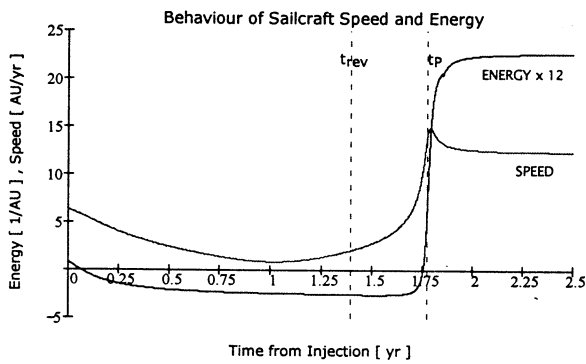
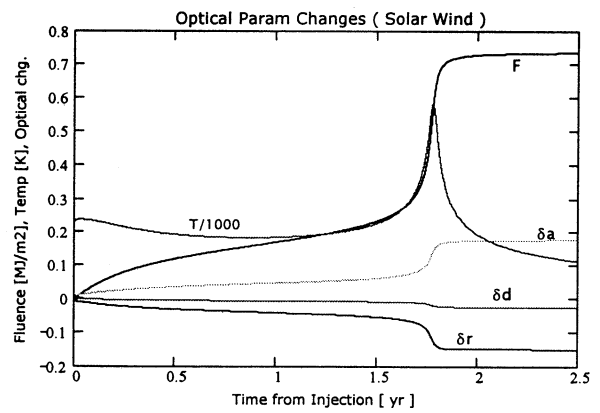


Figure IV.6.4-12



Case id:  $\sigma=2.00 \text{ g/m}^2$ , r.m.s.  $\delta=0 \text{ nm}$ , Degradation=off, perihelion=0.20 AU

Figure IV.6.5-1

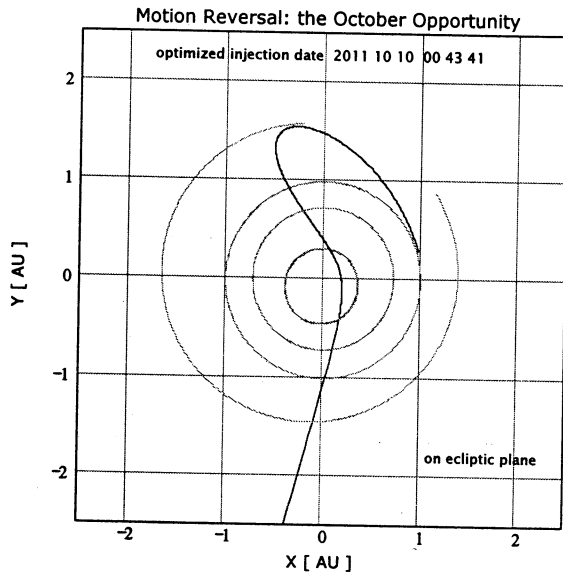


Figure IV.6.5-2

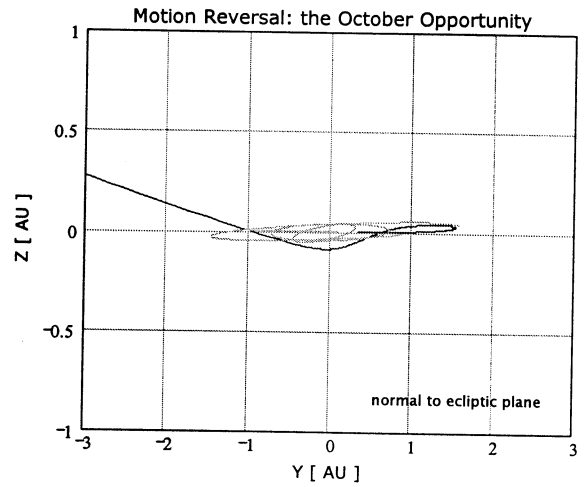


Figure IV.6.5-3

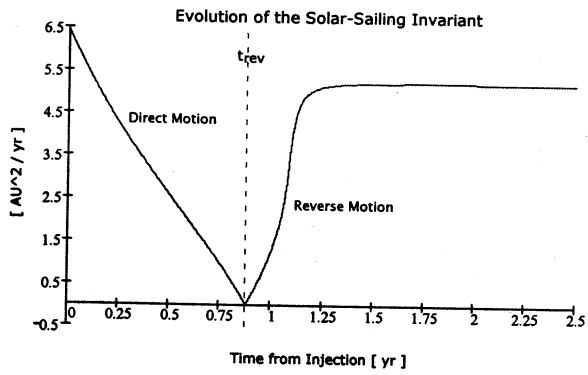


Figure IV.6.5-4

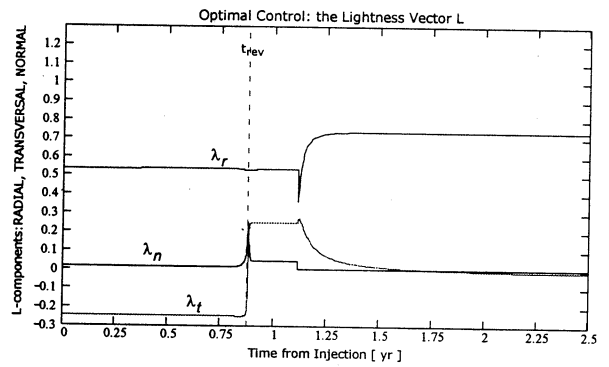


Figure IV.6.5-5

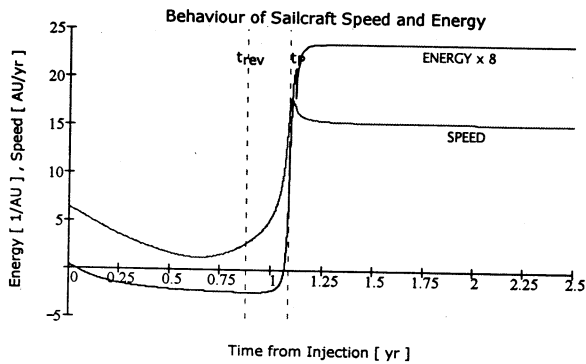
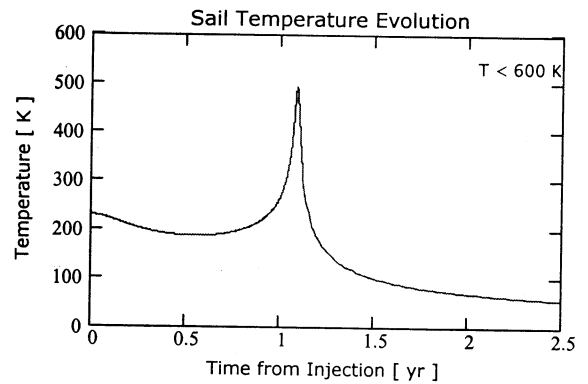


Figure IV.6.5-6



Case id:  $\sigma=2.00 \text{ g/m}^2$ , r.m.s.  $\delta=10 \text{ nm}$ , Degradation=off, perihelion=0.20 AU

Figure IV.6.5-7

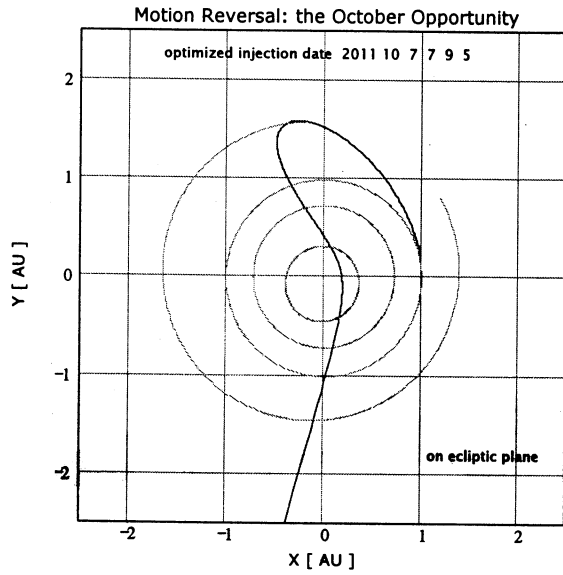


Figure IV.6.5-8

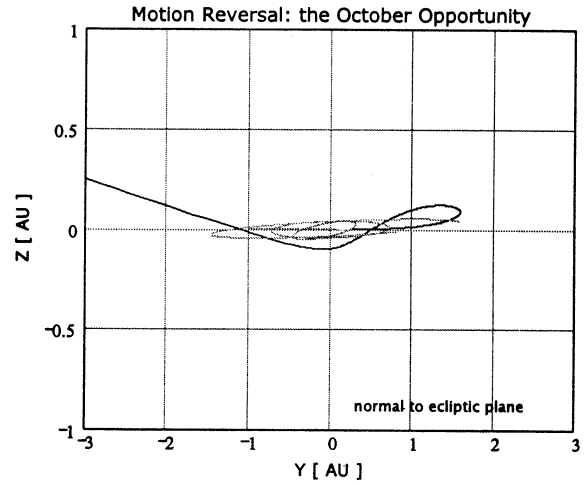


Figure IV.6.5-9

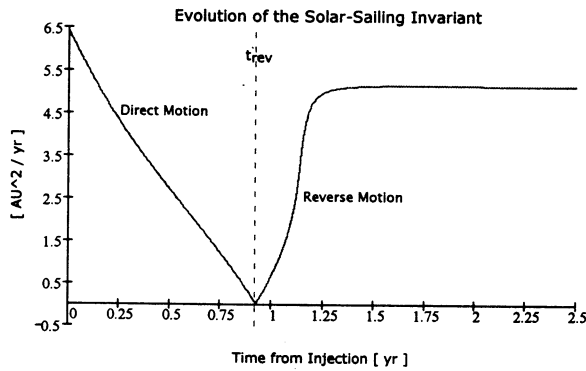


Figure IV.6.5-10

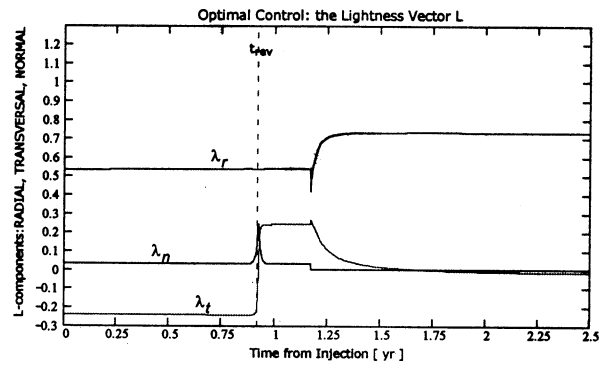


Figure IV.6.5-11

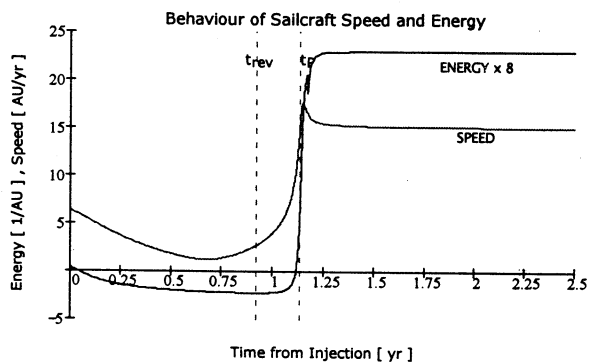
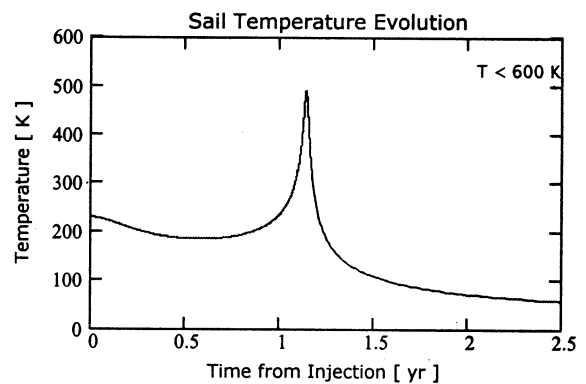


Figure IV.6.5-12



Case id:  $\sigma=2.00 \text{ g/m}^2$ , r.m.s.  $\delta=20 \text{ nm}$ , Degradation=off, perihelion=0.24 AU

Figure IV.6.5-13

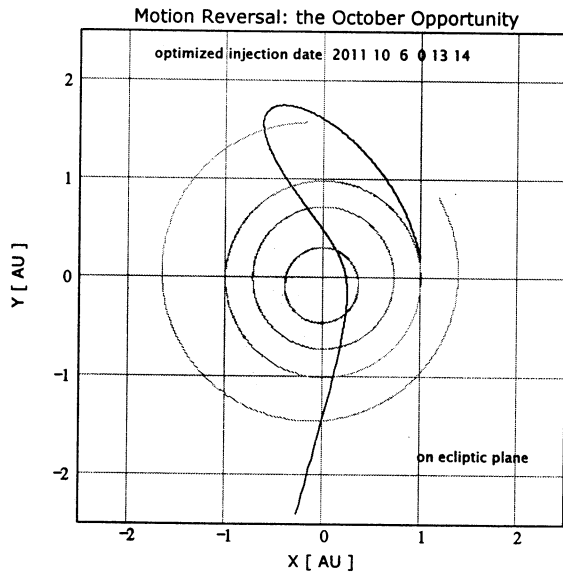


Figure IV.6.5-14

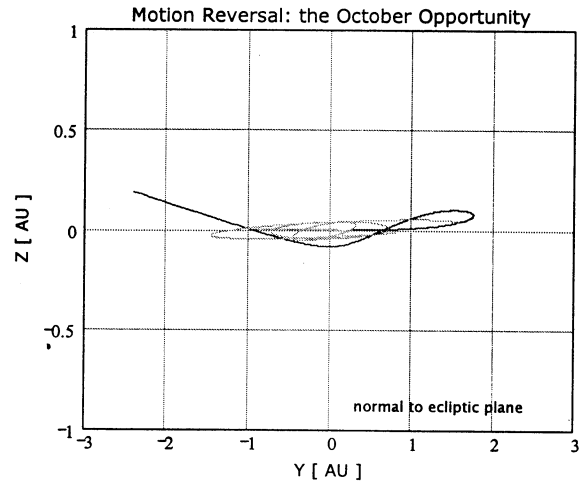


Figure IV.6.5-15

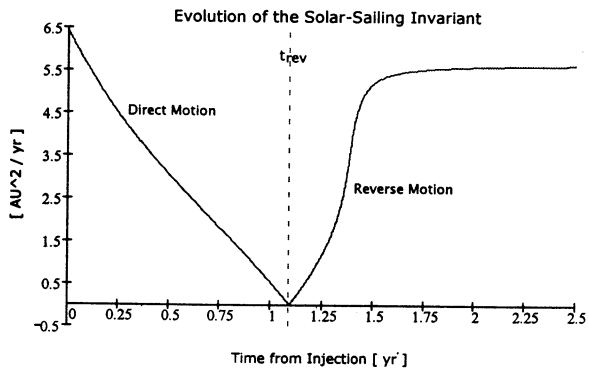


Figure IV.6.5-16

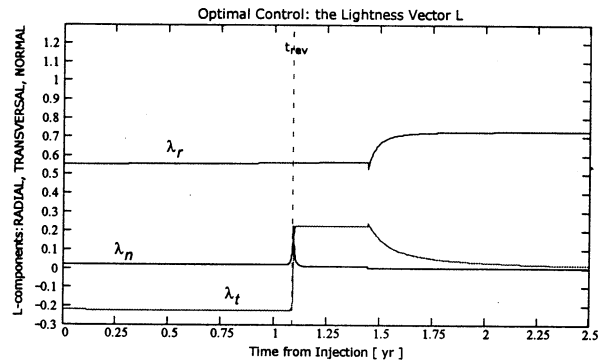


Figure IV.6.5-17

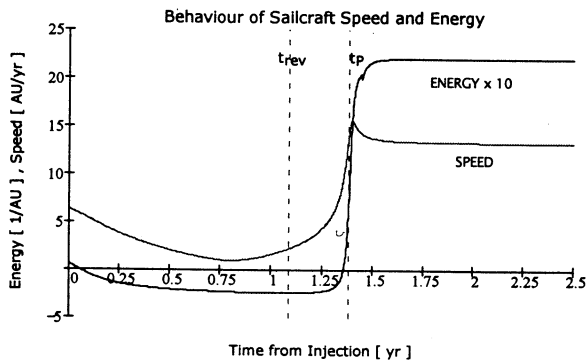
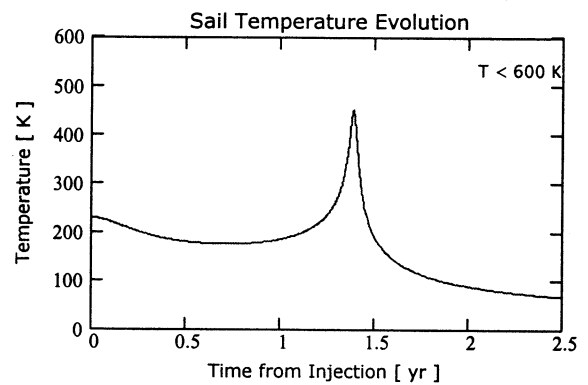


Figure IV.6.5-18



Case id:  $\sigma=2.00 \text{ g/m}^2$ , r.m.s.  $\delta=20 \text{ nm}$ , Degradation=ON, perihelion=0.24 AU

Figure IV.6.5-19

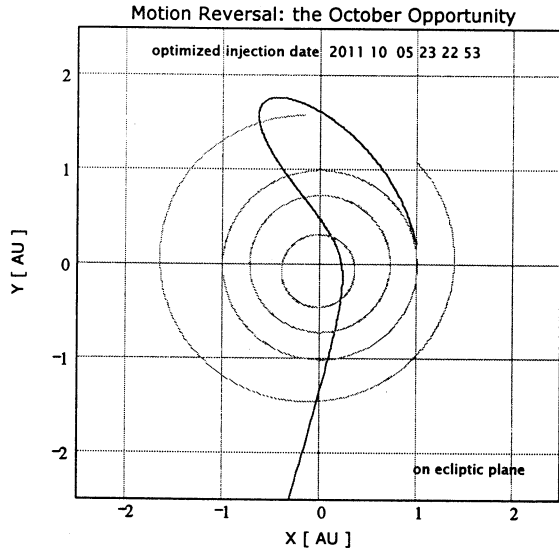


Figure IV.6.5-20

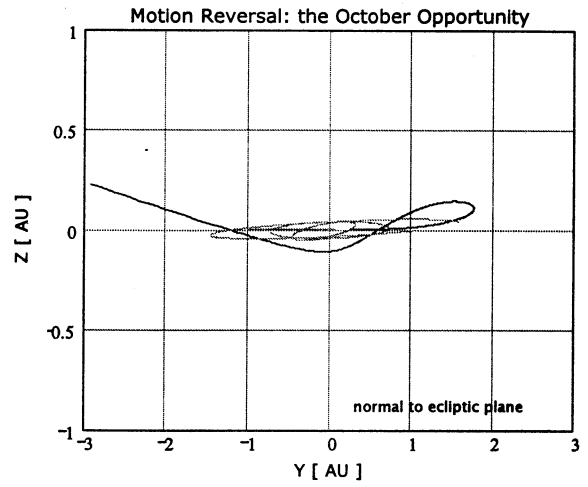


Figure IV.6.5-21

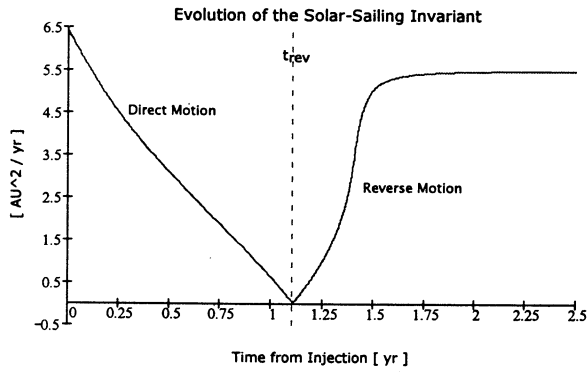


Figure IV.6.5-22

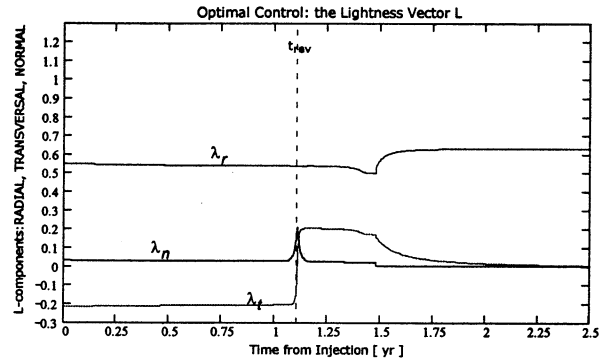


Figure IV.6.5-23

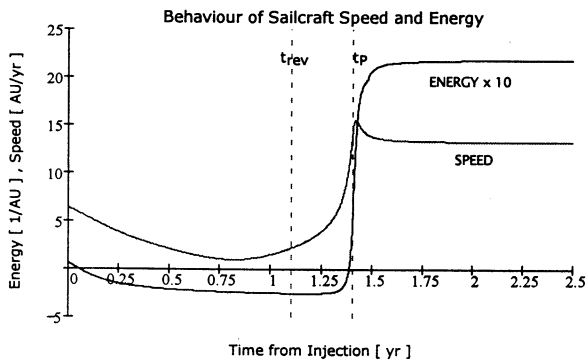
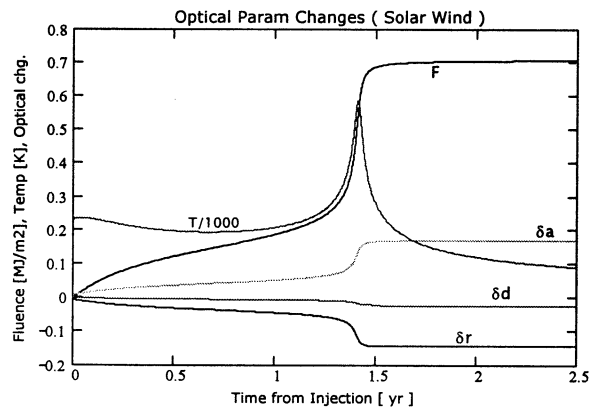


Figure IV.6.5-24



Case id:  $\sigma=1.80 \text{ g/m}^2$ , r.m.s.  $\delta=20 \text{ nm}$ , Degradation=off, perihelion=0.20 AU

Figure IV.6.6-1

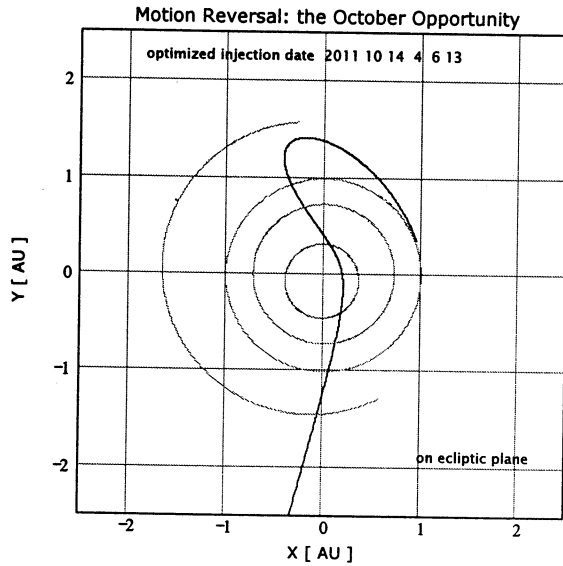


Figure IV.6.6-2

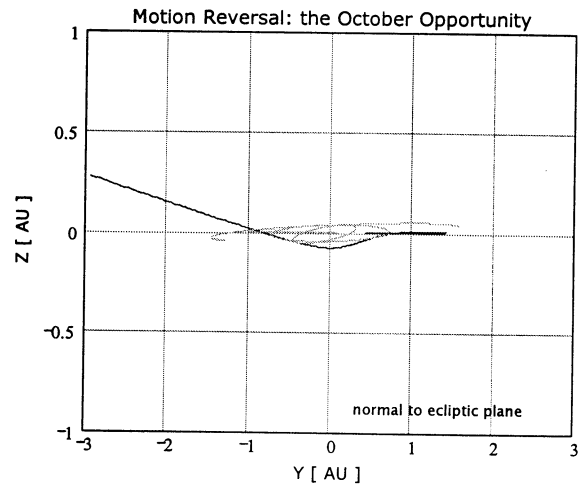


Figure IV.6.6-3

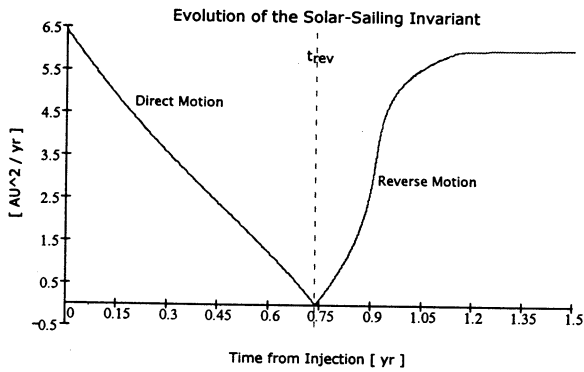


Figure IV.6.6-4

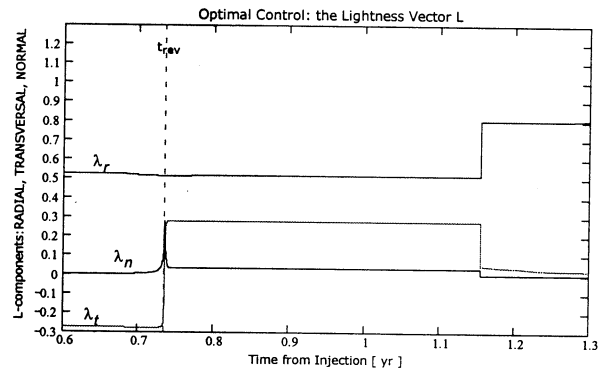


Figure IV.6.6-5

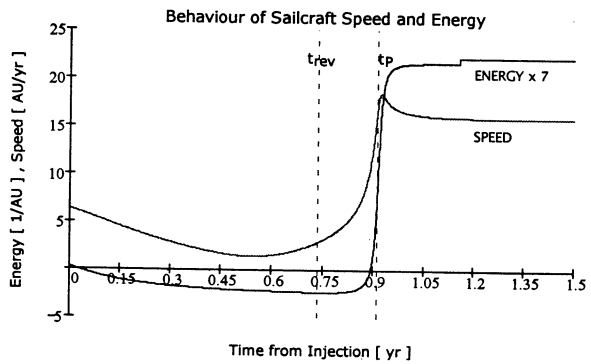
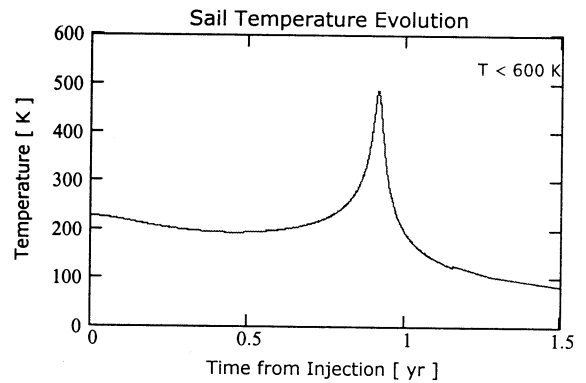


Figure IV.6.6-6



Case id:  $\sigma=1.80 \text{ g/m}^2$ , r.m.s.  $\delta=20 \text{ nm}$ , Degradation=ON, perihelion=0.22 AU

Figure IV.6.6-7

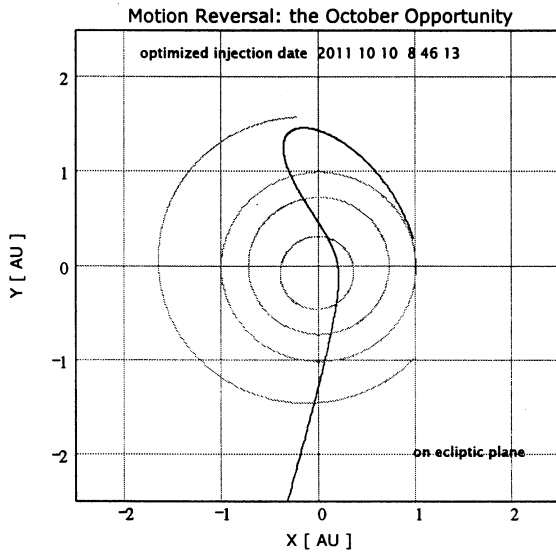


Figure IV.6.6-9

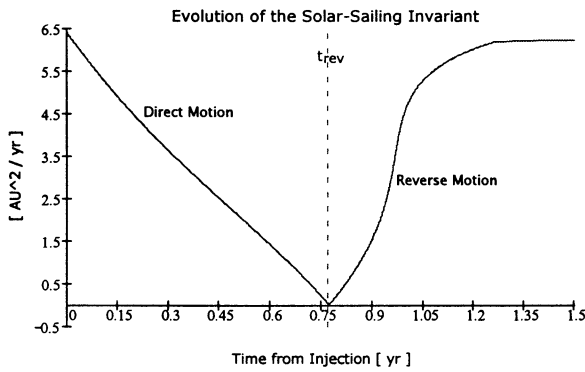


Figure IV.6.6-11

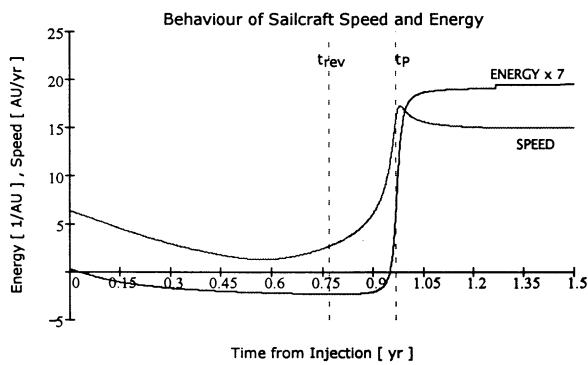


Figure IV.6.6-8

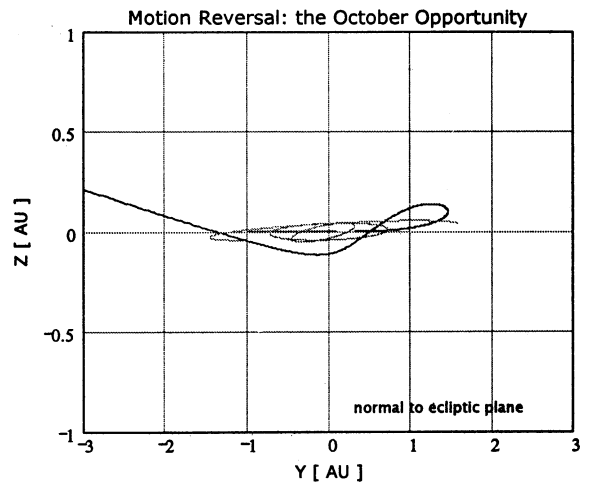


Figure IV.6.6-10

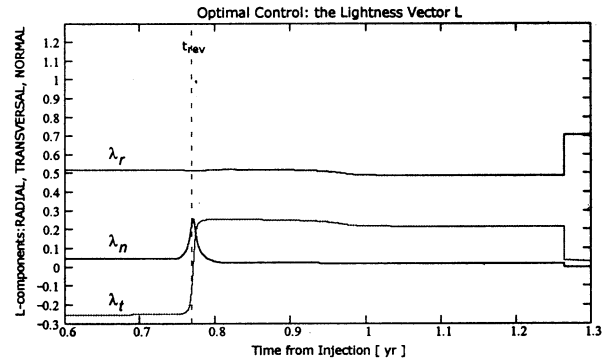
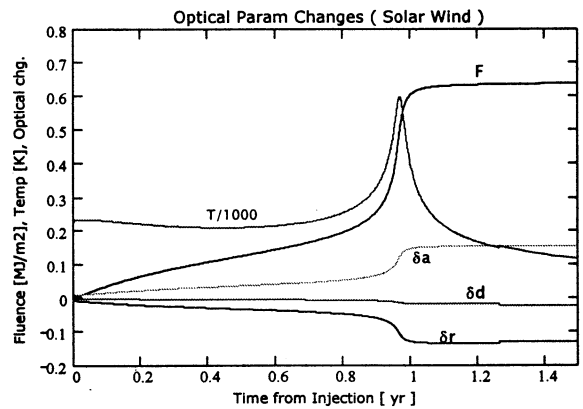


Figure IV.6.6-12



Case id:  $\sigma=1.28 \text{ g/m}^2$ , r.m.s.  $\delta=20 \text{ nm}$ , Degradation=off, perihelion=0.20 AU

Figure IV.6.8-1

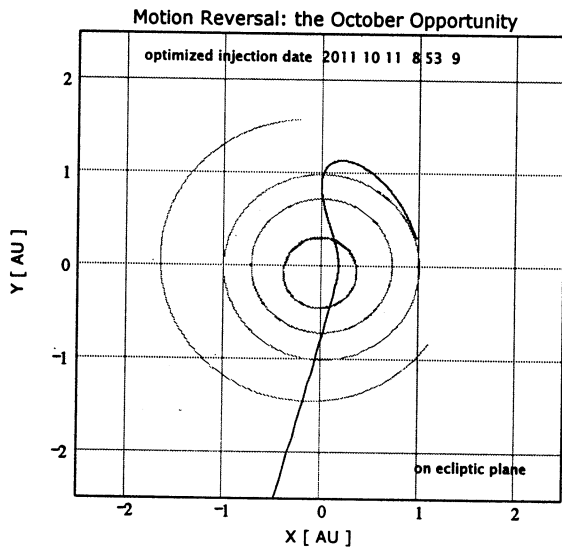


Figure IV.6.8-2

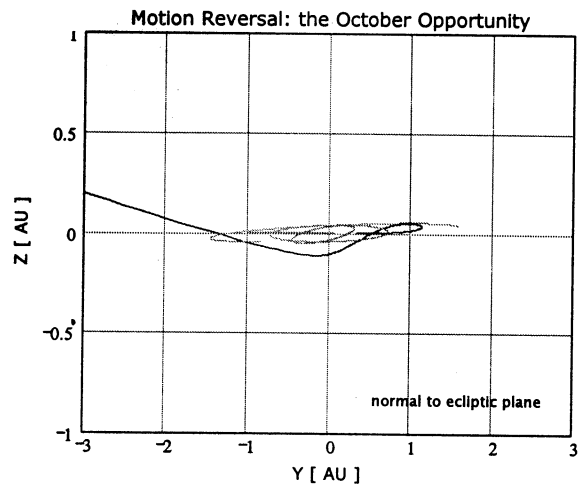


Figure IV.6.8-3

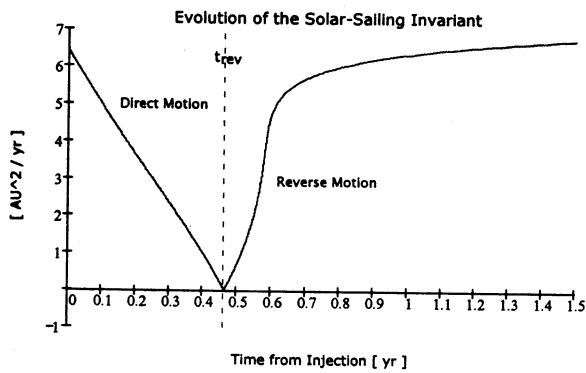


Figure IV.6.8-4

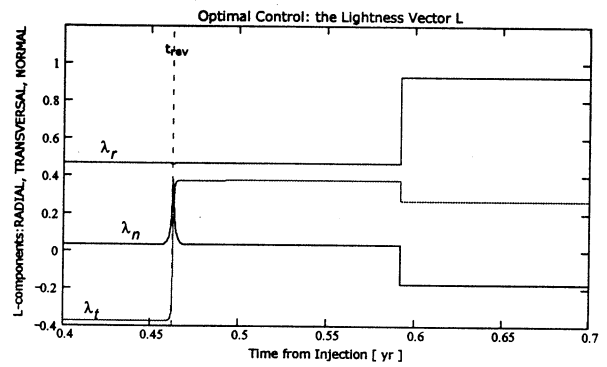


Figure IV.6.8-5

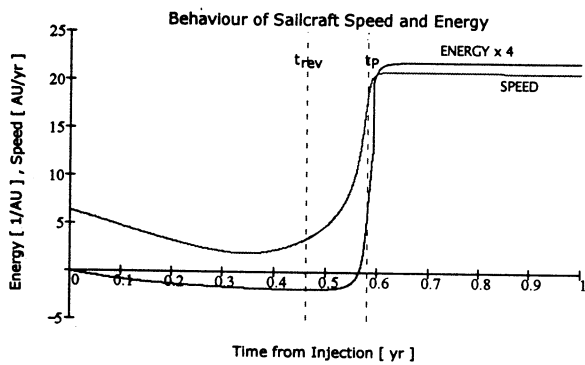
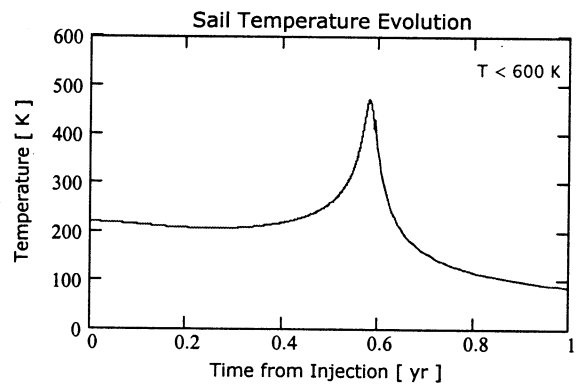


Figure IV.6.8-6



Case id:  $\sigma=1.28 \text{ g/m}^2$ , r.m.s.  $\delta=20 \text{ nm}$ , Degradation=ON, perihelion=0.20 AU

Figure IV.6.8-7

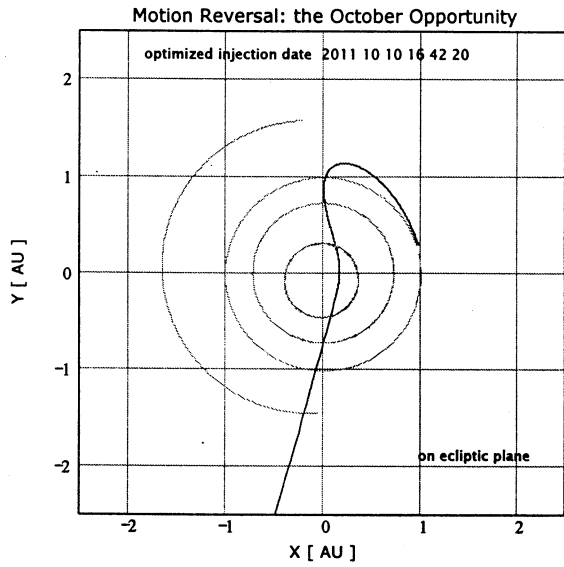


Figure IV.6.8-8

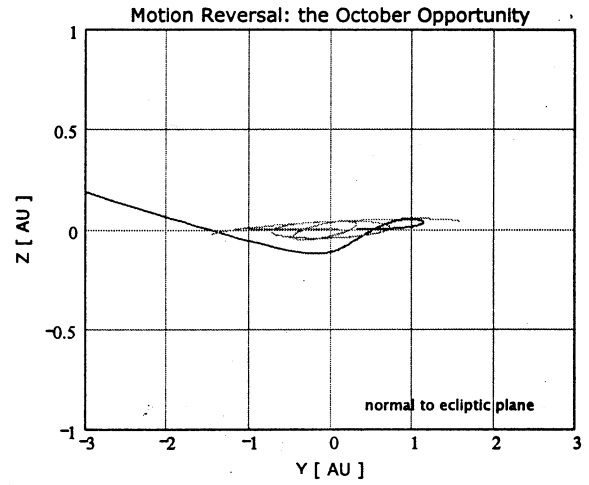


Figure IV.6.8-9

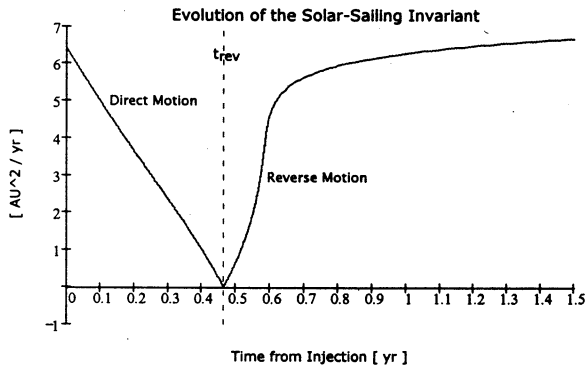


Figure IV.6.8-10

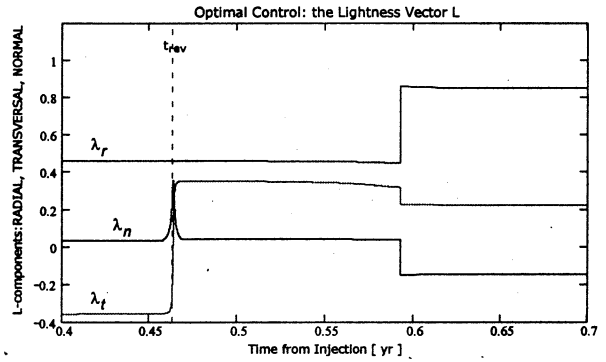


Figure IV.6.8-11

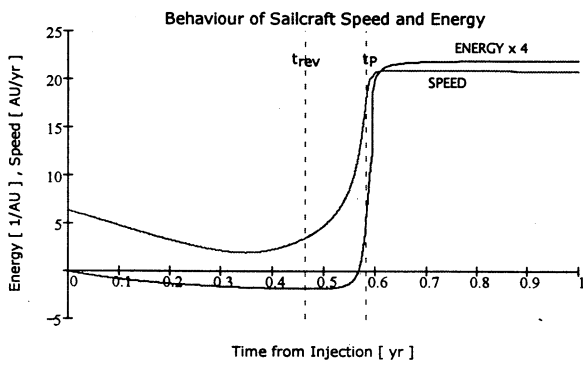
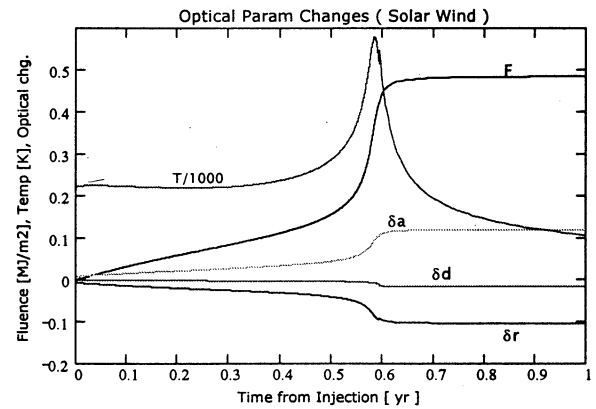


Figure IV.6.8-12



Case id:  $\sigma=1.00 \text{ g/m}^2$ , r.m.s.  $\delta=20 \text{ nm}$ , Degradation=off, perihelion=0.20 AU

Figure IV.6.9-1

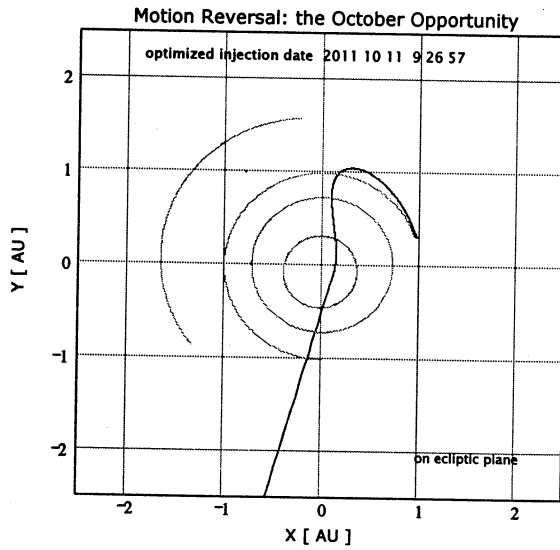


Figure IV.6.9-2

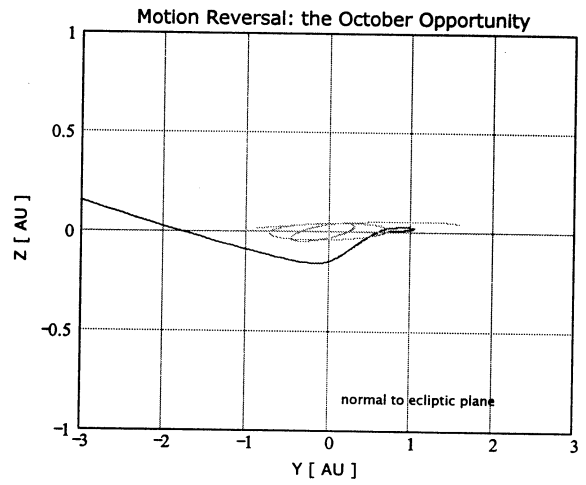


Figure IV.6.9-3

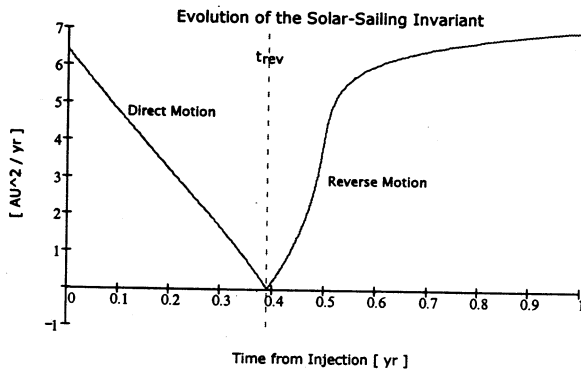


Figure IV.6.9-4

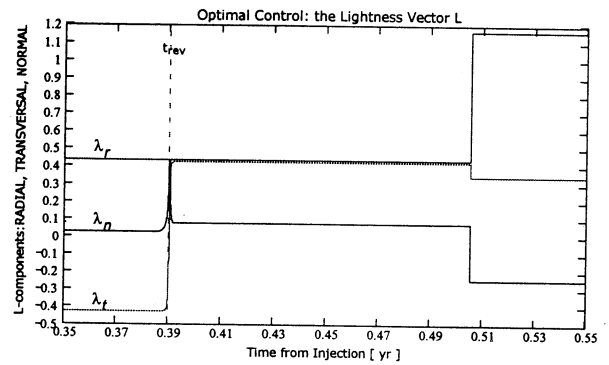


Figure IV.6.9-5

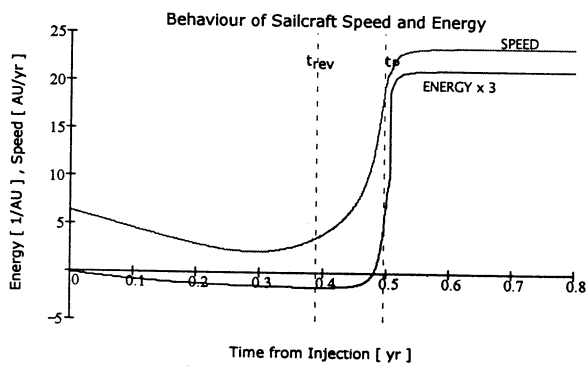
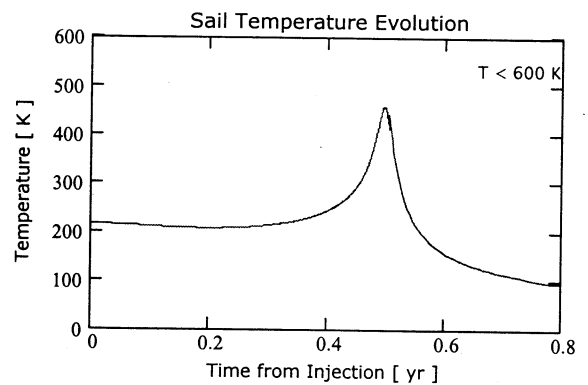


Figure IV.6.9-6



Case id:  $\sigma=1.00 \text{ g/m}^2$ , r.m.s.  $\delta=20 \text{ nm}$ , Degradation=ON, perihelion=0.20 AU

Figure IV.6.9-7

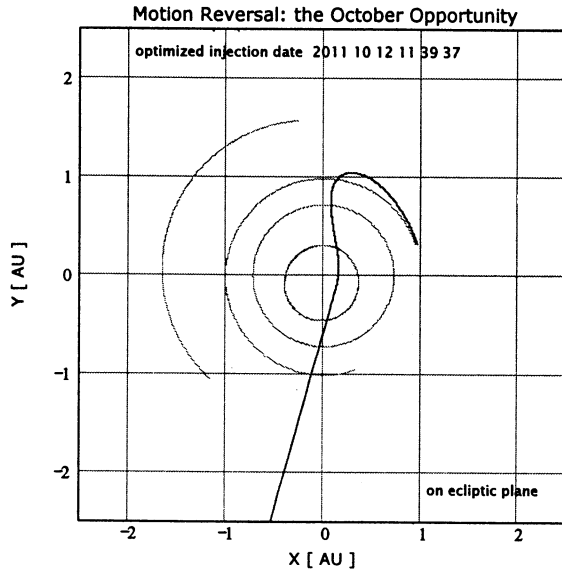


Figure IV.6.9-9

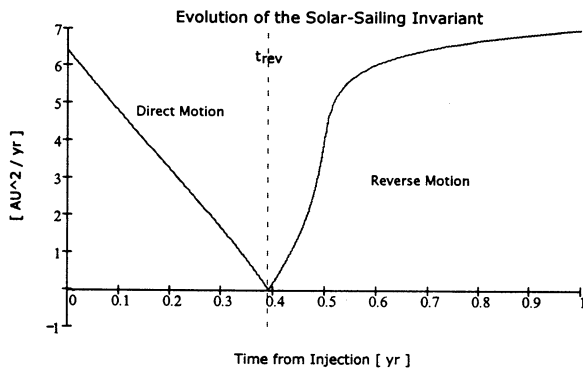


Figure IV.6.9-11

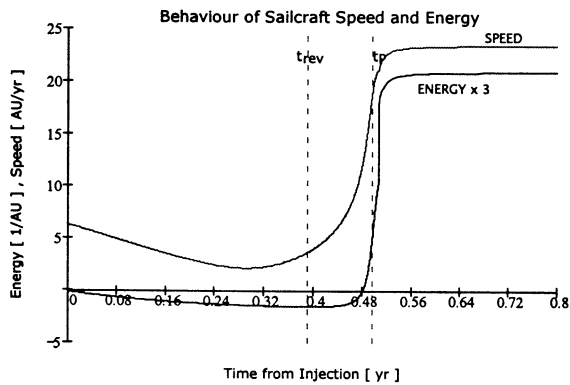


Figure IV.6.9-8

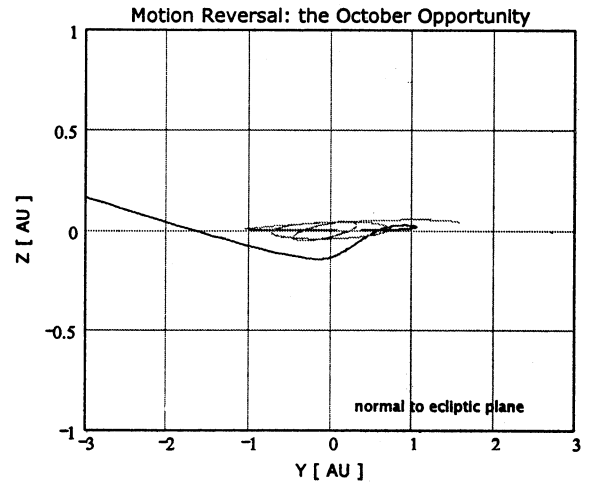


Figure IV.6.9-10

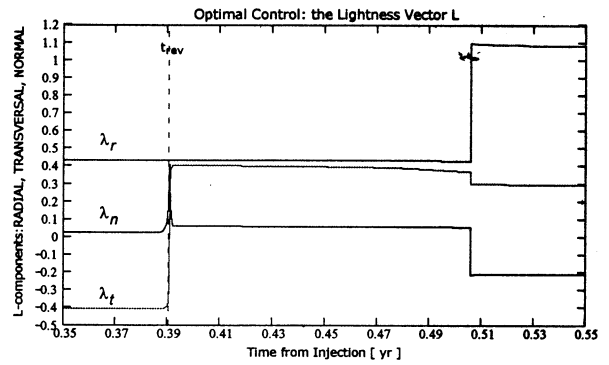
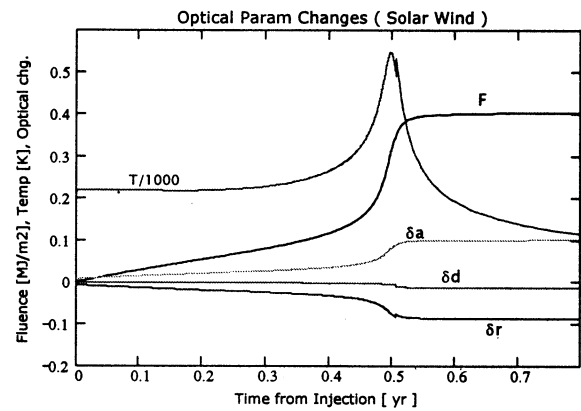


Figure IV.6.9-12



## IV.7 Summary Table

Table IV.7-1. ISP H-reversal trajectory opportunity: main features from the optimal profiles discussed in §IV.6. Constraint violation is marked bold. *Italic* figures in the rightmost column represent the flight time of the extended mission to 400 AU.

$\sigma$ [g/m <sup>2</sup> ]	$\delta$ [nm]	Optical Degradation	Perihelion distance [AU]	<i>Aphelion</i> in pre-perihelion arc [AU]	Time to <i>Aphelion</i> [year]	Time to H-reversal [year]	Time to Perihelion [year]	Max Sail Temperature [K]	Speed at 200 AU [AU/yr]	Time to 200   400 AU [year]
2.20	20	Off	<b>0.175</b>	2.130	0.931	1.492	1.776	530	14.34	15.698   29.65
2.20	20	ON	0.261	2.636	1.283	1.934	2.470	574	11.02	<b>20.565</b>   <b>38.71</b>
<i>2.10</i>	<i>20</i>	<i>Off</i>	0.204	1.938	0.806	1.258	1.543	490	13.20	16.667   31.82
<i>2.10</i>	<i>20</i>	<i>ON</i>	0.248	2.118	0.922	1.393	1.773	584	12.23	<b>18.096</b>   <b>34.45</b>
2.00	00	Off	0.20	1.570	0.556	0.879	1.086	492	15.22	14.211   27.35
2.00	10	Off	0.20	1.613	0.583	0.922	1.137	490	15.04	14.424   27.72
2.00	20	Off	0.24	1.809	0.716	1.089	1.383	450	13.17	16.543   31.73
2.00	20	ON	0.24	1.827	0.726	1.105	1.405	587	13.13	16.611   31.84
<i>1.80</i>	<i>20</i>	<i>Off</i>	0.20	1.426	0.457	0.736	0.913	487	15.79	13.565   26.23
<i>1.80</i>	<i>20</i>	<i>ON</i>	0.22	1.470	0.485	0.769	0.967	597	14.84	14.429   27.91
1.28	20	Off	0.20	1.158	0.257	0.462	0.581	471	20.79	10.201   19.82
1.28	20	ON	0.20	1.159	0.257	0.464	0.582	578	20.79	10.202   19.82
<i>1.00</i>	<i>20</i>	<i>Off</i>	0.20	1.099	0.201	0.390	0.496	458	23.57	8.986   17.47
<i>1.00</i>	<i>20</i>	<i>ON</i>	0.20	1.099	0.201	0.391	0.496	547	23.46	9.026   17.55

## IV.8 Feasibility of ISP from Trajectory Design Viewpoint

These following considerations complement those made in §IV.6.10. As it is well known, Interstellar Probe is not only a sophisticated scientific mission concept; among the main things, it should prove that it is possible to travel fast to distant targets with low cost and high reliability. These features generally depend on sailcraft operations, no other propulsion (apart from lifting off, of course), strong increase of the launch window, higher number of missions per time unit (e.g. on a quinquennium basis) and so forth. Thus, the existence of an additional launch opportunity for the ISP mission concept should be of high concern. Previous sections have, no doubt, shown that there exists such an opportunity for ISP sailcraft, in October of every year. This could be accomplished by utilizing one of the several peculiarities of space sailing: the fly-by of the Sun via motion reversal. A spectrum of fourteen optimized mission profiles have been computed by a code that takes into account a high number of real effects. Distinct trajectories correspond to different key parameters such as the sailcraft sail loading, sail roughness and optical sail degradation due to solar wind. (Ultraviolet-photon degradation was not considered by lack of experimental data appropriate to solar sailing). Solar wind fluence has been recognized relevant to a sailcraft approaching the Sun closely. In addition, a major item has consisted of dealing with integro-differential equations for modeling sailcraft motion appropriately. Optical degradation, with constraints on temperature, perihelion and flight time, has resulted in a key item for designing some fast sailcraft trajectory to many hundreds of AU. By considering both baseline and extended mission concepts, ISP is certainly feasible from *motion-reversal* trajectory viewpoint if the sailcraft sail loading is lower than  $2.1 \text{ g/m}^2$ . The current literature value of the ISP-sailcraft sail loading is very close to  $2 \text{ g/m}^2$ . This is a value sufficiently lower than the above threshold to allow the following time line (since injection): (1) launching in October, (2) flying-by the Sun at 0.24 AU after 1.40 years, (3) achieving 200 AU after 16.6, (4) extending the mission to 400 AU by 15.2 years more. (A slightly lower value of the sailcraft sail loading in the range  $[1.9, 1.95] \text{ g/m}^2$  is suggested to deal with small attitude control errors). These ones and the other numerical results, discussed in this document, should be considered *realistic* enough due to the many key elements and detailed features included in the present dynamical model of sailcraft motion.

## IV.9 Conclusions and Future Research

The analysis performed so far, and presented in this report, is sufficiently general in some aspects to allow us to suggest some major lines for future investigation. They may be expressed as follows

- A. ISP feasibility: additional aspects are to be investigated and improved, of course; however, it is hard that the ISP concept may result unfeasible from mission viewpoint. That is enforced by *two* launch opportunities per year. By considering how complex and various are solar-sailing trajectories, it would be interesting to investigate whether there is some other opportunity.
- B. Optical sail degradation: there is the need for additional experimental data about solar wind and new data on UV. Once again, we stress that the evolution of the optical sail parameters is one of the major aspects of solar sailing. Other potential missions close to the Sun may benefit from such data; for instance, a solar-sail mission to solar poles, with final orbit achieving  $90^\circ$  in heliographic latitude, should be investigated with respect to this critical point as well. Furthermore, a future interplanetary sail shuttle might be limited in lifetime by optical degradation before any other system fails.
- C. A sensitivity analysis on the baseline ISP profile is strongly recommended. The optimization process performed in this work was rather complicated; although not reported here since beyond the present aims, however it revealed that many decision parameters affect the solar sailcraft flyby very differently.
- D. Aluminum-Chromium is appropriate for the ISP of first generation (400 AU). Assessing feasibility for second-generation ISP (800-1000 AU) with perihelion at 0.15 AU would deserve a dedicated study. New sail materials, e.g. according to the line open by Matloff (Matloff, 1997-2000), should be investigated for third-generation ISP that, for instance, may achieve 10 light-days in one human job time, or less.

## IV.10 References

- Johnson, L., *Options for Interstellar Probe*, private communication, June 2001
- Matloff, G. L. and Mallove, E. F., *The Interstellar Solar Sail: Optimization and Further Analysis*, Vol. 36, No. 5, pp. 201-209, 1983
- Matloff, G. L., *Interstellar Solar Sailing: Consideration of Real and Projected Sail Materials*, JBIS, Vol. 37, No. 3, March 1984
- Matloff, G. L., *Interstellar Solar Sails: Projected Performance of Partially Transmissive Sail Films*, paper IAA-97-IAA.4.1.04, the 48<sup>th</sup> International Astronautical Congress, Turin - Italy, 1997
- Matloff, G. L., *Deep Space Probes*, Springer-Praxis, ISBN 1-85233-200-X, 2000
- McInnes, C. R., *Solar Sailing – Technology, Dynamics and Mission Applications*, Springer-Praxis, ISBN 1-85233-102-X, 1999
- Mewaldt, R. A., Liewer, P. C., *An Interstellar Probe Mission to the Boundaries of the Heliosphere and Nearby Interstellar Space*, Space 2000, Long Beach (CA), Sept. 19-21, 2000
- Liewer, P. C., Mewaldt, R. A., Ayon, J. A., Garner, C., Gavit, S., Wallace, R. A., *Interstellar Probe Using a Solar Sail: Conceptual Design and Technological Challenges*, COSPAR Colloquium, The Outer Heliosphere: the next frontiers, Potsdam, Germany, July 24-28, 2000
- Maccone, C., *Sun-Lensing the Cosmic Microwave Background from 763 AU by virtue of NASA's Interstellar Probe*, 3<sup>rd</sup> IAA Symposium on Realistic Near-Term Advanced Scientific Space Missions, Aosta, Italy, July 3-5, 2000
- Genta, G., and Brusa, E., *The AURORA Project: a New Sail Layout*, Acta Astronautica, 44, No. 2-4, pp. 141-146 (1999)
- Stuckey, W. K., Meshishnek, M. J., *Solar Ultraviolet and Space Radiation Effects on Inflatable Materials*, Aerospace Report TR-2000 (8565)-9, August 20, 2000
- Scaglione, S., and Vulpetti, G., *The AURORA Project: Removal of Plastic Substrate to Obtain an All-Metal Solar Sail*, Acta Astronautica, 44, No. 2-4, 147-150 (1999)
- Vulpetti, G., *3D High-Speed Escape Heliocentric Trajectories by All-Metallic-Sail Low-Mass Sailcraft*, 2<sup>nd</sup> IAA International Conference on Low-Cost Planetary Missions (Laurel, Maryland, April 1996) and Acta Astronautica, Vol. 39, No. 1-4, pp. 161-170, July-August 1996
- Vulpetti, G., *Sailcraft at High Speed by Orbital Angular Momentum Reversal*, Acta Astronautica, Vol. 40, No. 10, pp. 733-758, 1997
- Vulpetti, G., *General 3D H-Reversal Trajectories for High-Speed Sailcraft*, Acta Astronautica, Vol. 44, No. 1, pp. 67-73, 1999a
- Vulpetti, G., *The AURORA Project: Estimation of the Optical Sail Parameters*, Acta Astronautica, Vol. 44, No. 2-4, pp. 123-132, 1999b
- Vulpetti, G., *Sailcraft-Based Mission to The Solar Gravitational Lens*, STAIF-2000, Albuquerque, New Mexico, Jan-30 – Feb-3, 2000
- Vulpetti, G., *Solar Sailing: Symmetry Groups*, in progress research, 2001 (unpublished)
- Werts, G. E., Edwards, D., Hubbs, W., *Space Environmental Effects Testing and Characterization of Candidate Solar-Sail Material Aluminized Mylar*, Test Report, August 2000, Work Request WR-ED 32-243
- Wright, J. L., *Space Sailing*, Gordon and Breach Science Publishers, Amsterdam, 1993
- Ziegler, J. F., and Biersack, J. P., *SRIM-2000, Ion Beam Interactions with Matter, version 40 (Feb. 2001)*, <http://www.SRIM.org>

## **Chapter V: A Prototype Holographic Message Plaque for ISP**

Members of the International Academy of Astronautics (IAA) Committee on Space : Society, Culture, and Education suggested to committee member C Bangs, that she curate an art show in conjunction with the meeting *Missions to the Outer Solar System and Beyond, 3rd IAA symposium on Realistic Near-Term Advanced Scientific Space Missions*, in Aosta, Italy on July 3-5 2000 , chaired by Giancarlo Genta of Politecnico di Torino. Through the not-for-profit gallery/alternative-space she is affiliated with (Art Resource Transfer Inc., 210 11th Avenue, New York, NY 10011, phone : 212-691-5956), Ms. Bangs posted a "Call for Art."

Approximately 35 artists participated in this show, which was called "Messages from Earth." The premise was to show what a selection of artists would mount on an interstellar probe as a message plaque. The work was submitted on 21 X 27.5 centimeter color xeroxes. Copies of these are in the permanent collection of the Aosta City Hall. Copies of many of these pieces are permanently installed at Marshall Spaceflight Center in the office of Les Johnson, Space Transportation Directorate.

One of the participants in the Aosta IAA Symposium was Dr. Robert Forward, who suggested to Ms. Bangs that holography was a good medium for the art in an interstellar message plaque. As well as encouraging Ms. Bangs, Dr. Forward suggested to Les Johnson that some funds should be devoted to this effort.

A monochromatic hologram is produced by the interaction of two mutually-coherent laser beams. One is the unmodified original or reference beam; The second is separated from the original beam by an optical beam splitter, passed around the target object and then recombined with the original beam. The interference pattern of the two beams is recorded on a photographic plate. If the exposed photographic plate is then placed within the monochromatic reference beam, a three-dimensional photograph, or hologram, of the original object, can be viewed (Caulfield, 1979 and Saxny, 1988).

A rainbow or 'Benton' hologram utilizes the interference of two partially-coherent polychromatic beams to produce a three dimensional image of an object that can be viewed in white or polychromatic light. The "master" hologram, produced in monochromatic light is masked off to a narrow horizontal slit which forms an image hologram in which the vertical information in the master is replaced by a diffraction grating. When the image hologram is flipped, the slit image is projected close to the eye of the viewer. When the image hologram is illuminated with polychromatic light, the slit's image varies in position as a function of wavelength. The viewer sees a three-dimensional image in white light of the original object, in which the spectral hue depends upon the height of the viewpoint. Variations in the image-exposure process on the master can result in a polychromatic rainbow hologram.

It is possible to expose many "multiplexed" holographic images on the same rainbow hologram. Individual images are viewed in white light by altering the angle between the viewer and the photographic plate.

The hologram prepared by Ms. Bangs has seven independent images. One is an Apollo 16 photograph of the full Earth that is printed on acetate and serves as a backdrop to the holographic images. The six holographic images include two-

dimensional and three-dimensional representations. The four two-dimensional representations include equations of solar-sail acceleration, a representation of ISP trajectory and Earth's location in the solar system and galaxy and line drawings of two figures. These figures include an adult human male with his palm raised in greeting and an adult human female standing for scale near a representation of the ISP payload. In the spirit of the Pioneer 10 /11 message plaque (Sagan, 1975), both figures incorporate features of an amalgam of the various human races. The two three-dimensional images are sculpted and painted representations of a woman and man.

The rainbow hologram was created at the Holocenter : Center for Holographic Arts (45-10 Court Square, Long Island City, NY 11101 , phone 718-784-5065) during Spring 2001. Holocenter staff assisting with the preparation of the rainbow hologram included Sam Moree, Ana Maria Nicholson, and Dan Schweitzer. The dimensions of the holographic plate are 40 X 50 centimeters. The finished piece was framed by Simon, Liu Inc. 645 Dean Street, Brooklyn, New York 11238 (718) 638-7292. In framing the piece the acetate with the image of the Earth had to be separated from the actual hologram.

The finished and framed rainbow hologram was delivered to Les Johnson of the MSFC Space Transportation Directorate during summer 2001. Under normal illumination, all but one of the images (that being the image of the ISP trajectory and Earth location) can be readily viewed. Photographs of the images on the rainbow hologram in sunlight were shot in July 2001. Some of these are included as Fig. 5-1.

In his NASA / ASEE Summer 2001 faculty fellowship presentation, the PI attempted to estimate the information content of holographic interstellar message plaque. This estimate is partially based upon discussions with Dan Schweitzer of the Holocenter, who states that at least 30 separate multiplexed images can be exposed on one holographic plate.

Assume that the active portion of the photographic plate has dimensions 35 x 46 cm. A rainbow hologram can store three-dimensional reduced-size images. Assume that each stored image has dimensions of 2 X 2 cm and is placed on one face of a three-dimensional cube. Each multiplexed image stored on the holographic plate can include more than 250 cubes or more than 1000 reduced-size images. Since 30 separate multiplexed images can be included on one rainbow hologram, more than 30,000 separate reduced-size images can be included on one 35 x 46 cm rainbow hologram. A rainbow hologram's minimum thickness is in the micron range. John Caulfield of Fisk University suspects that a state-of-the-art holographic message plaque could accommodate as many as 300,000 reduced-size images.

### Chapter 5 References

H. J. Caulfield ed. , *Handbook of Optical Holography*, Academic, NY (1979).

C. Sagan, *The Cosmic Connection*, Dell, NY (1975).

G. Saxby, *Practical Holography*, Prentice-Hall, NY (1988).

Fig. 5-1. Photographs of Some Images on Prototype Holographic Message Plaque.

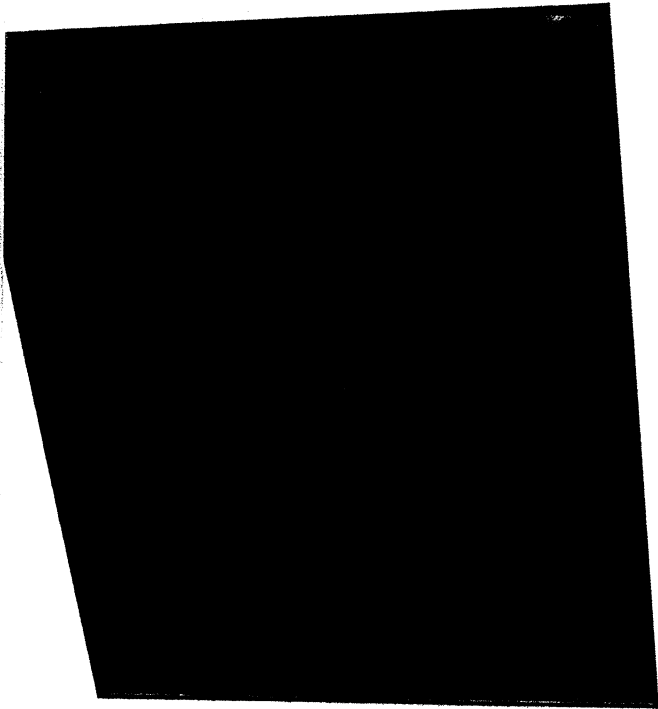
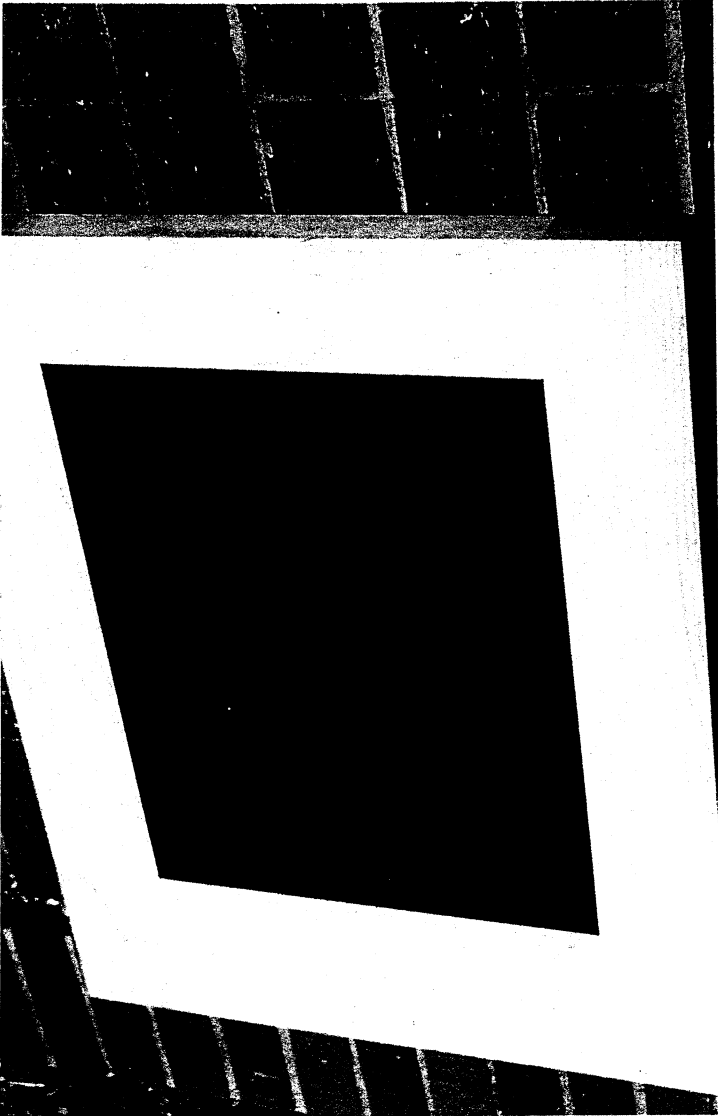
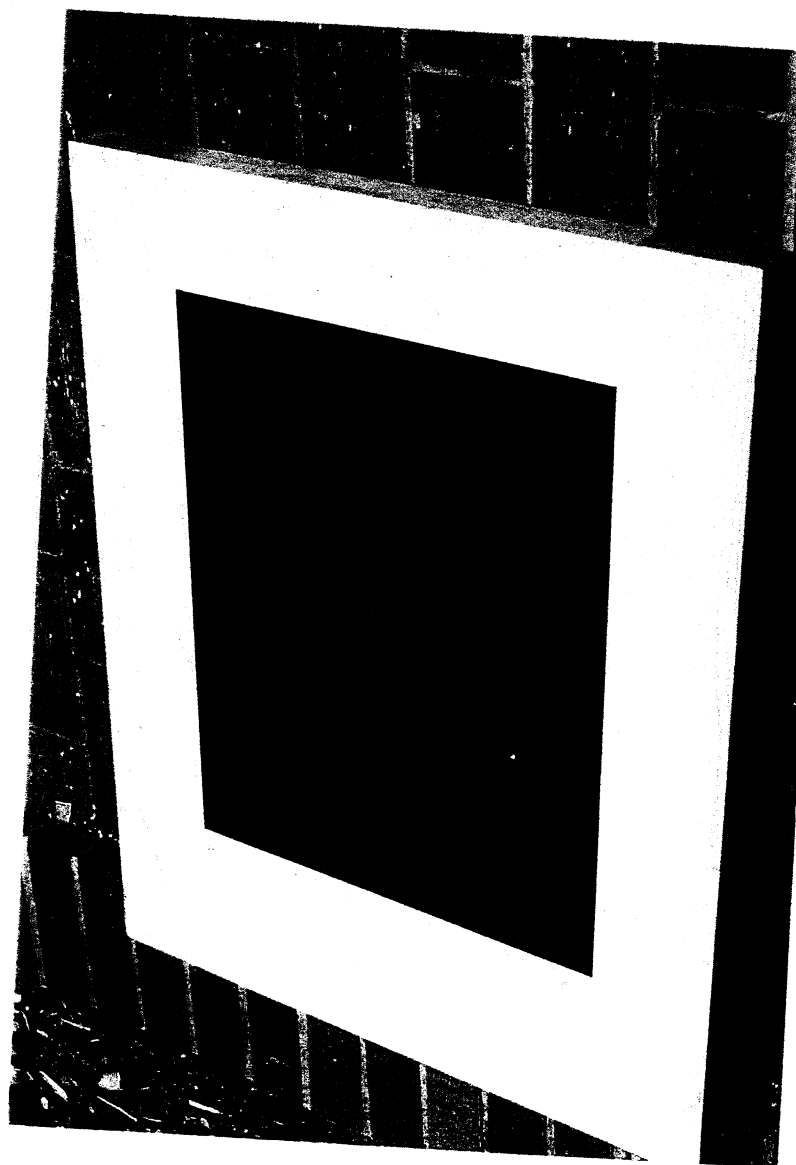
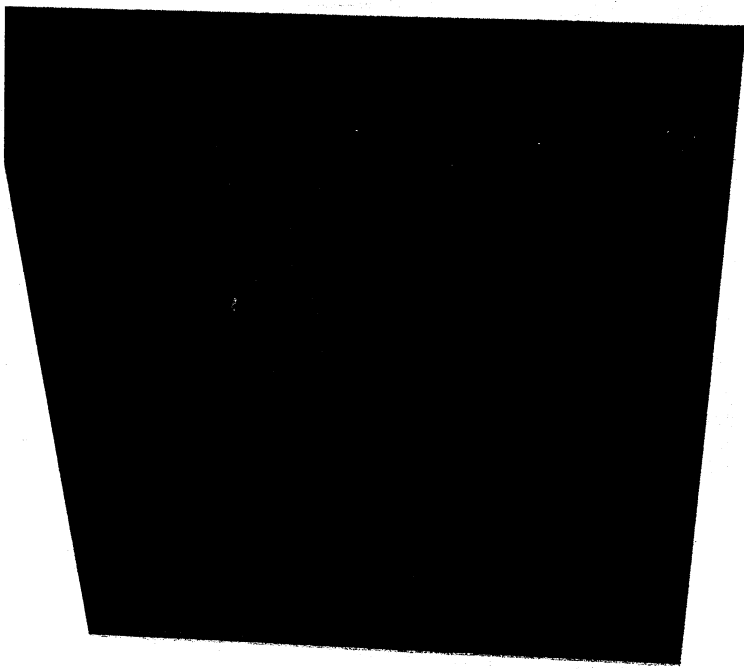


Fig. 5-1. Photographs of Some Images on Prototype Holographic Message Plaque.



## Chapter VI : Simulated Space Environmental Effects on Holograms

In early June 2001, a series of meetings took place at the Space Environment facility at NASA MSFC and the National Space Science Technology Center (NSSTC) at University of Alabama, Huntsville. Attendees included the authors of this report (with the exception of Dr. Vulpetti), members of the Space Environments team and MSFC Space Transportation Directorate, and holograph expert Dr. John Caulfield, who is currently affiliated with Fisk University.

A strategy was developed to test commercial sample white-light holograms for their resistance to simulated long-term exposure to solar-wind radiation, perform a literature search for previous studies of radiation effects on holograms, and investigate applications of holography in space in addition to the holographic message plaque described in the preceding chapter.

Most of the results of the studies are presented in this chapter. A possible application of holography to in-space propulsion is discussed in the Appendix to this report.

### VI.1 Radiation Test Strategy

The first step was to obtain commercial holographic samples. During the late winter of 2001, C Bangs discussed with staff members of the Holocenter (see Chap. 5) the availability of commercial white-light hologram samples. Following their leads, she contacted Spectratek Technologies Inc., 5405 Jandy Place, Los Angeles, CA 90066. An initial packet of sample holograms was mailed to her by Sandra Rychly of Spectratek. One application of these commercial holograms is holographic wrapping paper.

Spectratek was contacted in early June 2001 after the first set of meetings at MSFC and NSSTC. Sample holograms of many varieties were promptly mailed to the Space Environments team by Barry Levenson of Spectratek.

The following strategy was used to test the samples. It was first necessary to select a subset of holographic varieties to be tested. Samples of each variety were baked at 100 C for 48 hours under high vacuum to remove impurities, after an unbaked sample (denoted by "U") was put aside. The four Spectratek varieties selected for study were "ripple", "rain", "hyperplaid," and "sparkles"

One baked sample of each variety was then stored as the Control (or "C") sample. Samples 1, 2, and 3 of each variety were then exposed to various dosages of simulated solar-wind radiation (10, 50, and 100 Mrad respectively). Instead of utilizing alpha and proton accelerators to simulate solar-wind radiation, a high-energy electron accelerator was used and electron dosages were modeled using standard MSFC Space Environments procedures to simulate proton / alpha dosages. Ryan Haggerty will present a paper at STAIF-2002, in Albuquerque, NM, in which the procedures are discussed in greater detail.

The MSFC Space Environments plan for testing commercial white-light holograms for solar-radiation resistance is summarized in Table VI.1-1.0

**Table VI.1-1 MSFC Space Environment Team test Plan for Commercial White-Light Holograms**

**Test Plan for Hologram Testing**

1. Select 8 candidate materials
2. Identify samples to be exposed and set-aside control sheets of identical material
3. Cut samples to be exposed into squares 1.25 inch on a side
4. Perform thermo-optical measurements (alpha, emissivity, transmission)
5. Bakeout samples at 100 C for 48 hours under high vacuum
6. Perform thermo-optical measurements on baked-out samples
7. Take photographs of baked-out samples side-by-side with control samples
8. Mount 4 samples in exposure system
9. Expose samples to 1<sup>st</sup> radiation dose and UV.
10. Remove samples and perform thermo-optical measurements
11. Take photographs of exposed samples side-by-side with control samples
12. Place remaining 4 samples in exposure chamber
13. Expose samples to 1<sup>st</sup> radiation dose and UV
14. Remove samples and perform thermo-optical measurements
15. Take photographs of exposed samples side-by-side with control samples
16. Place 4 new samples in exposure chamber
17. Expose to 2<sup>nd</sup> radiation dose and UV
18. Remove samples and perform thermo-optical measurements
19. Take photographs of exposed samples side-by side with control samples
20. Place remaining 4 samples in exposure chamber
21. Expose to 2<sup>nd</sup> radiation dose and UV
22. Remove samples and perform thermo-optical measurements
23. Take photographs of exposed samples side-by-side with control samples
24. Place 4 new samples in exposure chamber
25. Expose to 3<sup>rd</sup> radiation dose and UV
26. Remove samples and perform thermo-optical measurements
27. Take photographs of exposed samples side-by-side with control samples
28. Place remaining 4 samples into exposure chamber
29. Expose to 3<sup>rd</sup> radiation dose and UV.
30. Remove samples and perform thermo-optical measurements
31. Take photographs of exposed samples side-by side with control samples
32. Select best 4 samples types
33. Place 4 samples in test chamber and expose to UV for \_\_\_hours at \_\_\_ UV suns
34. Perform thermo-optical measurements
35. Take photographs

## VI.2 Radiation Test. Quantifiable Optical Results

After sample selection, preparation, and irradiation, a number of optical tests were performed by Ryan Haggerty and the Space Environments team to quantify radiation resistance of the samples selected. Control and irradiated samples were tested for changes in fractional absorption to simulated solar electromagnetic (EM) radiation ( $\alpha$ ) and emittance ( $\epsilon = \text{emitted} / \text{absorbed solar EM}$ ).

Results are summarized in Table VI.2-1 and are described in greater detail in Haggerty's forthcoming paper at STAIF-2001. Simulated solar-wind radiation between 10 and 100 Mrad has little or no effect on the fractional solar EM absorption and emittance of the commercial white-light hologram samples tested.

**Table VI.2-1. Effects of Simulated Solar-Wind Irradiation upon Fractional Simulated Solar EM Absorption ( $\alpha$ ) and Emittance ( $\epsilon$ ) of Commercial Holographic Samples.**

$\alpha$ (10 Mrad)	Trial #1	#2	#3	#4	Avg. $\alpha$	% $\Delta$ $\alpha$ I
ripple	0.094	0.093	0.096	0.101	0.096	3.125
rain	0.127	0.121	0.116	0.117	0.120	4.575
hyperplaid	0.144	0.173	0.198	0.182	0.174	27.007
sparkles	0.138	0.123	0.146	0.139	0.137	5.182

$\alpha$ (50 Mrad)	Trial #1	#2	#3	#4	Avg. $\alpha$	% $\Delta$ $\alpha$ I
ripple	0.112	0.105	0.102	0.102	0.105	1.942
rain	0.122	0.125	0.120	0.121	0.122	2.521
hyperplaid	0.155	0.154	0.153	0.161	0.156	8.333
sparkles	0.145	0.132	0.132	0.127	0.134	4.688

$\alpha$ (100 Mrad)	Trial #1	#2	#3	#4	Avg. $\alpha$	% $\Delta$ $\alpha$ I
ripple	0.102	0.101	0.101	0.106	0.103	1.463
rain	0.123	0.121	0.119	0.119	0.121	7.589
hyperplaid	0.181	0.173	0.189	0.151	0.174	16.430
sparkles	0.129	0.133	0.132	0.138	0.133	-0.075

Control	ripple $\alpha/\epsilon$	rain $\alpha/\epsilon$	hyperplaid $\alpha/\epsilon$	sparkles $\alpha/\epsilon$
#1	0.098	0.114	0.162	0.128
#2	0.093	0.127	0.137	0.147
#3	0.103	0.119	0.144	0.128
#4	0.101	0.112	0.149	0.134
Avg. $\alpha$ I/ $\epsilon$ I	0.098	0.114	0.156	0.131
	0.099	0.117	0.150	0.134

Emittance	10 Mrad	50 Mrad	100 Mrad	Avg $\epsilon$ I
ripple	0.032	0.030	0.034	0.025
rain	0.030	0.038	0.032	0.025
hyperplaid	0.038	0.033	0.036	0.029
sparkles	0.038	0.036	0.037	0.034

### VI.3 Effects of Space Radiation on Holograms--Literature Search

On June 13 and 14, 2001, C Bangs and G. Matloff followed the advice of H. J. Caulfield of Fisk University and performed a literature search at the NASA Marshall Spaceflight Center and Redstone Scientific and Technical Information Center (RSTIC), both in Huntsville Alabama. the purpose of this search was to locate previous references in the open literature that relate to the survival of holograms in the space environment.

Three significant English-language studies were discovered. These include a 1988 paper in *Optics Letters* by J. P. Golden, G. P. Summers, and W. H. Carter, all of the US Naval research Laboratory; a 1989 *SPIE* paper by A. McKay and J. White of National Technical Systems, Inc., in Los Angeles, CA; and a 1993 report to the USAF Rome Laboratory, Air Force Material Command, Griffiss Air Force Base, New York. The Rome report was co-authored by S. P. Hotaling of Rome and G. Manivannan, R. Changkakoti and R. A. Lessard, who were all affiliated with Laval University, in Quebec, Canada.

Golden et al (1988) reported that holograms made in Polaroid DMP128 photopolymer can withstand a total dose of 2 Mrad of 63-MeV protons and 2-Mrad of  $^{60}\text{Co}$  gamma rays without loss of diffraction efficiency. Diffraction efficiency was defined by plotting incident-intensity fraction vs. diffraction angle in degrees from normal before and after exposure. Separate exposures to protons and gamma rays resulted in minimal degradation. Since a LEO satellite receives an electron / proton dose in the neighborhood of 1 Mrad per year, this material seems to be sufficiently hard for space holographic applications.

McKay and White (1989) exposed dichromated gelatin holograms to a simulated space environment including UV (ultraviolet) radiation, particle radiation and vacuum effects. The vacuum corresponded to a 500-km altitude. In the vacuum tests, a significant issue was the level of outgassing from holographic coatings. Outgassing, which was ascertained by comparing sample weight before and after exposure to vacuum conditions, amounted to only a few percent of sample weight. Most outgassing occurred during the first 24 hours of exposure and is probably do to water vapor. Charged-particle exposure utilized 4 MeV protons at fluences simulating the effects of 0.5-5 years exposure in the space environment. prior to exposure, test-sample optical density varied 4.0-4.5. Exposure to 5 years of simulated space charged-particle radiation resulted in a mean optical density loss of 1.6 and a mean loss of 0.15. this was probably do to breaking of covalent bonds and resulting changes in density and refractive index. The spectral peaks of the samples moved slightly towards the blue by about 9 nm, from a pre-exposure spectral peak of 540-550 nm. Ultraviolet effects were tested for 1104 simulated days of exposure to exo-atmospheric sunlight. The peak wavelength decreased once agin by 6-20 nm for all samples tested. for most samples tested, UV did not significantly effect optical density.

Hotaling et al (1993) considered the survivability of dichromated (vinyl alcohol) holograms in the space environment. Diffraction efficiency was used as the degradation criterion and holographic thin-films were exposed to combinations of ionizing radiation, temperature, and atomic oxygen simulating the LEO environment. A

cobalt-60 gamma-ray source was varied to produce 0, 2.5, and 10 Mrads. Once again, the combined effects resulted in no significant degradation to the optical performance of the sample holograms.

#### VI.4 Effects of Space Radiation on Holograms--A New Experimental Formalism

The previous studies discussed in the last section utilize diffraction efficiency as the operational parameter in considering radiation effects on holograms. Such an approach requires monochromatic light sources of various wavelengths to be directed upon the interference pattern that constitutes the hologram. The transmitted (or reflected) light acts as though it has interacted with a diffraction grating. Diffraction efficiency considers the relative amount of output light from the hologram in the 0<sup>th</sup>, 1<sup>st</sup>, or 2<sup>nd</sup> order of the diffraction pattern from control and irradiated sample holograms.

None of the studies cited in the previous section considers the replicability and repeatability of the experimental results. This is not surprising, since diffraction efficiency, by its very nature, has many possibilities for error. The small changes in the performance of irradiated holograms in some of the cited studies should therefore not be taken too seriously.

We therefore desired to develop a method of irradiated-hologram evaluation that would be less susceptible to experimental error and would have replicability that could be determined by experiment. The following procedure was proposed by the PI, after discussions with C Bangs and two Brooklyn, NY based artists who assisted with preparation of the prototype holographic message plaque described in Chapter V-- David Wister Lamb and Lajos Szobozlai. After discussions, the procedure was approved and implemented by Dr. David Edwards, team leader of the MSFC Space Environments Team.

After baking and irradiation, control and irradiated hologram samples were transferred (care being taken to avoid contact with human hands and other impurities) to the tray of a scanner connected to a PC (Personal Computer). The computer was equipped with Adobe Photoshop™, a software package designed for commercial and artistic image processing application.

After images of the hologram samples were scanned into Photoshop, the Image Histogram utility of the software package was activated. This allows the utility to ascertain image quality in three primary colors, R (red), B (blue), and G (green). Image quality in a selected color is quantified by the relative number of image pixels in that color. Because of the relative nature of the histogram output, it was decided to define image quality (iq) in the three primary colors as follows :

$$R_{iq} = \frac{R}{R + B + G}, \quad B_{iq} = \frac{B}{R + B + G}, \quad G_{iq} = \frac{G}{R + B + G} \quad (6-1)$$

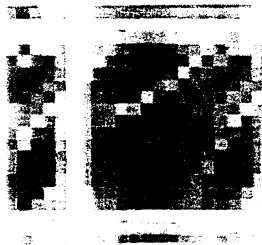
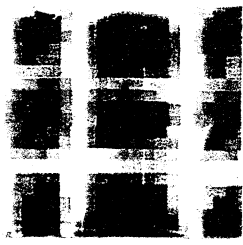
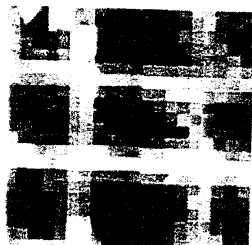
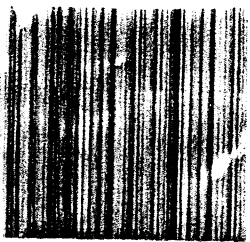
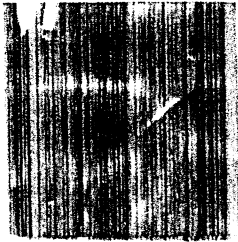
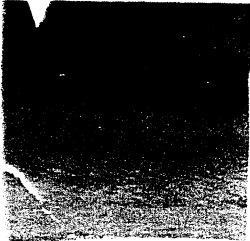
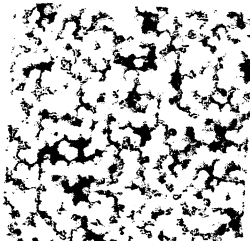
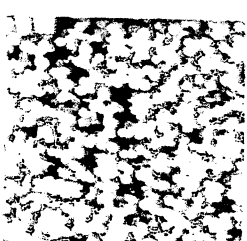
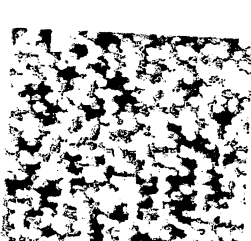
where R, B, and G here refer to the histogram pixel counts in the various colors.

In considering experimental repeatability, consideration revealed that there are two readily identifiable sources of error. Because of variations in electrical line power in the MSFC Space Environments facility, scanned-image histogram data might be slightly different from one experimental run to the next. Also, different portions of the scanner surface might have different spectral sensitivity.

VI.5 Effects of Space Radiation on Holograms-- Experiments and Repeatability

Holographic samples were prepared for scanning by Ryan Haggerty and the MSFC Space Environments team in late June 2001. In early July, the samples were scanned by C Bangs; results were evaluated by the C Bangs and the PI using the Photoshop software package. Figure 6-1 presents printouts of the scanned images of control and irradiated holograms

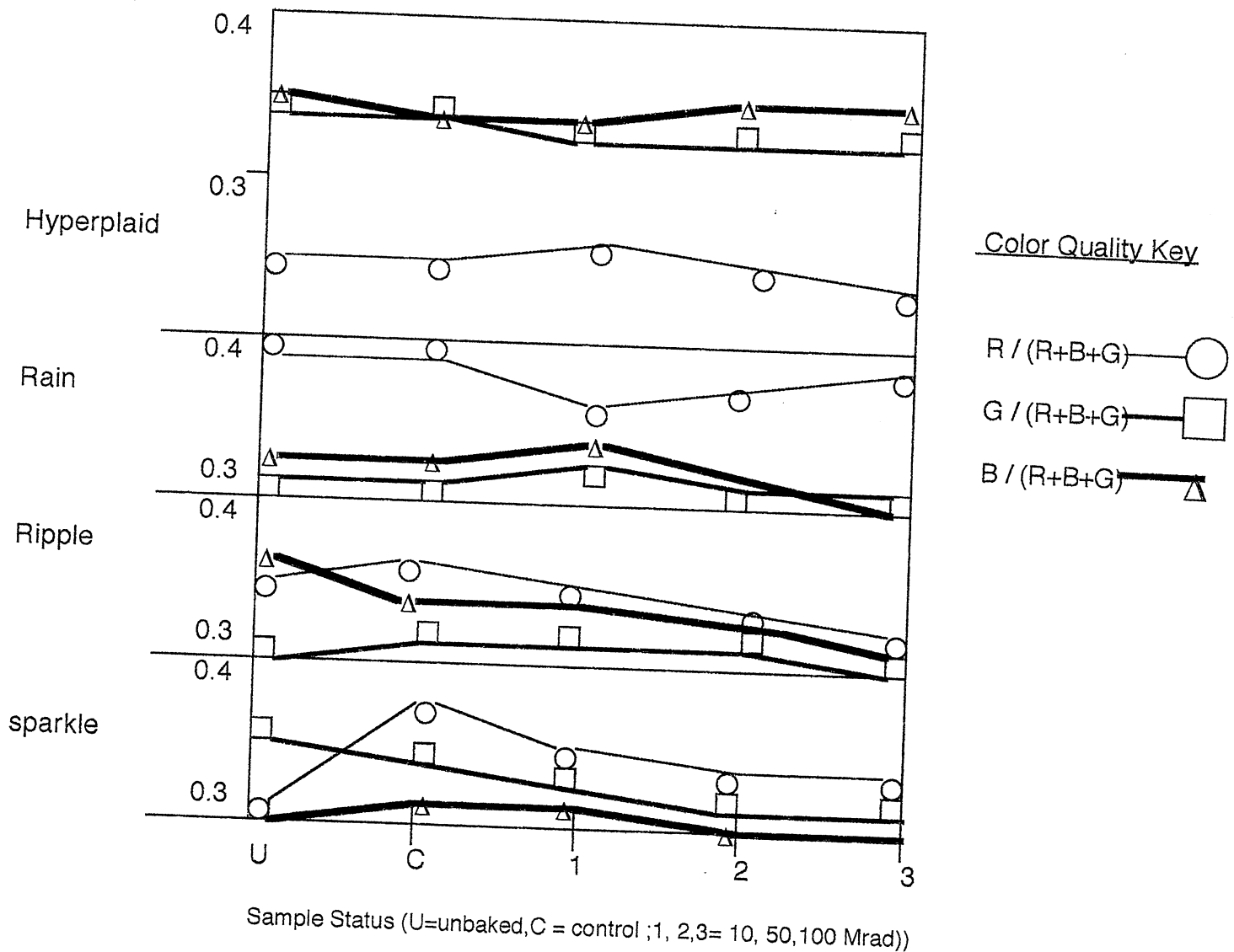
Fig. 6-1. Scanned Images of Some Control and Irradiated Commercial Holograms

<u>Variety</u>	<u>Control</u>	<u>10 Mrad Exposure</u>	<u>100 Mrad Exposure</u>
Hyperplaid			
Rain			
Ripple			
Sparkle			

The indentations on the upper left of some of the samples in Fig. 6-1 were for alignment purposes. The eye is not sensitive enough to discern differences between the control and irradiated commercial hologram samples in this figure.

After printing out the scans presented in Fig. 6-1, these scans were evaluated using the formalism presented in Section VI.4 of this chapter. Results are presented as fig. 6-2, where U = unbaked, C = control, 1 = 10 Mrad exposure, 2 = 50 Mrad exposure, and 3 = 100 Mrad exposure.

Fig. 6-2. Holographic Sample Color-Quality Variation with Irradiation



Color-quality variations with irradiation are almost always less than about 7% for the samples tested. Before considering the significance of the small variations in this quantity presented in Fig. 6-2 by repeatability investigations, we also prepared plots of mean luminosity vs. irradiation. Mean luminosity is essentially the sum of R, B, and G pixels listed in the Photoshop™ histogram. Luminosity increased with baking for Rain and Hyperplaid, and decreased with baking for Ripple and Sparkle. In all cases, small amount of electron irradiation increased luminosity. For Ripple, higher dosages had little effect on mean luminosity. Luminosity decreased with increasing irradiation for the other three samples.

We next evaluated the repeatability of this experimental procedure. This was done in two ways. **First**, a holographic sample was placed in a fixed location on the scanner. Power to the equipment was turned on, the sample was scanned and histogram results recorded. Power was then turned off and the procedure was repeated without moving the sample. In the **Second** repeatability test, power to the PC and scanner were left on and the sample was repeatedly scanned at different portions of the scanner surface. Results are summarized in Table VI.5-1.

**Table VI.5-1. Scanned Hologram Repeatability Tests.**

Test 1 : Power off/on. Hologram variety : Rain. Sample location : mid-center of scanner.

<u>Trial</u>	<u>Sample</u>	<u>Mean Luminosity</u>	<u>Mean Red (R)</u>	<u>Mean Green (G)</u>	<u>Mean Blue (B)</u>
1	Rain C	185.54	210.10	173.81	181.37
2	(control)	196.38	217.49	190.21	171.95
3		197.82	218.14	191.94	173.98
1	Rain 2	182.87	202.64	173.66	178.32
2	(50 Mrad)	197.82	218.14	191.94	173.98

Test 2: Power on . Hologram sample : Rain control (C): various scanner locations

<u>Scanner Location</u>	<u>Mean Luminosity</u>	<u>Mean Red (R)</u>	<u>Mean Green (G)</u>	<u>Mean Blue (B)</u>
mid-center	196.38	217.49	190.21	171.95
top-right	174.22	196.03	163.80	170.65
bottom-right	194.92	219.98	185.64	176.42
mid-left	212.84	224.23	210.13	195.82
bottom-left	221.22	231.61	220.49	196.80
top-left	174.22	196.03	163.80	170.65
mid-right	214.49	224.98	213.80	189.51
top-tight	174.22	196.03	163.80	170.65

Power on-off tests (Test 1 in Table VI.5-1 results in maximum experimental errors in the vicinity of 7% in R, B, and G pixel counts. Variations in sample location on the scanner results in R, B, and G experimental errors of about the same magnitude.

Care was taken in the performing the operational scans that resulted in Fig. 6-2 to keep the experimental sample as close to the center of the scanner as possible. Even so, the maximum precision of the data obtained using this technique is about 7%.

Therefore, the small variations in hologram color quality with irradiation presented in Fig. 6-2 must be considered to be insignificant. Our results are therefore in agreement with those of the cited studies from the literature. Simulated solar-wind irradiation, at least up to 100 Mrads, has little or no effect upon the quality of a commercial white-light hologram. We may reasonably expect that space-qualified holograms will do well even under much higher levels of irradiation.

#### VI.6 Effects of Space Radiation on Holograms-- Photographic Tests

A final investigation of simulated solar-wind radiation effects on commercial white light holograms was performed by NASA / MSFC photographer Emmett Given. Control and 100 MRad samples of the holographic varieties tested were photographed side-by-side using a high resolution camera and direct, overhead lighting. The results are presented as Fig. 6-3.

The photographer reported to us that control, and irradiated samples are essentially identical. The small differences between control and irradiated samples in the photographs are due to positioning of camera and lights.

#### Chapter 6 References

J. P. Golden, G. P. Summers, and W. H. Carter, "Resistance of Holograms made in Polaroid DMP128 Photopolymer to Ionizing Radiation Damage," *Optics Letters*, 13, 949-951 (1988).

A. McKay and J. White, "Effects of Simulated Space Environments on Dichromated Gelatin Holograms," *SPIE*, 1044, 269-276 (1989).

S. P. Hotaling, G. Manivannan, R. Changkakoti and R. A. Lessard, "The Performance and Survivability of Dichromated Poly (Vinyl Alcohol) Holograms for Space-Based Photonic Applications, RL-TR-93-131, Rome Laboratory, Griffiss Air Force Base, Rome, NY (July 1993).

Fig. 6.3b Photographs of Control (Top) and 100-Mrad Irradiated "Rain"

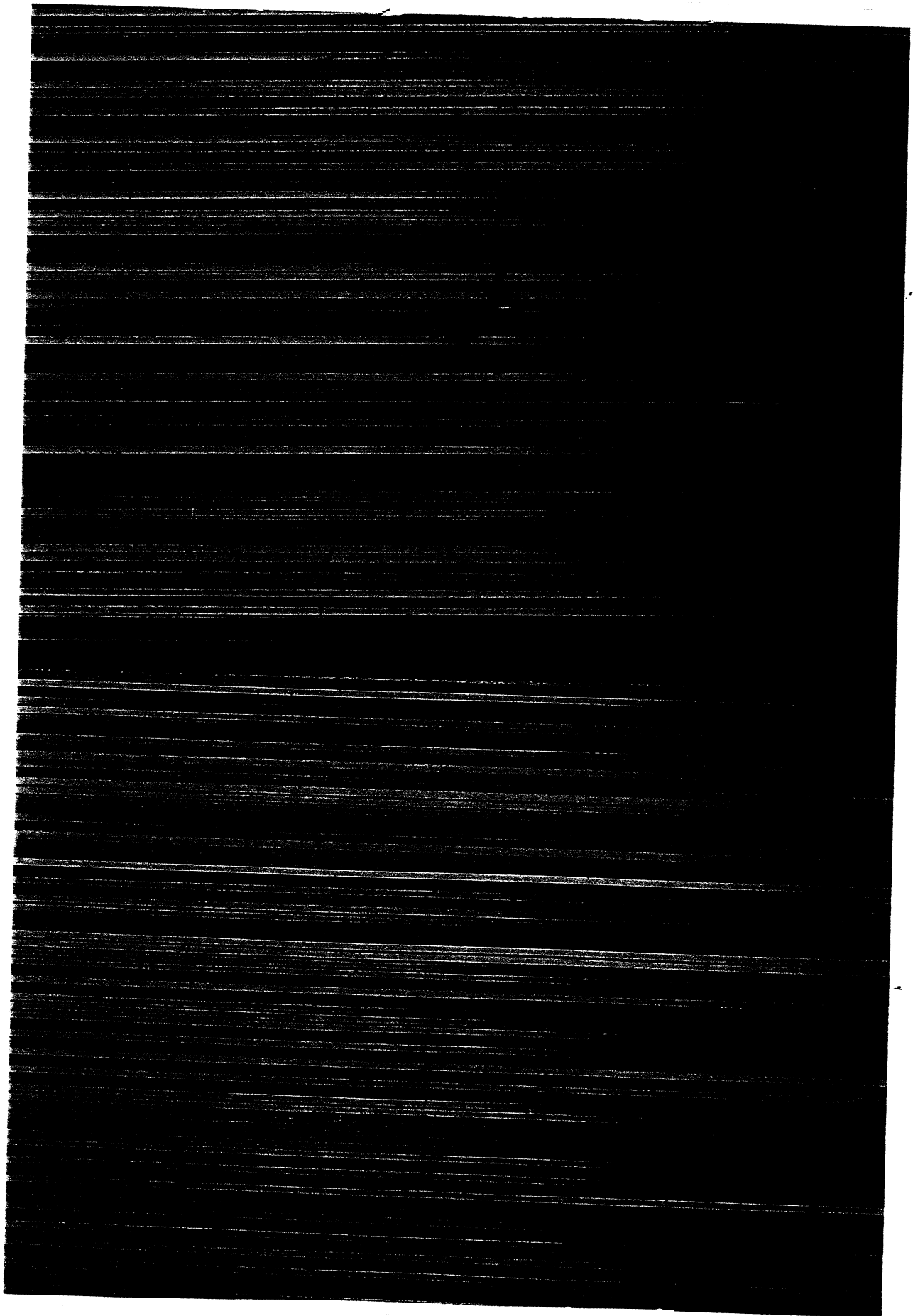
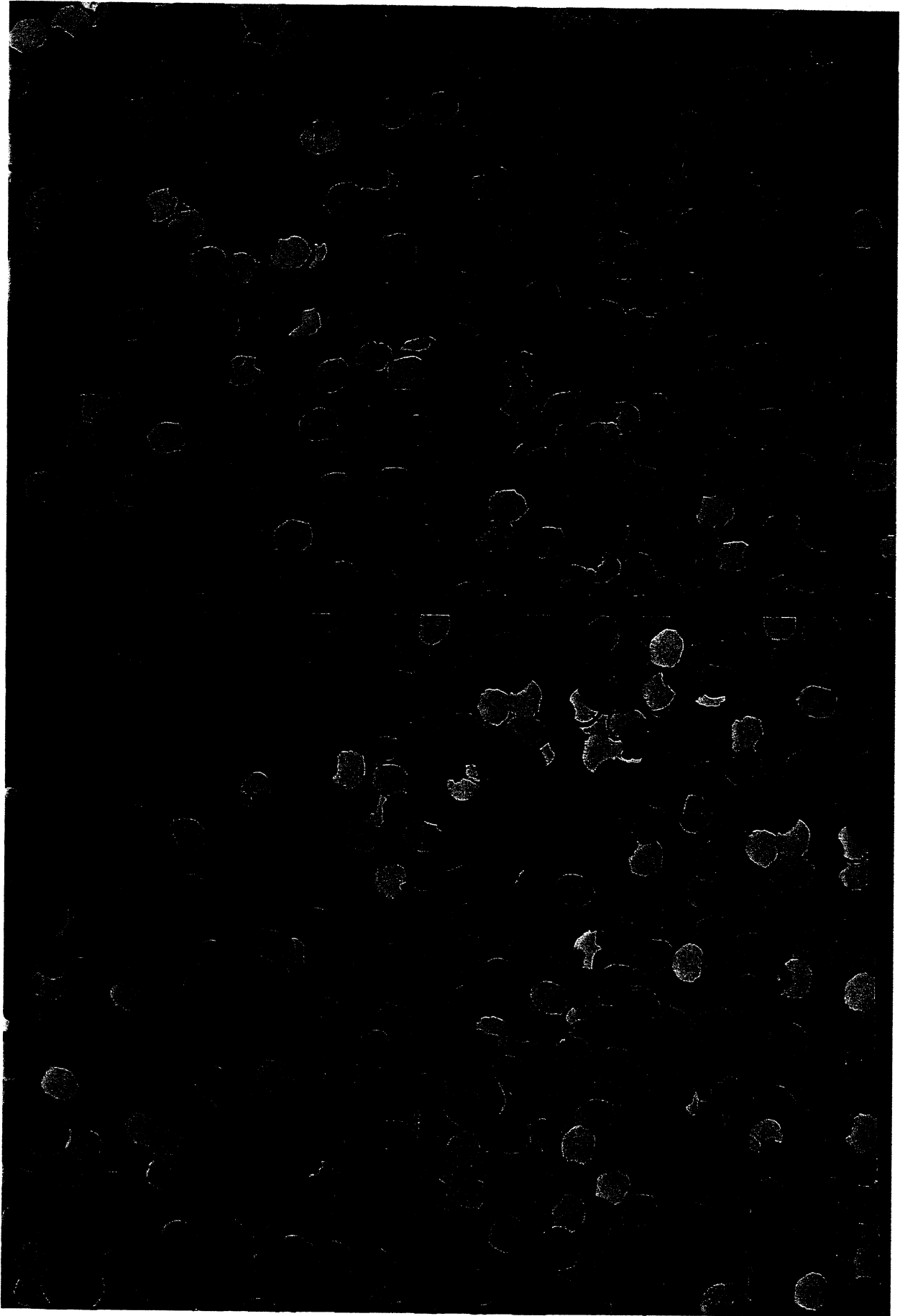


Fig. 6.3d Photographs of Control (Top) and 100-Mrad Irradiated "Sparkle"



## Chapter VII : Conclusions

Instead of merely summarizing the study results summarized in the previous chapters, this Conclusions chapter attempts to outline some directions for future research.

- (1) First, the sail-launched Interstellar Probe (ISP) mission remains feasible. Nothing in our study detracts in the slightest from the goals of this proposed mission, or demonstrates that the 2010-2015 time frame for launch is infeasible.
- (2) Mission planners should give further attention to the option of maintaining sail operation past Jupiter's orbit, unless sail interference with planned scientific experiments can be conclusively demonstrated. Not only will terminal interstellar cruise velocity increase by as much as several percent, but it is possible that the sail could be integrated into the experiment suite.
- (3) Both reverse and direct pre-perihelion sail trajectories should be considered by mission planners. This will allow two rather than one launch window per year for flights to the "nose" of the heliopause.
- (4) Mission planners at NASA / JPL and elsewhere should incorporate exact models of sail reflectance and other optical properties into their trajectory projections. Lack of including such parameterization can introduce errors approaching 10%. Approximate screening models have been useful up to the present time for rough interstellar-sail performance projections. But a more elaborate and exact model, such as that of Dr. Vulpetti's, should be applied in the next phase of mission design.
- (5) One major advantage of improved sail-trajectory models is the capability of investigating the advantages of a wide range of mission options. Vulpetti's discovery of a class of sail trajectories in which sail technological requirements can be relaxed by utilization of a higher Earth-escape velocity, is only an example of the possibilities.
- (6) Future work might consider as well the possibilities of giant-planet gravity assists in improving interstellar-sail terminal velocity. Also to be considered are the possible advantages of combining solar-proton sailing with solar-photon sailing in missions scheduled for the 2010-2015 time frame.
- (7) Construction of the prototype white-light holographic message plaque demonstrated that such a device is possible. A thin-film plaque carrying many thousands of messages is certainly very possible for the 2010-2015 time frame. Further investigations could consider the design of such a complex message plaque and its application as a unifying project of global scope. Such a project could directly involve many people in the space-exploration effort and internationalize the effort.
- (8) A series of investigations with holograms revealed that they are relatively

immune to simulated solar-wind irradiation of commercial holograms up to 100 MRad. This work included literature searches and experimental studies. It should be pointed out that the scanned and photographic evidence presented in this report does not in any way do justice to the intrinsic beauty and information-carrying capability of the holographic medium.

(9) Holography gives the capability of embossing reflective, transmissive, and absorptive layers and functional images of optical components on the same surface. The possibility of holographic applications to solar-sail propulsion should therefore not be ignored. One such application is further considered in the Appendix to this report. There may be others.

## BIBLIOGRAPHY

- A. Bond and A. R. Martin, "World Ships -- An Assessment of the Engineering Feasibility," *JBIS*, 37, 254-266 (1984).
- H. J. Caulfield ed. , *Handbook of Optical Holography*, Academic, NY (1979).
- F. Dyson, "Interstellar Transport," *Physics Today*, 21, No. 10, 41-45 (October, 1968).
- R. L. Forward, "Solar Photon Thruster," *J. Spacecraft*, 27, 411-416 (1990).
- G. Genta and E. Brusca, "The Aurora Project " A New Sail Layout : *Acta Astronautica*, 44, 141-146 (1999).
- R. Haggerty and T. Stanaland, "Application of Holographic Film in Solar Sails," to be delivered, STAIF-2002, Albuquerque, NM 9Feb. 3-7, 2002).
- J. Heidmann and C. Maccone, "ASTROsail and SETIsail : Two Extrasolar System Missions to the Sun's Gravitational Focus," *Acta Astronautica*, 37, 409-410 (1994).
- L. D. Jaffe, C. Ivie, J. C. Lewis, R. Lipes, H. N. Norton, J. W. Sterns, L. D. Stimpson, and P. Weissman, "An interstellar Precursor Mission," *JBIS*, 33, 3-26 (1980).
- L. Johnson, "Options for Interstellar Probe," private communication, June, 2001
- L. Johnson and S. Leifer, "Propulsion Options for Interstellar Exploration," AIAA-2000-3334.
- P. C. Liewer, R. A. Mewaldt, J. A. Ayon, C. Garner, S. Gavitt, and R. A. Wallace, "Interstellar Probe using a Solar Sail : Conceptual Design and Technological Challenges," presented at COSPAR Colloquium, *The Outer Heliosphere : The Next Frontier*, Potsdam, Germany, July 24-28, 2000.
- C. Maccone, "Sun-Lensing the Cosmic Microwave Background from 763 AU by Virtue of NASA's Interstellar Probe," in *Missions to the Outer Solar System and Beyond : Third IAA Symposium on Realistic Near-Term Advanced Scientific Space Missions*, Aosta, Italy, July 3-5, 2000, ed. G. Genta, Levrotto & Bella, Torino, Italy (2000).
- E. Mallove and G. L. Matloff, *The Starflight Handbook*, Wiley, NY (1989).
- A. R. Martin, ed., "Project Daedalus : The Final Report on the BIS Starship Study," supplement to *JBIS* (1978).
- A. R. Martin, "World Ships -- Concept, Cause, Cost, construction, and Colonization," *JBIS*, 37, 243-253 (1984).

G. L. Matloff, "Interstellar Solar Sails : Consideration of Real and Projected Sail Materials," *JBIS*, 37, 135-141 (1984).

G. L. Matloff, "interstellar Solar Sails : Projected Performance of Partially Transmissive Sail Films," IAA-97-IAA.4.1.04

G. L. Matloff, *Deep-Space Probes*, Springer-Praxis, Chichester, UK (2000).

G. L. Matloff and K. Parks, "Hyperthin and Perforated Solar Sails in Low Earth Orbit (LEO) : A Step to the Moon, Mars, and Beyond," AIAA-89-2442

G. L. Matloff and E. Mallove, "Solar Sail Starships : the Clipper Ships of the Galaxy," *JBIS*, 34, 371-380 (1981).

G. L. Matloff and E. Mallove, "The Interstellar Solar Sail : Optimization and Further Analysis," *JBIS*, 36, 201-209 (1983).

C. R. McInnes, *Solar Sailing -- Technology, Dynamics, and Mission Applications*, Springer-Praxis, Chichester, UK (1999).

R. A. Mewaldt and P. C. Liewer, "An Interstellar Probe Mission to the Boundaries of the Heliosphere and Nearby Interstellar Space, presented at Space 2000, Sept. 19-21, 2000, Long Beach, CA.

C. Sagan, *The Cosmic Connection*, Dell, NY (1975).

G. Saxby, *Practical Holography*, Prentice-Hall, NY (1988).

S. Scaglione and G. Vulpetti, "The AURORA Project : Removal of Plastic substrate to Obtain an All-Metal Solar Sail," *Acta Astronautica*, 44, 147-150 (1999).

W. K. Stuckey and M. J. Meshishnek, "Solar Ultraviolet and Space Radiation Effects on Inflatable Material," Aerospace Report TR-2000 (8565)-9, August 20, 2000.

G. Vulpetti, "The Aurora Project : Flight Design of a Technology Demonstration Mission," in *Missions to the Outer Solar System and Beyond*, 1st IAA Symposium on Realistic, Near-Term Scientific Space Missions, ed. G. Genta, Levrotto & Bella, Turin, Italy (1996), pp 1-16.

G. Vulpetti, "3D High-Speed Escape Heliocentric Trajectories by All-Metal Sail, Low-Mass Sailcraft," *Acta Astronautica*, 39, 161-170 (1996).

G. Vulpetti, "Sailcraft at High Speed by Orbital Angular Momentum Reversal," *Acta Astronautica*, 40, 733-758 (1997).

G. Vulpetti, "General 3D H-Reversal Trajectories for High-Speed Sailcraft, *Acta Astronautica*, 44, 67-73 (1999).

G. Vulpetti, "The Aurora Project : Estimation of the Optical Sail Parameters," *Acta Astronautica*, 44, 123-132 (1999).

G. Vulpetti, "Sailcraft-Based Mission to the Solar Gravitational Lens," STAIF-2000, Albuquerque, NM, Jan. 30-Feb. 3, 2000.

G. Vulpetti, "Solar-Sailing : Symmetry Groups," unpublished (2001).

G. E. Werts, D. Edwards, W. Hubbs, " Space Environmental Effects Testing and Characterization of Candidate Solar-Sail Material Aluminized Mylar," NASA / MSFC Test Report, Work Request WR-ED 32-243, August 2000.

J. L. Wright, *Space-Sailing*, Gordon and Breach, Philadelphia, PA (1993).

J. F. Ziegler and J. P. Biersack, " SRIM-2000, Ion Beam Interactions with Matter," version 40 (Feb. 2001) [http : //www. SRIM.org](http://www.SRIM.org)



## **APPENDIX : A NEAR-EARTH APPLICATION FOR HOLOGRAPHIC SOLAR SAILS**

The following pages present use of the solar photon thruster (a multi-sail solar sail that can redirect the reflected photon vector) with holographic optical elements to allow solar-sail operation between low Earth orbit (LEO) and higher drag-free orbits. The color graphic was prepared for the PI by NASA / MSFC artist Bruce Shelton, senior media developer with Computer Sciences Corporation, in consultation with C Bangs.

A number of presentations at NASA / MSFC and NSSTC during the summer of 2001 featured the following pages. The audiences included Randy Baggett, Helen Cole, John Cole, Les Johnson and Jonathan Jones of NASA / MSFC and John Caulfield of Fiske University.

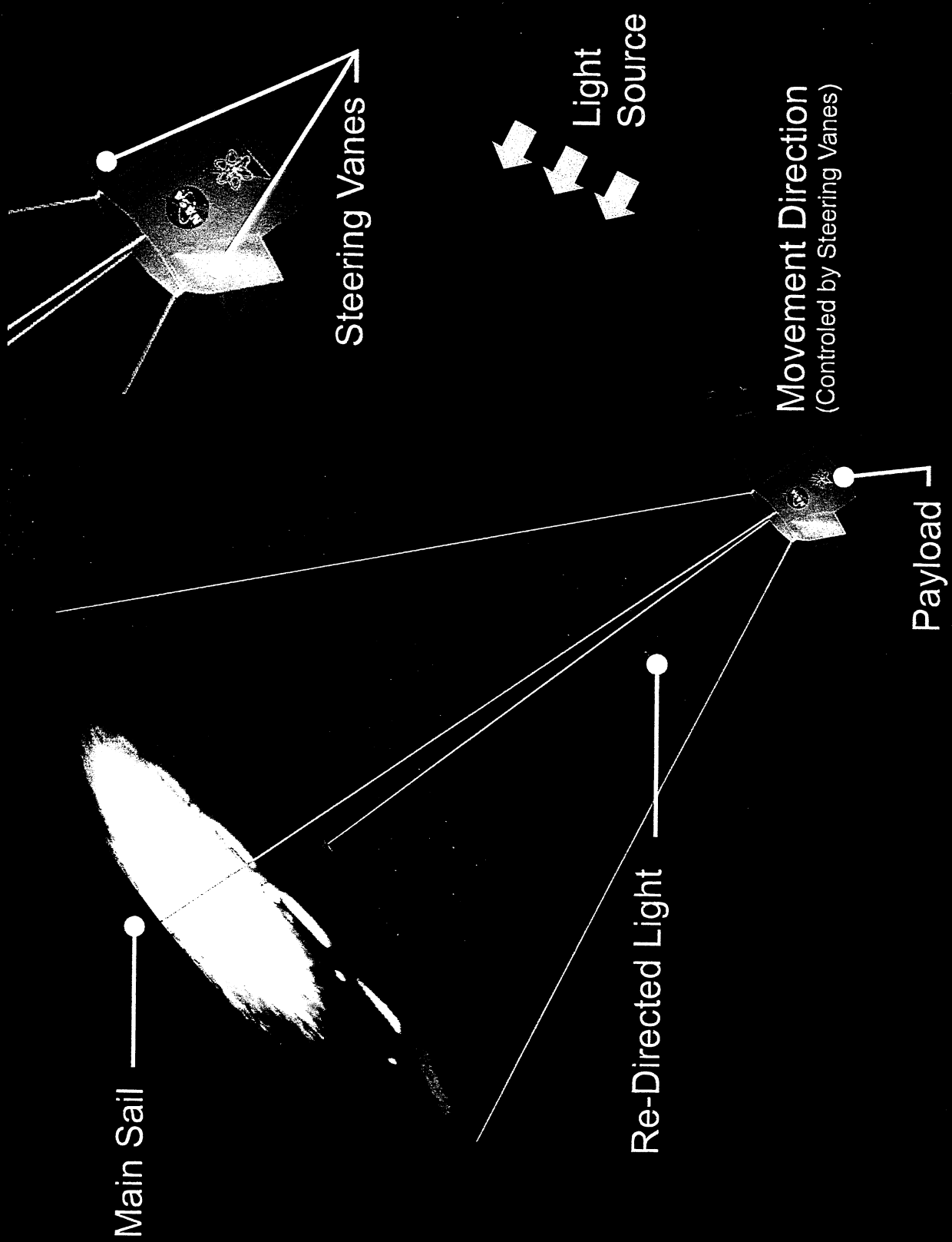
Jonathan Jones pointed out a dynamical issue with the solar-photon thruster as configured here, utilized in the high-atmospheric-drag environment of LEO, about 500 km above Earth's surface. Namely, the reflected photon radiation-pressure and atmospheric-drag vectors do not operate along the same line. This would result in a torque.

One way of correcting this problem would be to incorporate additional reflectors such that the photon exhaust is co-planar with the sail. This would introduce additional complexity and slightly degrade projected performance.

Figure AP-1 presents another possibility, as suggested by John Caulfield. Holographic images of corner-cube reflectors could be incorporated in a holographic main sail. These could, in principle, rotate the photon stream by 90 degrees within the main sail, removing the necessity for additional thruster elements.

Figure AP-1 was prepared by the PI. With the exception of the color graphic, all other Appendix figures were created by C Bangs or with the assistance of C Bangs

# Holographic Solar-Proton Thruster



# The Holographic Solar-Photon Thruster

Dr. Greg Matloff, summer 2001 MSFC / ASEE Faculty Fellow

Original solar-photon thruster idea was proposed by Forward (see Ref. 1)

Rainbow Holograms are white-light transmission holograms.

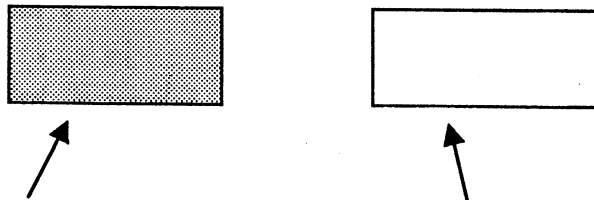
This means that the reconstruction beam is on side of plate opposite viewer.

Holographic images can be very reflective, highly radiation resistant, and of micron thickness

Many holographic images can be stored on a single plate. This means that an angular shift of a few degrees relative to the light source can dramatically alter optical properties.

## SPACE APPLICATIONS :

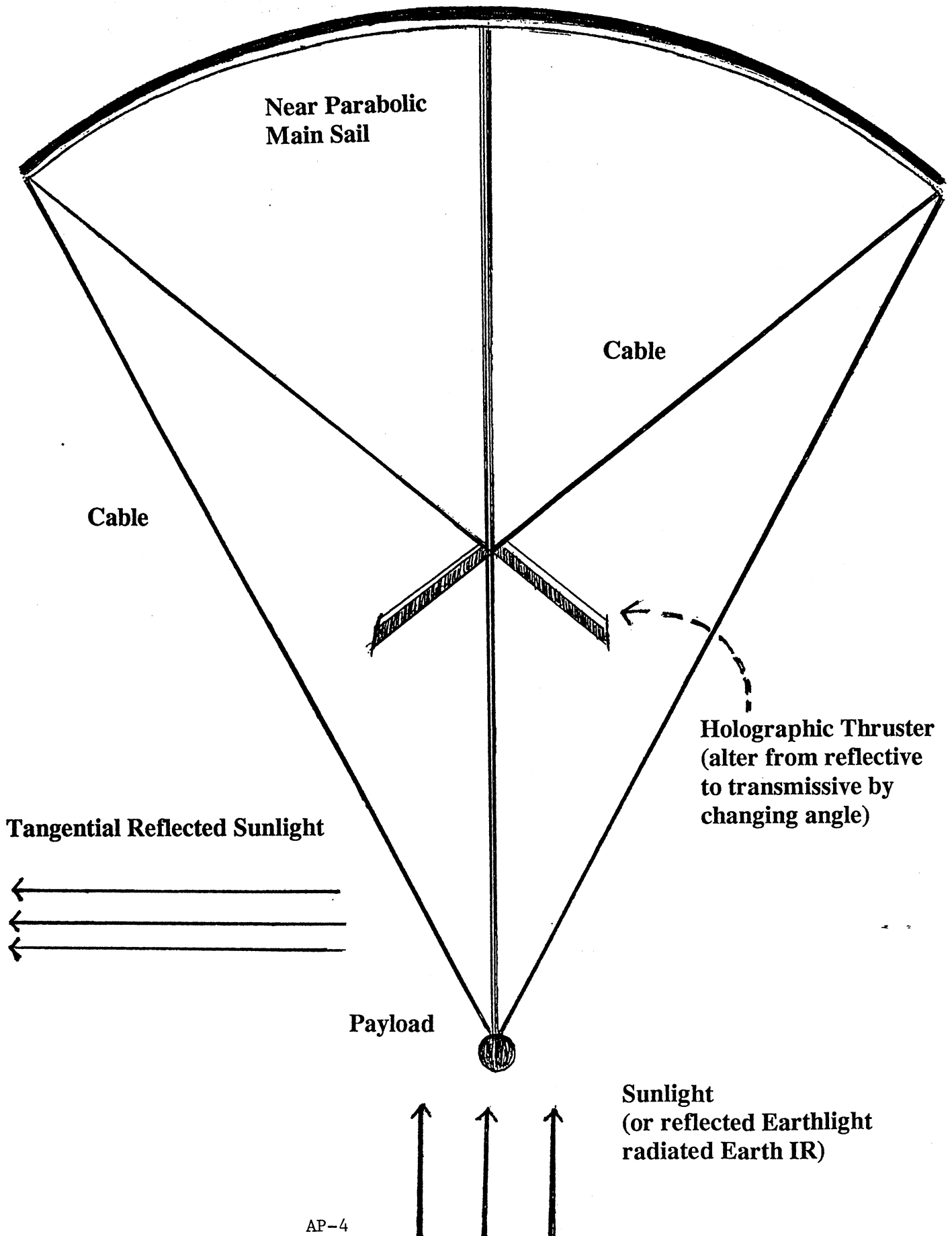
1. **Attitude Control:** steering vanes affected by solar radiation pressure that change reflectivity when slightly rotated



Example : absorptive hologram changes to reflective after a 5 degree rotation. Photons off reflective vane transfer as much as 2X momentum than those off absorptive vane.

2. **Primary propulsion :** sail can be used to implement Trailblazer mission (effectively unfurl rapidly near Sun) or for LEO—GEO orbit raising if configured as a solar-photon-thruster (SPT). In LEO (about 500 km), a primary parabolic reflector focuses light on a much smaller thruster element, which allows for a tangential thrust component. The thruster element would be holographic, so that a small rotation could change reflection to transmission. As well as curvature, holographic Fresnel Lenses could be used to focus light on thruster element. To reduce atmospheric drag, main sail would be normal to direction to earth center. Top of main sail would be emissive, bottom reflective to visual and IR. This reduces direct solar back pressure and increases acceleration by reflected Earthlight and reradiated solar energy absorbed by the Earth

**HOLOGRAPHIC SOLAR PHOTON THRUSTER :  
(Alternative Configuration)**



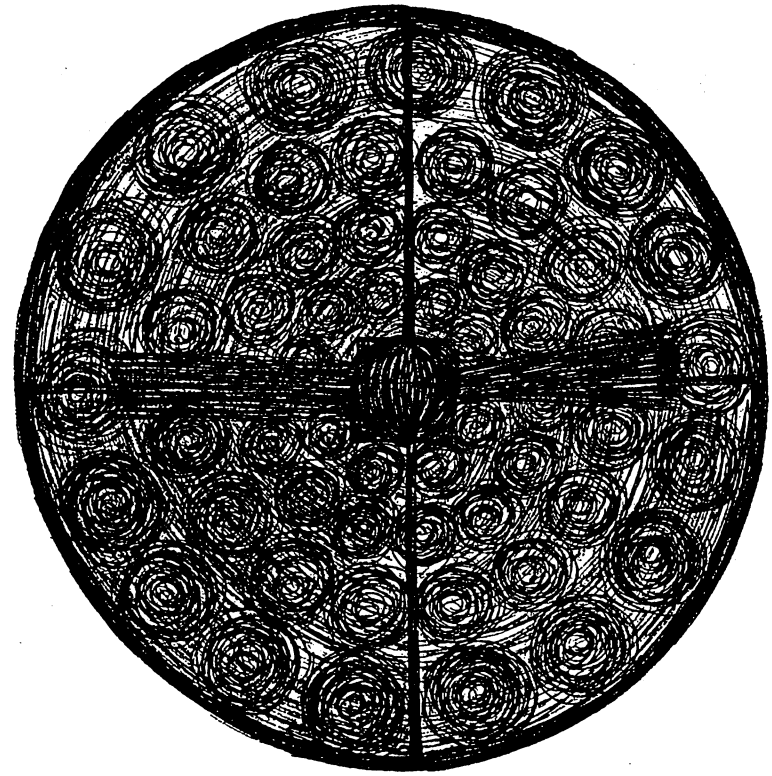
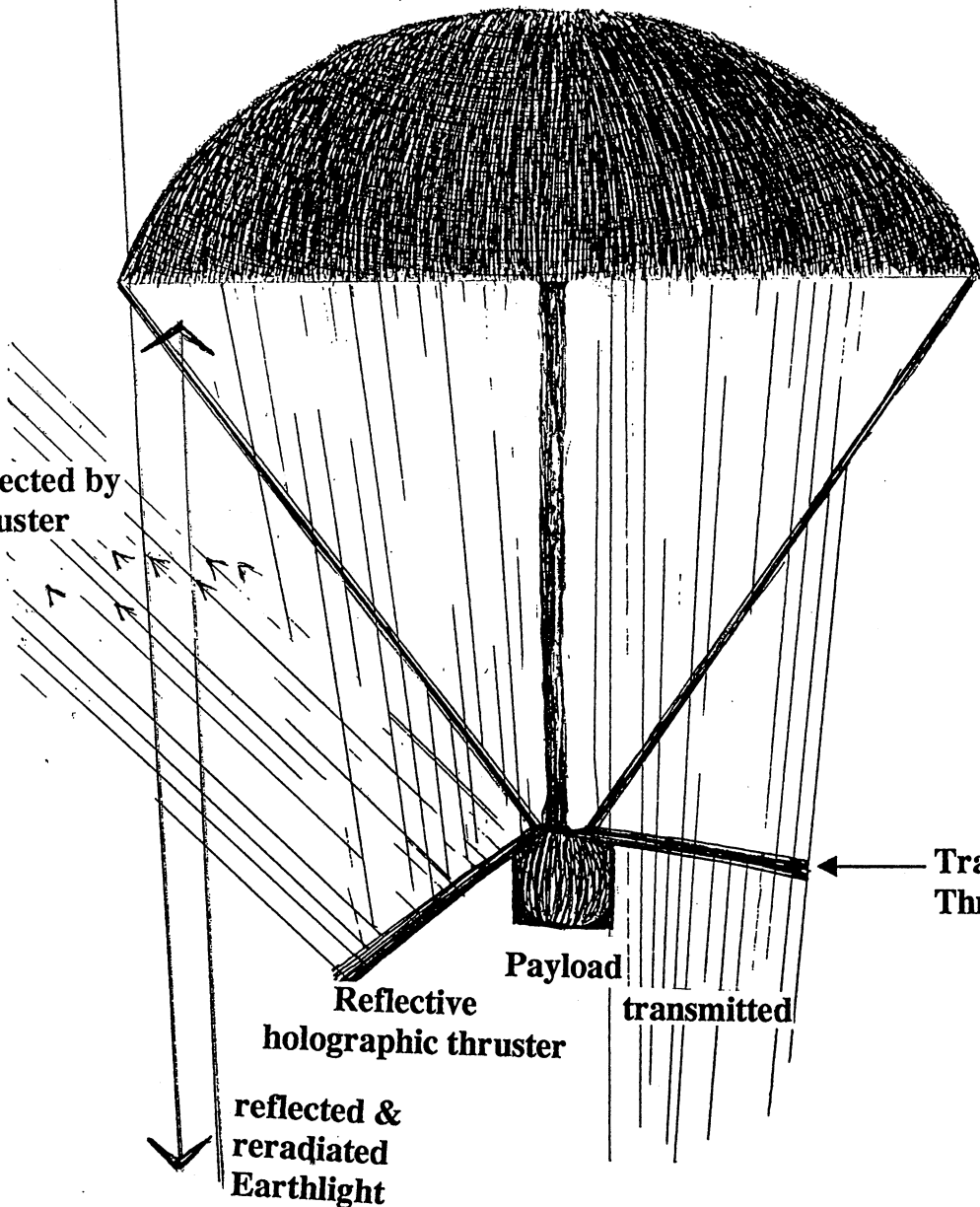
Direct insolation  
(zenith Sun)

Dark emissive layer on main sail top

Spacecraft velocity and tangential  
acceleration

AP-5

Reflected by  
Thruster



reflected &  
reradiated  
Earthlight

Transmissive holographic  
Thruster

Reflective (lower)  
Main sail layer &  
holographic Fresnel  
lenses

*Holographic Solar-Photon Thruster*

**SPT Operation Between LEO and GEO : A Comm-Sat Tug :**

**THREE ORBITAL POSITIONS , Three photon streams (P)**

- $P_1 = S =$  direct solar insolation (solar constant) = 1368 watt /m<sup>2</sup>  
 $P_2 = A_e S =$  Earth-reflected sunlight ,  $A_e =$  Earth albedo  
 $P_3 = (1-A_e) S =$  solar radiation absorbed by Earth and later reradiated as IR  
 $K_1 =$  reflectivity of emissive, upper main sail to direct solar insolation  
 $K_2 =$  reflectivity of lower reflectivemain sail to  $P_2$   
 $K_3 =$  reflectivity of lower reflective main sail to  $P_3$   
**RF =** radial force on main sail  
**TF =** tangential force on thruster (90% reflective, 45 degree angle)  
 $c =$  speed of light ,  $A_s =$  area of main sail

**Position 1 : Zenith Sun**

Turn thruster off  
to reduce downward  
radial force

$$RF = [-(1+K_1) + A_e (1+K_2) + (1-A_e) (1+K_3)] SA_s / c$$

**Position 2 : Nadir Sun**

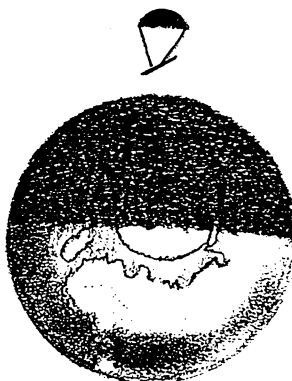
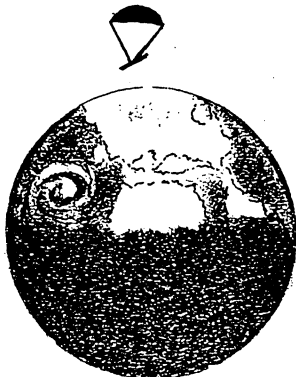
No direct sunlight  
since it's night  
Turn thruster off  
to reduce net  
downward radial  
force on thruster  
(0.7RF)

$$RF = [(1-A_e) (1+K_3)] SA_s / c$$

**Position 3 / 4 : Dawn/Dusk Sun**

No direct sunlight on  
main sail  
Dawn direct Sun on  
thruster cancels dusk  
direct Sun on thruster

$$RF = [A_e / 2 (1+K_2) + (1-A_e) (1+K_3)] SA_s / c$$



**SPT Operation Between LEO and GEO : A Comm-Sat Tug :**

**THREE ORBITAL POSITIONS , Three photon streams (P)**

$P_1 = S =$  direct solar insolation (solar constant) = 1368 watt /m<sup>2</sup>

$P_2 = A_e S =$  Earth-reflected sunlight ,  $A_e =$  Earth albedo

$P_3 = (1-A_e) S =$  solar radiation absorbed by Earth and later reradiated as IR

$K_1 =$  reflectivity of emissive, upper main sail to direct solar insolation

$K_2 =$  reflectivity of lower reflectivemain sail to  $P_2$

$K_3 =$  reflectivity of lower reflective main sail to  $P_3$

RF = radial force on main sail

TF = tangential force on thruster (90% reflective, 45 degree angle)

$c =$  speed of light ,  $A_s =$  area of main sail

**Position 1 : Zenith Sun**

**Position 2 : Nadir Sun**

**Position 3 / 4 : Dawn/Dusk Sun**

-----  
 Turn thruster off  
 to reduce downward  
 radial force

-----  
 No direct sunlight  
 since it's night  
 Turn thruster off  
 to reduce net  
 downward radial  
 force on thruster  
 (0.7RF)

-----  
 No direct sunlight on  
 main sail  
 Dawn direct Sun on  
 thruster cancels dusk  
 direct Sun on thruster

$$RF = [-(1+K_1) + A_e (1+K_2) + (1-A_e) (1+K_3)] SA_s/c$$

$$RF = [ (1-A_e) (1+K_3)] SA_s/c$$

$$RF = [A_e/2 (1+K_2) + (1-A_e) (1+K_3)] SA_s/c$$

**ESTIMATING RADIAL FORCE**, let  $K_1=0.5$ ,  $K_2=K_3=0.9$ ,  $A_e = 0.4$ ,  $1-A_e=0.6$

Radial Force (RF) on thruster = - 0.7 Radial Force on main sail from reflected and reradiated Earthlight, for 45 degree angle

(Actually slightly smaller if thruster is 90% reflective)

**POSITION 1**:  $RF_1 = [SA_s/c] [-1.5 + 0.4 (1.9) + 0.6 (1.9)] = 0.4 SA_s/c$  {ZENITH SUN}

If thruster is on, net radial force on s/c = -0.7  $SA_s/c$

**POSITION 2** :  $RF_2 = 0.6 (1.9) SA_s/c = 1.14 SA_s/c$  . If thruster is on,  $RF_{net,2} = 0.3 SA_s/c$

**POSITION 3/4** :  $RF_{net,3} = 0.3 [0.2 (1.9) + 0.6(1.9)] = 0.5 SA_s/c$

If thruster is off in POSITIONS 1 and 2, average RF for an orbit is about 0.43  $SA_s/c$

If thruster is always on, average RF for an orbit is about 0.17  $SA_s/c$ .

**TANGENTIAL FORCE** =  $\cos(\text{degrees}) \times$  average radial force from  $P_2$  &  $P_3$ .

Average tangential force per orbit—average for positions 1,2,3,4

Average tangential force per orbit is about  $SA_s/c$

**Average Tangential Acceleration** is about  $SA_s/(M_{s/c} c)$ , where  $M_{s/c}$  is spacecraft mass.

---

**Three Possible SPT Configurations**—all with sail mass = 1/3 s/c mass, s/c areal mass thickness = 6 grams per square meter

-----

CASE 1 : DEMO flight---10 kg payload, 5 kg, sail-radius = 16 m

CASE 2 : Microsat – 500 kg payload mass, 250 kg sail mass, sail radius = 115 m

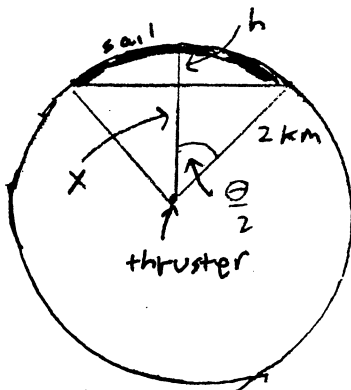
CASE 3 : Large Com Sat – 10000 kg payload, 5000 kg sail mass, sail radius = 515 m

If Fresnel Lenses are not used, we require a parabolic main sail—

Focal length = 0.5 (radius of curvature).

**ATMOSPHERIC DRAG ESTIMATE IN LEO**

Assume 500-m sail diameter. Use spherical approximation for sail shape. Assume 2 km sail-thruster distance.



$\theta/2 = 0.25/2 = 0.125$  radians = about 7.2 degrees

$\cos(\theta/2) = x/2000$ ,  $x = 1984$  m,  $h = 16$  m

cross-sectional area ( $A_{cr}$ ) seen by Earth's atmosphere is approximately 0.5 (16) (500) or 4000  $m^2$ .

From Ref. 2, LEO atmospheric-drag deceleration is  $-0.5 C_d A_{cr} \rho V_s^2 / M_{s/c}$ , where  $\rho$  is atmospheric density,  $C_d$  is drag coefficient (2—2.3) and  $V_s$  is spacecraft orbital velocity. We assume a 500-km minimum SPT operational orbital height, the maximum Shuttle orbit. At 500 km, is about  $10^{-12}$  kg/m<sup>3</sup> (From Ref. 1 and TRW *Space Data*. Drag deceleration is about  $10^{-4}$  m/sec<sup>2</sup>, since s/c orbital velocity is about 8 km/sec. Assuming a 3,500 kg spacecraft mass, drag deceleration is about 1/3 orbitally-averaged tangential acceleration.

Spacecraft requires about 200 days to go from LEO orbital velocity to Earth-escape velocity. This is an overestimate because at orbital heights greater than 1000 km or so, atmospheric drag becomes minimal. Sail can be rotated to use direct insolation for acceleration at these heights.

### THERMAL LIMITATIONS ON THRUSTER SIZE

From Chap. 2 of Ref. 3, solar power per unit area absorbed by the thruster is  $S (A_s / A_{th}) \{1 - R_{th}\}$ , where  $S$  is the solar constant,  $A_s$  is sail area,  $A_{th}$  is thruster area, and  $R_{th}$  is thruster reflectivity. Remembering that solar flux absorbed by the sail is absorbed by one sail face but emitted by two and applying blackbody theory, the thruster blackbody temperature can be expressed:

$$T_{th} = \{[S/(2\sigma)] (A_s / A_{th}) \{1 - R_{th}\}\}^{0.25} \text{ degrees Kelvin}$$

Where  $\sigma$  is the Stefan-Boltzmann Constant =  $5.67 \times 10^{-8}$  watt /m<sup>2</sup>-K<sup>4</sup>

If the sail/thruster area ratio is 10, 100, 1000, 10000, and 100000, the maximum thruster blackbody temperature is respectively 330, 588, 1045, 1860, and 3307 degrees Kelvin. For an aluminum thruster, maximum sail / thruster area is about 100. For an advanced thruster made out of 3000 degree Kelvin material, maximum sail / thruster area is about 100,000.

### REFERENCES

1. R. L. Forward, "Solar Photon Thruster," *J. Spacecraft*, 27, 411-416 (1990).
2. G. L. Matloff and K. Parks, "Hyperthin and Perforated Solar Sails in Low Earth Orbit (LEO) : A Step to the Moon, Mars, and Beyond," AIAA-89-2442.
3. G. L. Matloff, *Deep-Space Probes*, Springer-Praxis, Chichester, UK (2000).

## A POSSIBLE SPT ORIENTATION, for ORBITAL HEIGHT > 1000 KM

Above orbital heights 1000 km, SPT atmospheric drag becomes minimal. One way to accelerate the spacecraft tangentially is to turn off the thruster and rotate main sail so that the reflective side is always normal to the Sun, for every orbital "afternoon", as shown. Since the spacecraft spends half its time in daylight and positive-energy tangential solar radiation pressure acceleration is possible for half of every daylight pass, the tangential acceleration averaged over every orbit is approximately

$$(1+K_2) S A_s / (4 c M_{s/c}),$$

or about  $2.17 \times 10^{-6} A_s / M_{s/c}$  meters per second squared. If the thruster is activated for part of the orbit, the average acceleration will be increased. For heights not much greater than a few thousand kilometers, reflected and reradiated Earthshine will provide some additional positive tangential acceleration possibilities for the SPT.

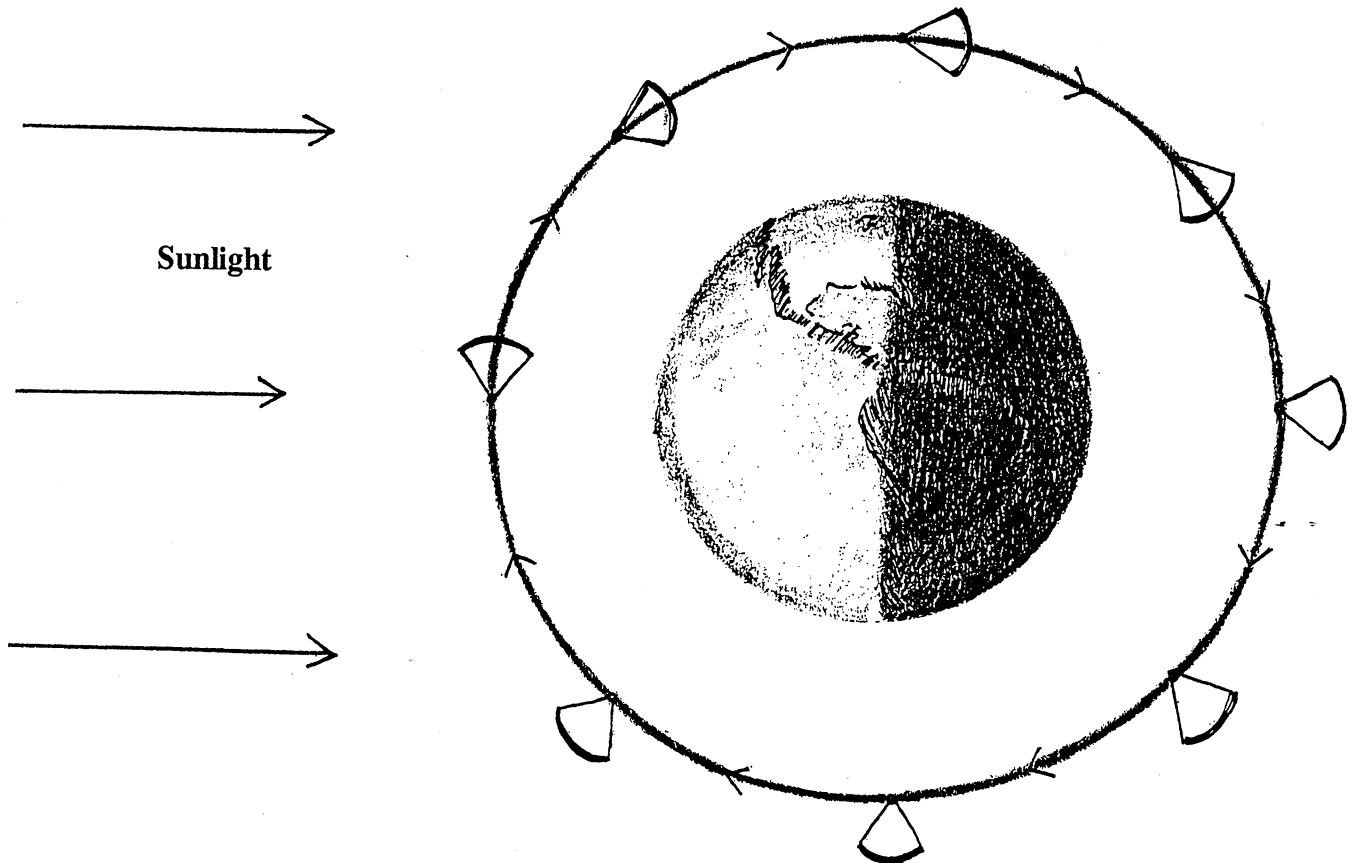
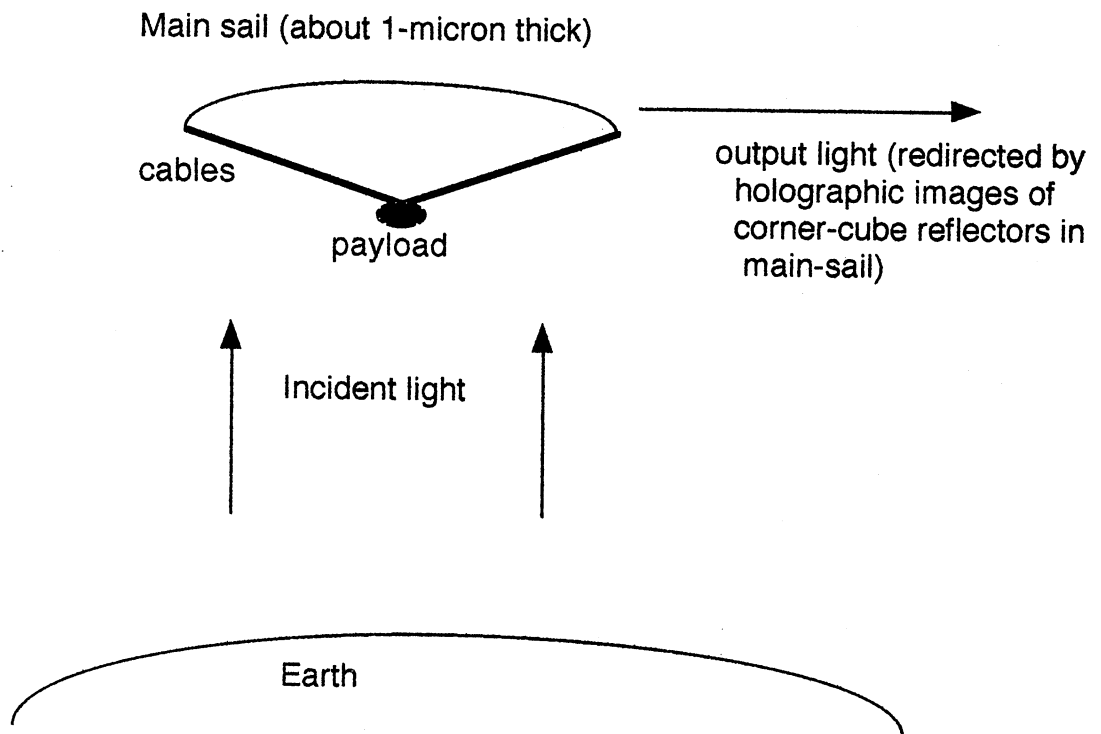


Fig. AP-1. Use of a Holographic Main Sail to Redirect Photon Radiation-Pressure Vector



REPORT DOCUMENTATION PAGE			Form Approved OMB No. 0704-0188	
Public reporting burden for this collection of information is estimated to average 1 hour per response, including the time for reviewing instructions, searching existing data sources, gathering and maintaining the data needed, and completing and reviewing the collection of information. Send comments regarding this burden estimate or any other aspect of this collection of information, including suggestions for reducing this burden, to Washington Headquarters Services, Directorate for Information Operation and Reports, 1215 Jefferson Davis Highway, Suite 1204, Arlington, VA 22202-4302, and to the Office of Management and Budget, Paperwork Reduction Project (0704-0188), Washington, DC 20503				
1. AGENCY USE ONLY (Leave Blank)	2. REPORT DATE June 2002	3. REPORT TYPE AND DATES COVERED Contractor Report (Final)		
4. TITLE AND SUBTITLE The Interstellar Probe (ISP): Pre-Perihelion Trajectories and Application of Holography			5. FUNDING NUMBERS  H-29712D	
6. AUTHORS G.L. Matloff,* G. Vulpetti,** C. Bangs,*** and R. Haggerty*				
7. PERFORMING ORGANIZATION NAMES(S) AND ADDRESS(ES) Pace University 1 Pace Plaza New York, New York 10038			8. PERFORMING ORGANIZATION REPORT NUMBER  M-1046	
9. SPONSORING/MONITORING AGENCY NAME(S) AND ADDRESS(ES) George C. Marshall Space Flight Center Marshall Space Flight Center, AL 35812			10. SPONSORING/MONITORING AGENCY REPORT NUMBER  NASA/CR-2002-211730	
11. SUPPLEMENTARY NOTES Prepared for Space Transportation Directorate *Pace University, **Telespazio Company, ***Art Resource Transfer, Inc. Technical Monitor: L. Johnson				
12a. DISTRIBUTION/AVAILABILITY STATEMENT Unclassified-Unlimited Subject Category 16 Standard Distribution			12b. DISTRIBUTION CODE	
13. ABSTRACT (Maximum 200 words) Between February and September 2001, a number of aspects of the solar-sail-launched Interstellar probe (ISP), which is under consideration by NASA for launch in the 2010-2015 timeframe, were researched. The effort was conducted in New York City (NYC) February-May, at Marshall Space Flight Center (MSFC) May-July (when the PI served as a NASA Summer 2001 Faculty Fellow), and in NYC August-September. In addition to the people listed on the title sheet, many people in NYC and at MSFC participated in this research.				
14. SUBJECT TERMS solar sail, in-space propulsion, space transportation, holography			15. NUMBER OF PAGES 88	
			16. PRICE CODE	
17. SECURITY CLASSIFICATION OF REPORT Unclassified	18. SECURITY CLASSIFICATION OF THIS PAGE Unclassified	19. SECURITY CLASSIFICATION OF ABSTRACT Unclassified	20. LIMITATION OF ABSTRACT Unlimited	